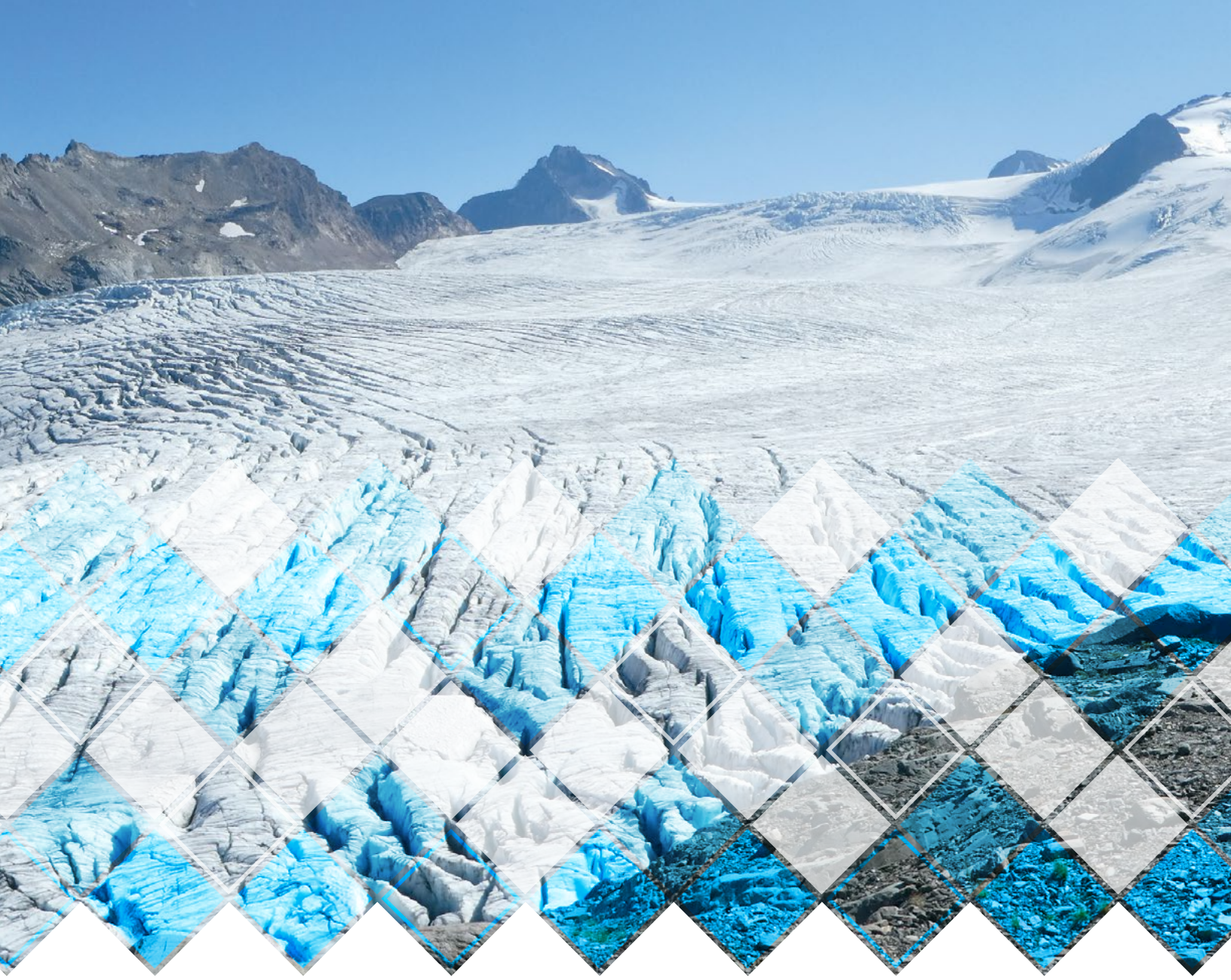

GLACIERS *in the* CANADIAN COLUMBIA BASIN

Technical Report

Table of Contents

CHAPTER 1: INTRODUCTION 1

1.0 Introduction 1
1.1 Columbia Basin Snow and Ice Research Network 2
1.2 Canadian Columbia Basin Glacier & Snow Research Network 2
1.3 Glacier supersites 4
1.4 Outline of the technical report 5

CHAPTER 2: CLIMATIC CONTEXT 6

2.1 Introduction 6
2.2 General climate science background 6
2.3 Regional geography and large-scale climate influences 8
2.4 Climatic variability in the Columbia River headwaters 12
2.4.1 Data and analysis 12
2.4.2 Results and discussion 13
2.5 The intensive monitoring period in climatic context 19

CHAPTER 3: SNOWPACK MONITORING 20

3.1 Introduction 20
3.2 Monitoring networks 20
3.2.1 BC Snow Survey Program 20
3.2.2 Alberta Environment Snow Survey Program 21
3.2.3 US NRCS SNOTEL and Manual Snow Monitoring Program Network 25
3.2.4 Canadian Avalanche Association Industry Information Exchange database 25
3.2.5 Environment and Climate Change Canada surface weather and reference climate stations 26
3.2.6 BC Ministry of Transportation and Infrastructure, Road and Avalanche Weather Stations 26
3.2.7 Parks Canada 26
3.2.8 UNBC LiDAR snow depth surveys 26
3.2.9 Other networks 27
3.2.10 Monitoring network gap analysis 27
3.2.10.1 *Review of the snowpack monitoring network in the Basin* 27
3.2.10.2 *InfoEx snow data* 28
3.2.10.3 *In situ snow monitoring of alpine areas* 28
3.3 Methods 30
3.3.1 Total depth of the snowpack 30
3.3.2 Total snow water equivalent 32
3.3.3 Average density of the total snowpack 32

3.4 Results and discussion 36
3.4.1 Characterization of the 2015-2019 snowpack 36
3.4.2 LiDAR-based snow gradients 37
3.4.3 Comparison of in situ and LIDAR snow depth 43

3.4.4 Comparison of in situ and LIDAR snow water equivalent 44
3.5 Summary 46

CHAPTER 4: GLACIER CHANGE 48

4.1 Introduction 48
4.1.1 Previous work 49
4.1.2 Glacier monitoring 49
4.2 Methods 51
4.2.1 Glaciological mass balance 51
4.2.2 Geodetic mass balance 54
4.2.2.1 *LiDAR post-processing* 55
4.2.2.2 *Density estimates* 58
4.2.3 Ice thickness data 60
4.2.4 Glacier mass change 60
4.3 Results 61
4.3.1 Mass change observations (5 year period) 61
4.3.1.1 *Glaciological vs. geodetic mass balance* 61
4.3.1.2 *Glaciological observations* 62
4.3.1.3 *Interannual and spatial variability* 63
4.3.1.4 *Balance gradients* 65
4.3.1.5 *Study glaciers vs. proximal glaciers* 67
4.3.1.6 *Glacier hypsometry* 68
4.3.2 Ice thickness observations 70
4.3.3 Area change 71
4.3.4 Regional mass change 71
4.4 Discussion 72
4.4.1 Mass change observations (5 year) 72
4.4.1.1 *Glaciological vs. geodetic balance* 72
4.4.1.2 *Glaciological observations* 72
4.4.1.3 *Geodetic observations* 73
4.4.1.4 *Interannual and spatial variability* 73
4.4.1.5 *Balance gradients* 74
4.4.1.6 *Study glaciers vs. proximal glaciers* 74
4.4.2 Ice Thickness 75
4.5 Conclusions 75
4.5.1 Glacier mass balance conclusions 76

CHAPTER 5: STREAMFLOW 77

5.1 Introduction 77
5.2 Streamflow data sources in the Basin 77
5.3 Streamflow regimes in the Columbia River Basin 81
5.3.1 Introduction 81
5.3.2 Methods 82
5.3.3 Results 82

5.3.4 Discussion 84
5.4 Glacier influences on the variability of August streamflow 84
5.4.1 Introduction 84
5.4.2 Methods 84
5.4.3 Results 85
5.4.3.1 *Temporal variability of hydroclimatic variables* 85
5.4.3.2 *Trend of August streamflow* 86
5.4.3.3 *Regression analysis* 87
5.4.3.4 *Trend analysis of the residuals* 88
5.5 Assessment of glacier wastage contributions to streamflow at Nordic and Zillmer glaciers 90
5.5.1 Introduction 90
5.5.2 Data sources 90
5.5.3 Results 91
5.6 Representativeness of the five-year enhanced monitoring period 92
5.7 Summary of key results 92

CHAPTER 6: SUMMARY OF FINDINGS AND IMPLICATIONS AND BIOGEOCHEMICAL AND ECOLOGICAL CONSEQUENCES OF GLACIER RECESSION 94

6.1 Introduction 94
6.2 Summary of major findings from the five year study 94
6.3 Implications in terms of water availability 96
6.4 Ecological and water quality implications 96
6.5 Directions for future work 98
6.5.1 Continued snow research 98
6.5.2 Continued glacier research 98
6.5.3 Continued streamflow research 99

REFERENCES 100

Acknowledgements

The work summarized in this technical report originated from research completed under the Western Canadian Cryospheric Network (WC^2N), a research network that operated between 2005-2012. A central objective of WC^2N was to project the fate of alpine glaciers in western Canada. In 2013, several co-PIs of that network (Menounos, Clarke and Moore) presented some of their initial findings to people living in the Columbia Basin in Golden, British Columbia. What became clear from that evening was that people in the Basin wished to know much more about glaciers and their fate. The research presented in this technical report represents a substantial commitment of human and financial resources to better quantify the current state of the Basin's seasonal snow and glaciers.

Our research would not have been possible without the financial support from the Columbia Basin Trust, BC Hydro, the Pacific Institute for Climate Solutions, the Natural Resources and Engineering Research Council of Canada, the Canada Chairs Program, and the Tula Foundation (Hakai Research Institute). Ben Pelto coordinated and led the glacier field work with the help of many invaluable volunteers. Thanks to Selkirk College Geospatial Research Centre for the mapping contributions as well as Marcus Schnorbus and Faron Anslow from the Pacific Climate Impacts Consortium (PCIC) for ongoing brainstorming of the study and report. We also acknowledge the participation of Tony Litke (BC Ministry of Environment) in discussions about the proposed work and its findings. This report benefitted from technical reviews from Andrew Fountain and Shawn Marshall. Thank you to Michelle Laurie for supporting network collaboration, communications and coordination of this technical report.

CHAPTER 1: INTRODUCTION

Authors: Brian Menounos and Ben Pelto

1.0 Introduction

The cryosphere - all forms of frozen water on Earth- plays a fundamental role in its climate system. Seasonal snow, mountain glaciers, ice sheets, and sea ice reflect much of the incoming shortwave radiation at high latitudes and in mountainous terrain back to space, helping to regulate the surface temperature of the planet. Accelerating concentrations of greenhouse gases (Solomon et al. 2009) are responsible for late twentieth and early twenty-first century tropospheric warming; this warming in turn drives large-scale changes in the cryosphere, with global implications that include changes in hemispheric circulation (Francis and Vavrus 2012), sea level rise (Gardner et al. 2013) and increased warming through ice-albedo feedbacks.

Electricity produced from surface runoff, from seasonal snowpack and alpine glaciers, accounts for approximately 90% of British Columbia's and 17% of Alberta's current electric power demand. This hydro-electric power generation reduces fossil fuel consumption (Deemer et al. 2016) and will help Canada to meet its carbon emission targets. Glaciers in western North America and the western Canadian Arctic are critical elements in the region's hydrologic cycle (Moore et al. 2009). The economic value of seasonal snow and alpine glaciers is difficult to quantify, but shrinking glaciers and less snow under a warming climate are estimated to exceed $500B (Sturm et al. 2017).

Glaciers provide much of the late summer inflows to several large reservoirs including those in the Canadian portion of the Columbia River Basin (Jost et al. 2012). In dry years, glacier runoff provides thermal and flow buffering required for many sensitive, aquatic species including salmon (Milner et al. 2017). Glaciers also provide financial returns to the provincial economies through tourism; these ice masses are national icons and, each year, they are visited by millions of tourists. The evidence of glacier recession in many of the National and Provincial parks provides a prime opportunity for educating the public about the effects of climate change. It is clear that seasonal snow and glaciers are important to Canada, but improved models are required to quantify regional rates of mass loss so Canada can adequately prepare for the changes that lie ahead.

1.1 Canadian Columbia Basin Glacier & Snow Research Network

The primary objective of this technical report is to summarize our findings about snow and ice in the Canadian portion of the Columbia River Basin. In 2014, the co-authors of this report and their respective organizations signed a Memorandum of Understanding to form the Canadian Columbia Basin Glacier and Snow Research Network (herein referred to as 'the Network'). The primary objectives of the Network were to:

1. Complete a literature review and gap analysis about glacier mass balance, snow cover and hydrologic impacts of a changing cryosphere in the Basin;
2. Establish environmental baselines for network research and monitoring activities;
3. Clarify processes important for the response of glaciers and seasonal snow cover under a changing climate;
4. Determine the downstream implications of current and projected changes to glaciers and snow cover in respect of both ecosystems and human use;
5. Coordinate research, monitoring and data sharing; and
6. Produce and disseminate information resources to support policy, planning and decision-making by communities, resource managers and agencies.

Unlike Europe (Zemp et al. 2019), few long-term records of glacier mass balance exist in western Canada. In situ records are extremely valuable for improving hydrologic and surface mass balance models. In 2010, Trubilwicz et al., (2010) co-authored a report to identify glaciers in the Basin that would represent ideal glaciers for long-term mass balance measurements. Several of those glaciers form the key sites described in Chapter 3.

1.2 The Canadian portion of the Columbia River Basin

The Columbia River Basin (the Basin) is a 668,000 km^2 transboundary watershed that spans seven U.S. states and British Columbia (BC), Canada. The Basin (Figure 1) represents 15% of the watershed's total area, yet provides around 30-40% of total runoff, largely due to the presence of mountainous terrain which enhances precipitation and allows glaciers to grow (Hamlet and Lettenmaier 1999; Cohen et al. 2000). Over 2,200 glaciers cover 1,760 km^2 in the Columbia Mountains (Bolch et al. 2010). The Columbia Mountains are subdivided into the Cariboo, Monashee, Selkirk, and Purcell ranges, each rising to over 3,000 m above sea level (asl).

The climate within the Canadian portion of the Basin is transitional between maritime and continental (Demarchi 2011). Monthly average temperatures in the Basin range from -9.2 °C in January to +13.3 °C in July (Najafi et al. 2017; Schnorbus et al. 2014a). General circulation is dominated by westerly flow, which brings consistent Pacific moisture, particularly in the winter months.

Approximately 65% of annual precipitation falls as snow, with snowfall possible at highest elevations throughout the year (Schnorbus et al. 2014a). The snow accumulation season in the Columbia Mountains extends from October to May, and the summer melt season runs from May through September.

Glaciers in the Basin lost 15% of their area from 1985 to 2005 (Bolch et al. 2010), and are forecast to shrink by 35 to 100% in area and volume by 2100 (Clarke et al. 2015). Despite the importance of glaciers to the flow of the Columbia River and its tributaries, and the projected declines in glacier volume and area, little is known about the glaciers which feed the Columbia River. Previous work suggests that glacier melt can represent up to 25-35% of surface flows during late summer months, especially during times of drought (Jost et al. 2012). Glaciers act as frozen reservoirs (Viviroli et al. 07/2007), storing water in the form of snow and ice, and then releasing a portion of that water in the form of melt during the ablation season, June-September in the Columbia Basin. Glacier runoff peaks in the driest, hottest months in the Basin, when water demand is high, and salmon runs are occurring. Streams typically experience their lowest flows during this period, which makes glacier contributions a buffer against low streamflows (Nolin et al. 2010) which can be detrimental to fish and aquatic species due to thermal stresses (Fleming and Dahlke 2014). For most portions of the Basin, glacier contribution to runoff is unquantified (Jost et al. 2012), and changes in snowpack over the glaciers also have not been studied in any detail. We are thus poorly situated to understand and adapt to the coming changes in the Basin. The Columbia River is largely snow and glacier-fed yet little is known of the high elevation cryosphere in the Basin, which forms the backbone of the river discharge. Our work aims to establish current rates of glacier mass change, and glacier runoff contributions. By elucidating glacier response to climate change, we provide the first large-scale estimates of glacier mass change in the Basin. This improved understanding of the current rate of change allows for improved forecasts of continued glacier response to climate change in the Basin (Clarke et al. 2015).

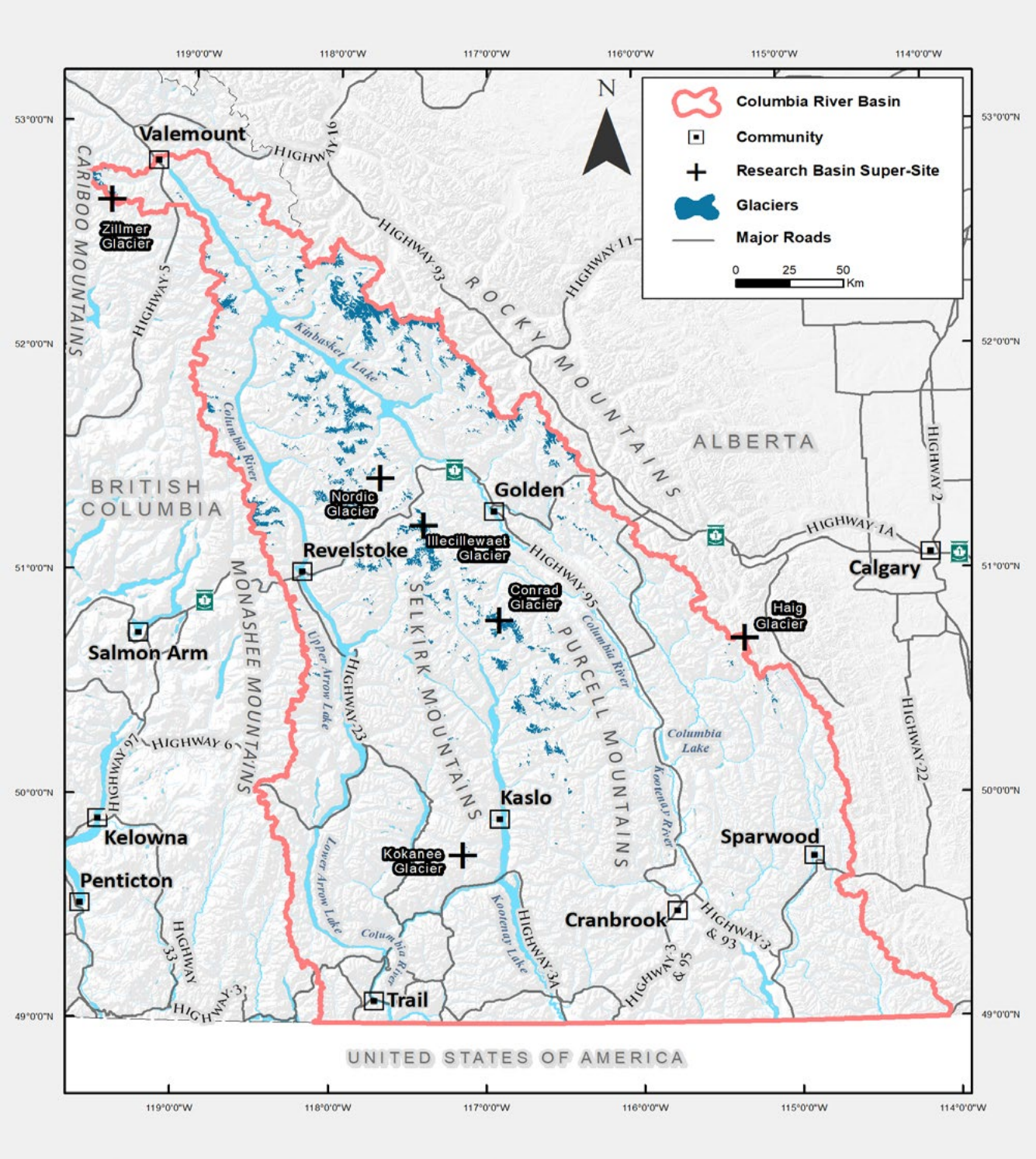

Figure 1 *The Canadian portion of the Columbia River Basin and glacier supersites of coordinated research.*

1.3 Glacier supersites

Glaciers in this study were selected based upon the following criteria: 1) have a large elevation range to maximize information on vertical gradients of accumulation and melt, 2) will not disappear over the next few decades, 3) located within a gauged catchment between 10 and 1000 km^2, 4) relatively close to one or more climate stations, snow courses, or snow pillows, 5) be safe to travel and work on, and 6) have relatively easy access (Trubilowicz et al. 2010).

1.4 Outline of the technical Report

This report is organized into a set of chapters that identify research gaps and describe research about snow and ice in the Basin over the last five years. Chapter two provides a summary of the Basin's climate and puts meteorological conditions of the last five years into a long-term perspective. Chapter three describes the Basin's seasonal snow cover, its climatological and topographic controls, and snow observational methods and current state of the monitoring network in the Basin. Chapter four provides an assessment of glaciers and glacier change with a focus on describing the research undertaken at key glaciers in the Basin. The importance of glaciers on the Basin's streamflow is described in Chapter five. The implications of our research and areas for future work are described in Chapter six.

CHAPTER 2: CLIMATIC CONTEXT

Authors: Sean W. Fleming and R.D. (Dan) Moore

2.1 Introduction

The objective of this chapter is to provide the climatic context for understanding cryospheric dynamics, and their hydrologic consequences, to be covered in chapters 3, 4 and 5. The chapter covers spatial variability in key climatic variables that are associated with snow accumulation and glacier ablation, as well as temporal patterns extending through the twentieth century to present. This report focuses on snow and ice monitoring and analysis, and no original climatological research was performed in this project. However, information about background climatic conditions and variability supports interpretation of the detailed scientific outcomes of the Canadian Columbia Basin Glacier & Snow Research Network over the five year intensive monitoring period. As such, this chapter provides verbal descriptions of both general climate science context and prior specific research on the characteristics, variability, and change of climate in the Canadian Columbia Basin, and illustrates some key climate features using visualization and analysis of existing climatic datasets corresponding to the study supersites.

2.2 General climate science background

Climate is defined as the average weather at a location; it is a central determinant of the depth and extent of seasonal snow cover and whether glaciers exist in a given location. How much precipitation there is, how much of it falls as snow, and how warm or cloudy or windy it is, are all key controls on downstream river runoff and all influence whether a glacier ultimately can persist at a given location. Some additional general background around climate variability and change is provided below. This short summary is intended only to orient the reader with some motivation and context for our description and analysis of climatic context to water, snow, and ice in the Basin.

Climate varies greatly between locations, across a vast variety of length scales. At the largest (planetary) scales, climate gradually cools from the equator toward the poles as the sun's incident radiation strikes the earth's surface at shallower angles, reducing the heat flux. This differential heating across latitudes also sets up large-scale convective atmospheric circulation patterns called Hadley cells: adiabatic cooling of rising air at the equator gives abundant rainfall and makes the tropical rainforests possible, and when that air, deprived of its moisture, then sinks in the subtropics, it helps create many of the world's great deserts, such as the Sahara. At slightly smaller continental scales, proximity to the ocean – which forms a

tremendous solar energy reservoir due to the high heat capacity of water – controls how moderate climate is, with warmer winters and cooler summers near the ocean and stronger seasonal extremes in continental interiors. At somewhat smaller scales still, topography is a tremendous influence on spatial variation in climate: higher elevations are cooler, and rain shadows form on the downwind side of mountain ranges. At the smallest spatial scales, microclimates exist.

Climate also varies significantly over time. This of course complicates the definition of climate as the long-term average of weather, as that average shifts as well, a statistical property known as nonstationarity. It is therefore perhaps more useful to think of climate as the overarching, interconnected framework of atmospheric chemical composition, incident solar radiation, ocean circulation, and land surface processes and feedbacks that in tandem control the typical weather at a location, and which can change over time.

As with spatial variations in climate, temporal variations are spread across a continuum of scales. Year-to-year fluctuations reflect the complex and unpredictable dynamics of the coupled ocean-atmosphere circulation. Over years to decades, more organized modes of variability exist. Examples of these quasi-periodic phenomena relevant to the Columbia Basin include El Niño-Southern Oscillation (ENSO) and the Pacific Decadal Oscillation (PDO) (Fleming and Whitfield 2010; Gobena et al. 2013; Hsieh et al. 2003; Mantua et al. 1997; Whitfield et al. 2010). At timescales of centuries, other forms of variability appear. Examples include the Medieval Warm Period (Osborn and Briffa 2006) and the Little Ice Age (Luckman 2000). Their origins are less clear but they may be associated with modulation of atmospheric chemistry by both volcanism and fluctuations in the sun's radiative output (e.g. Crowley 2000). Over timescales of tens to hundreds of thousands of years, wobbles in the Earth's orbit known as Milankovitch cycles drove the waxing and waning of the ice ages throughout the Pleistocene. At the longest timescales, tectonic forces have also changed climate, such as the rise of Himalayas, which affected atmospheric circulation, and the closing of the Isthmus of Panama, cutting off circulation between the Pacific and Atlantic oceans. This superposition of many timescales of variability leads to such phenomenological climate properties as fractal dynamics, which by definition lack a single characteristic timescale and make it even more challenging to define a mean climate state (Huybers and Curry 2006; Fleming 2008, for additional details see 2017). Moreover, overprinted upon all these natural processes are anthropogenic climate changes. There are two forms. One is local to regional: human modification of the land surface alters local climate, and the effect is most noticeable in cities, creating "urban heat islands" which tend to be considerably warmer than their rural or wilderness surroundings. The other is global climate change. This refers to an artificial increase in the net planetary atmospheric concentration of greenhouse gases resulting from a combination of human activities, such as fossil fuel combustion, industrial livestock operations, and massive deforestation, in turn corresponding to certain technological choices, economic growth, and population growth. Its general global impacts include rising temperatures and increased amplitude of the hydrologic cycle.

Recognizing that climate is changeable can be crucial. The archetypal example is the Colorado River Compact. This 1922 legal agreement allocated the water of the Colorado River among several, mostly arid, western US states. The allocations were based on the historical hydroclimatic datasets available in the region at that time, which corresponded to the then-recent settlement of the western US and were therefore very short. In the 1970s, paleoclimatic data (Jacoby 1976; Woodhouse et al. 2006) showed that the short datasets upon which this legal agreement was based happened to coincide with one of the wettest periods in the region in centuries, known as the North American Pluvial (Cook et al. 2011), and that the "droughts" and resulting water supply shortages in several of the intervening decades since 1922 in fact represented more normal conditions for the Colorado River Basin. Similar issues have been experienced in western Canada (Fleming and Sauchyn 2013). The North American Pluvial is believed to have been a natural event; superposed upon such natural variability we are now seeing the impacts of global anthropogenic climate change, making long-term climatic context even more important.

Thus, climate, and therefore suitable "habitat" for snow and glaciers, and all the downstream impacts of the cryosphere on river hydrology and water resources, varies substantially, and recognizing such variability is important for assessing the data collected over the five-year window of the intensive monitoring program. The following represents a simple snapshot assessment, based on review and synthesis of existing literature and visualization of data from established climatic databases, of how three relatively well-monitored climate variables important for snow, glacier, and hydrologic conditions – specifically, winter (November-April) total precipitation and summer (May-September) means of minimum and maximum daily air temperature – are variable over space and time in the Canadian Columbia Basin, and how the five-year monitoring window fits into this larger climatic context.

2.3 Regional geography and large-scale climate influences

The topography of the Columbia River headwaters is dominated by the Columbia Mountains, which comprise the Monashee, Selkirk and Purcell Mountains (in order from west to east), with the Rocky Mountains defining the eastern slope. The regional climate is dominated in autumn and winter by the passage of frontal-cyclonic weather systems that travel eastward across the north Pacific before traversing southern BC. In summer, anticyclonic systems tend to dominate, leading occasionally to extended spells of clear, dry weather (Moore, R.D., Spittlehouse, D.L., Whitfield, P.H. and Stahl, K. 2010).

The mountain chains are oriented roughly perpendicular to the dominant westerly circulation, which gives rise to a range of orographic influences on local climatic conditions, with contrasts between windward and lee slopes. Precipitation increases dramatically from the valley bottoms to the mountain peaks, while

temperature decreases. The Monashees, Selkirks and the west slope of the Purcells are dominated by cool-cold, moderately wet winters and warm, moderately dry summers (Chilton 1981). The east slope of the Purcells and the Rocky Mountains tend to be drier with colder winters than the western part of the catchment.

Climatic patterns are illustrated in Figures 2.1 to 2.4 based on the gridded PRISM climate product (Daly et al. 2008). Cold-season precipitation should be generally related to winter snow accumulation and glacier winter balance, while warm-season air temperature is an index of the energy available for melting snow and ice, which is a major control on glacier summer balance. As can be seen, the glaciers tend to occupy the coldest and wettest locations. Based on winter precipitation, Nordic and Illecillewaet glaciers should experience the highest winter accumulation, Haig and Yoho glaciers, the least, with the other glaciers being intermediate.

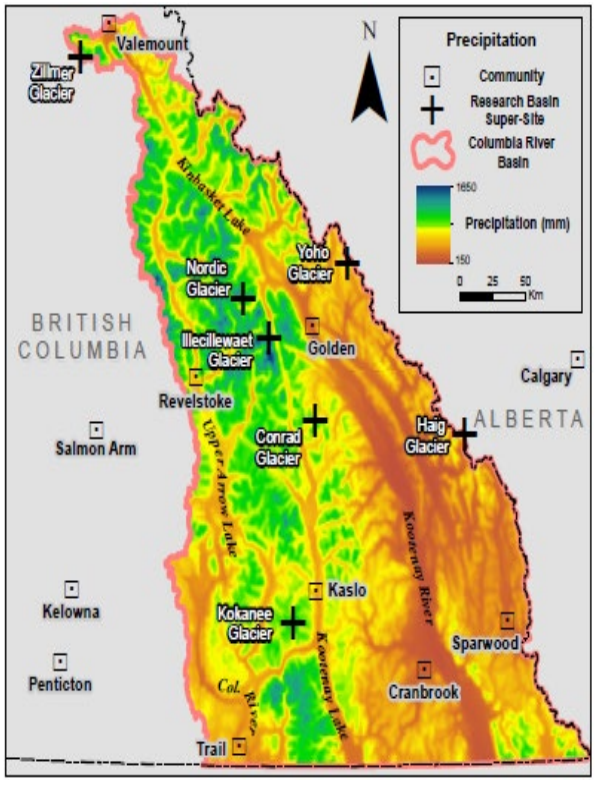

Figure 2.1 *Climatic normals of cold-season (November to April) precipitation based on the PRISM data set for the 1981–2010 period (provided by C. Belisle, I. Parfitt, and D. Hutchinson).*

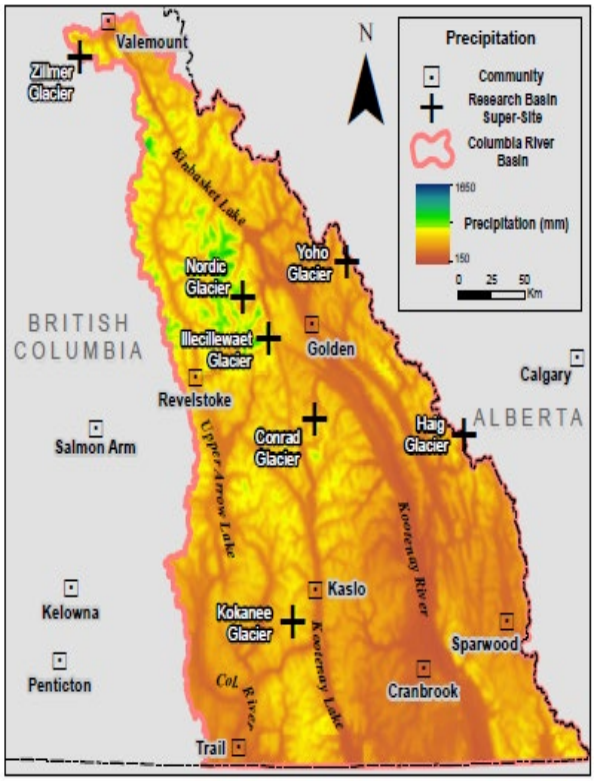

Figure 2.2 *Climatic normals of warm-season (May to October) precipitation based on the PRISM data set for the 1981–2010 period (provided by C. Belisle, I. Parfitt, and D. Hutchinson).*

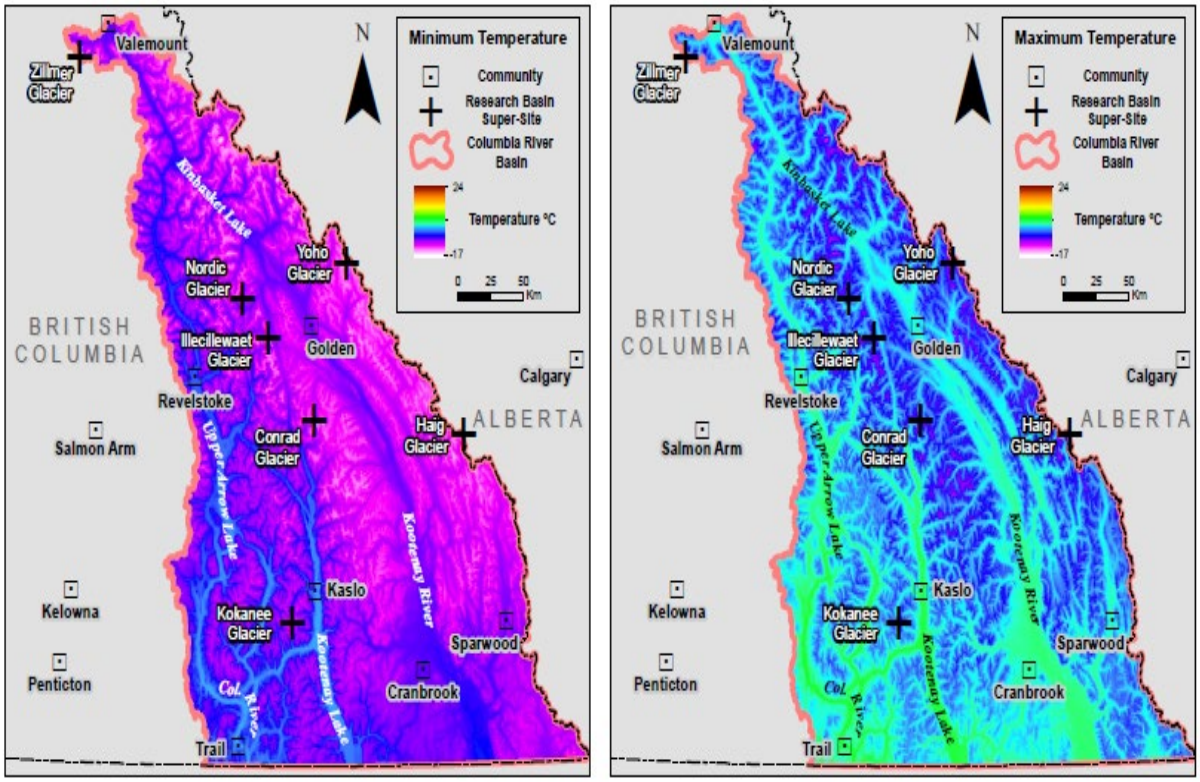

Figure 2.3 *Climatic normals of cold-season (November to April) minimum and maximum air temperature based on the PRISM data set for the 1981–2010 period (provided by C. Belisle, I. Parfitt, and D. Hutchinson).*

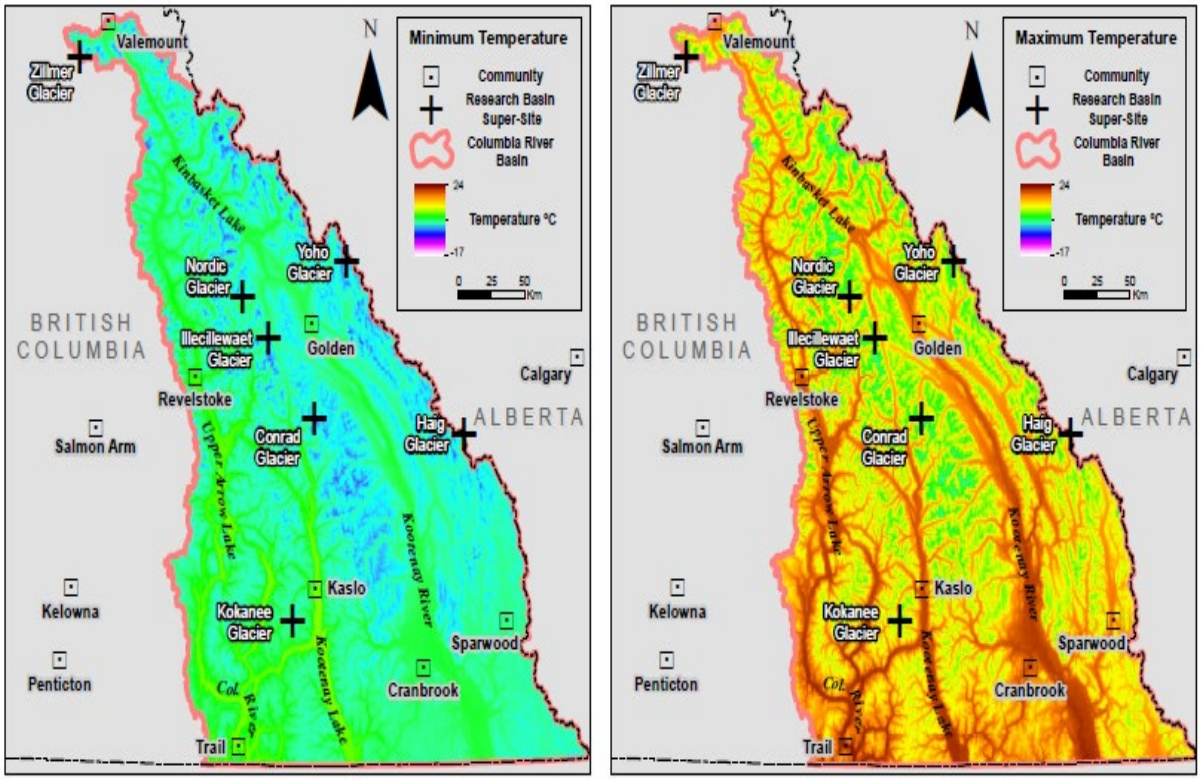

Figure 2.4 *Climatic normals of warm-season (May to October) minimum and maximum air temperature based on the PRISM data set for the 1981–2010 period (provided by C. Belisle, I. Parfitt, and D. Hutchinson).*

Interannual and interdecadal variations in air temperature and precipitation in the Columbia River headwaters are influenced in large part by two climatic teleconnection patterns, the El Niño–Southern Oscillation (ENSO) and the Pacific Decadal Oscillation (PDO), especially during winter (Fleming and Whitfield 2010; Gobena et al. 2013; Hsieh et al. 2003; Mantua et al. 1997; Stahl et al. 2006; Whitfield et al. 2010; Moore, R.D., Spittlehouse, D.L., Whitfield, P.H. and Stahl, K. 2010). ENSO is related to changes in complex coupled ocean–atmosphere circulation processes in the equatorial Pacific Ocean, including variations in the trade winds and upwelling of water off the equatorial coast of South America, and it tends to shift between warm (El Niño), and cool (La Niña), and neutral phases every two to seven years. In the Columbia River headwaters, years with La Niña conditions tend, on average, to be wetter than average and near or slightly below average for air temperature and cooler than average. El Niño winters tend to be near average to warmer than average and experience mixed conditions in relation to precipitation, and El Niño winters tend to exhibit the opposite anomalies (Moore, R.D., Spittlehouse, D.L., Whitfield, P.H. and Stahl, K. 2010).

The PDO pattern is related to variations in sea surface temperature patterns and associated shifts in wind patterns in the North Pacific Ocean (Whitfield et al. 2010). Like ENSO, PDO exhibits two dominant phases (positive/negative or warm/cool), somewhat akin to El Niño and La Niña events, but these instead tend to persist for multiple decades. Distinct shifts between phases occurred in about 1922 (cool to warm), 1947

(warm to cool) and 1977 (cool to warm); more recent shifts may have occurred as well but this is less clear. The Columbia River headwaters tends to experience warmer- and drier-than-average winters during the PDO warm phase, while the PDO cool phase tends to be associated with cooler and wetter winters (Stahl et al. 2006).

Climate variability experienced in the upper Columbia Basin is the net result of the superposition of many processes. While the impacts of some of these, like ENSO and the PDO, are well-studied and reasonably well-understood, it is an area of intensive ongoing research (e.g. Wu et al. 2005; Gobena et al. 2013; Fleming and Dahlke 2014). Other coherent large-scale patterns of climatic variability, such as the Arctic Oscillation and North Pacific Gyre Oscillation, may have significant impacts on Columbia River climate and water resources. Additionally, the nature and extent of teleconnection effects, particularly as related to their nonlinearities, continue to be refined as more data become available and more advanced data analysis methods are developed.

2.4 Climatic variability in the Columbia River headwaters

2.4.1 Data and analysis

Time series for the three key climatic variables were extracted from the ClimateWNA (v. 6.00) data product over 1901–2017 for each of seven locations corresponding to the glacier monitoring supersites (Table 2.1). ClimateWNA is a synthesis product that integrates climatic data from several sources into a single, seamless, relatively high-resolution spatiotemporal climate database (Wang et al. 2016). These results are presented as winter (November–April) and summer (May–September) seasons instead of annual averages (January–December) to represent conditions during the winter snow accumulation and summer ablation periods. As described below, the strong coherence of interannual variability for each variable across the supersites (Figures 2.5 to 2.7) allows data for a given variable to be averaged across the supersites on a year-by-year basis to create a regional average dataset (Figure 2.2); averaging simplifies interpretation and improves the signal-to-noise ratio, where signal is taken in this case to be the regionally coherent portion of climatic variability (Fleming and Barton 2015).

A LOWESS smoother was also applied to the spatially averaged time series (Figure 2) using the R scientific computing language (version 3.3.2 R Development Core Team 2013) in a RStudio (version 1.0.136) environment. LOWESS is a locally weighted polynomial regression (Cleveland 1979) that acts as a low-pass filter and helps to identify longer-term patterns of variation underlying year-to-year variability. Summary statistics were calculated to allow cross-site comparisons in climatic conditions. Correlation matrices based on the Pearson correlation coefficient (*r*), were also calculated to characterize the degree of coherence in interannual

variability among sites. Correlation coefficients were also calculated between each variable; some of these results are shown as a simple measure of linear trend.

Table 2.1 *Location of the six supersite glaciers and glacier-specific details.*

Glacier	Latitude	Longitude	Area	Max Elev.	Min Elev.	Mean Elev.	Length	Aspect
			(km^2)	(m)	(m)	(m)	(km)	
Zillmer	52.652	-119.562	5.43	2860	1860	2380	5.59	NW
Nordic	51.432	-117.703	3.39	2990	2065	2515	3.30	N
Illecillewaet	51.220	-117.416	7.72	2908	2015	2532	4.29	WNW
Haig	50.710	-115.301	2.62	2870	2461	2660	2.45	SE
Conrad	50.800	-116.914	11.45	3235	1825	2595	12.18	N
Yoho	51.616	-116.557	16.00	3146	2023	2630	11.5	SE
Kokanee	49.750	-117.147	1.79	2805	2220	2585	2.20	N

2.4.2 Results and discussion

The seven study glaciers experience somewhat different climatic conditions. Typical summer maximum and minimum temperatures are a few degrees higher at Kokanee than at Conrad and Yoho, for example, while Illecillewaet Glacier receives more than twice the winter precipitation than Conrad Glacier does. The severity of interannual fluctuations as captured by the standard deviations of the annually aggregated climate variables is consistent across the sites for temperature, but substantially differs for precipitation, with the wetter sites showing large year-to-year variations in winter precipitation, which should result in greater interannual variability in winter mass balance.

Although there are significant differences between the supersite climates (Table 2.2), the pattern of interannual climate variability is consistent between the sites (Figures 2.5 to 2.7): that is, the time series for a given climate variable (e.g., minimum temperature) strongly covaries among glaciers. Correlation coefficients between the same variables at different locations are greater than 0.7 in all cases and typically greater than 0.9.

This spatial coherence in the patterns of year-to-year variability in these climate variables may reflect, in part, the interpolation routines used to generate the ClimateWNA data product, but it is also typical of climate variability and change in western North America; for instance, the entire Pacific Northwest

responds to ENSO events in a roughly homogeneous way. Although a given climate parameter shows more-or-less uniform patterns of variability across the sites, each climate parameter tends to vary somewhat separately from the others due to local-scale influences on climatic conditions. For example, correlations between T_{min} and T_{max} at each site range from around 0.4 to a little over 0.5 indicating both similarities and differences in overall behavior. This is to be expected given that atmospheric controls on minimum and maximum temperature can differ; as one example, cloud cover tends (all else being equal) to decrease T_{max} and increase T_{min}. Overall, the picture painted by these data is one of fine-scale spatial variability in mean climate, due primarily to complex topography, and large-scale spatial coherence in the overall patterns of interannual variability, reflecting the dominance of synoptic-scale atmospheric processes such as North Pacific frontal storms and their dynamical controls, such as the position of the jet stream, and still larger-scale influences in turn, such as ENSO.

Table 2.2 *Summary statistics for some key climate variables at supersites, based on PRISM or ClimateNWA. "std dev" = standard deviation.*

	Conrad	Haig	Illecillewaet	Kokanee	Nordic	Yoho	Zillmer
Summer mean Tmax							
Average	8.2	10.9	9.5	11.4	10.8	9.6	9.5
Min	6.3	8.8	7.8	9.1	9.1	7.8	7.5
Max	10.9	13.5	12.2	14.2	13.4	12.0	12.3
Std dev	1.0	1.0	1.0	1.0	0.9	0.9	0.9
Summer mean Tmin							
Average	0.0	0.6	0.9	3.0	1.8	-0.3	0.4
Min	-1.5	-0.9	-0.5	1.2	0.5	-1.6	-1.0
Max	2.2	2.7	2.8	5.0	3.7	1.7	2.0
Std dev	0.7	0.7	0.7	0.8	0.7	0.7	0.7
Winter total P							
Average	893	587	1307	957	1224	737	1097
Min	493	351	746	470	718	426	683
Max	1481	911	2178	1635	2076	1193	1672
Std dev	185	127	268	198	248	162	204

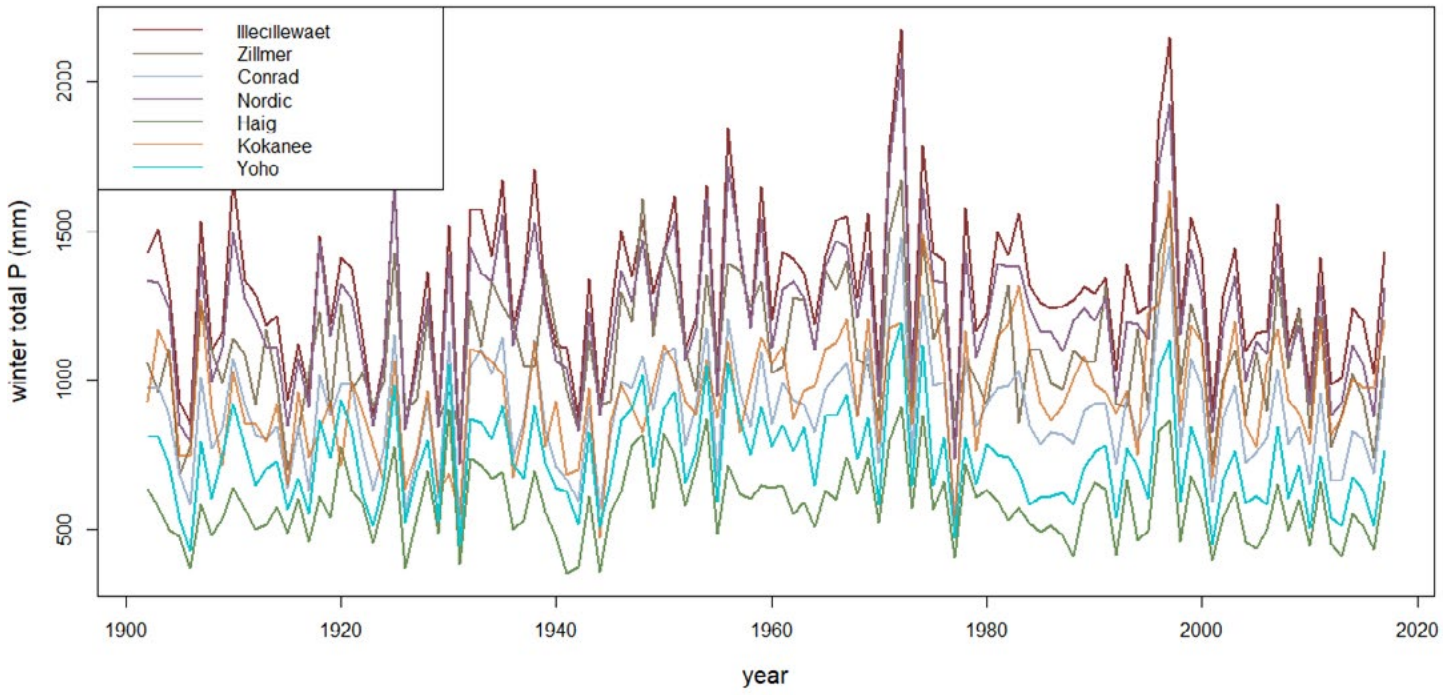

Figure 2.5 *Total winter precipitation at each of the supersites from ClimateWNA*

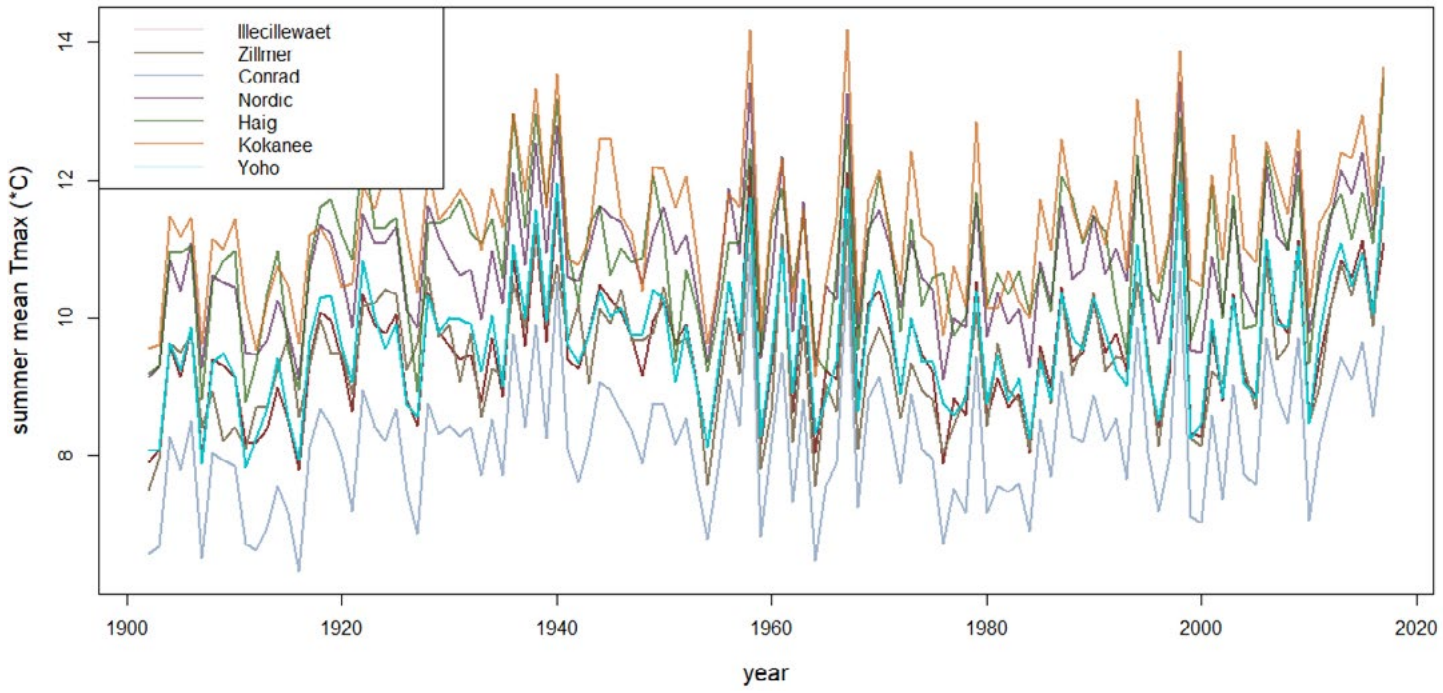

Figure 2.6 *Mean summer maximum temperature at each of the supersites from ClimateWNA*

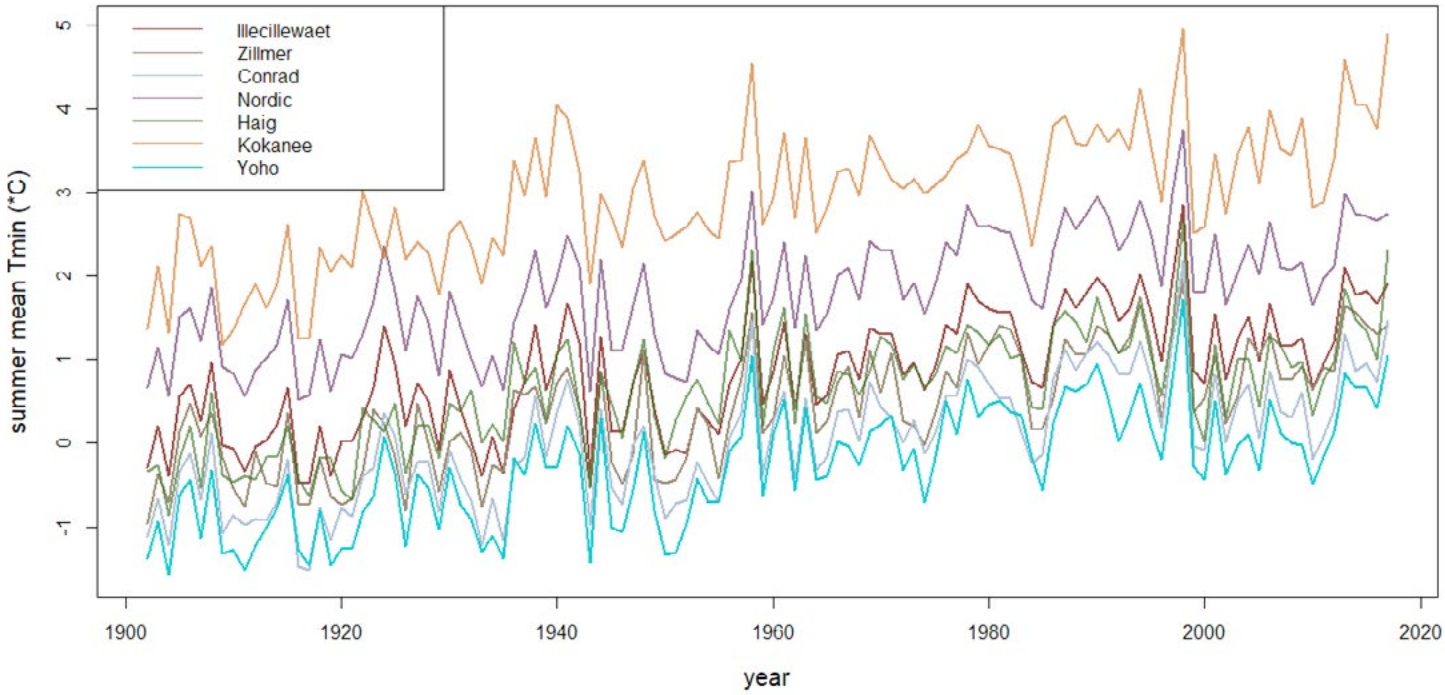

Figure 2.7 *Mean summertime minimum temperature at each of the supersites from ClimateWNA*

Regionally averaged precipitation, shown in Figure 2.8, shows little long-term monotonic trend, with no clear change toward towards wet or dry conditions. These observations are consistent with the lack of appreciable region-wide correlations ($-0.09 < r < 0.30$) between wintertime total P and the year of observation. Rather, precipitation appears to demonstrate a low-frequency oscillation consisting first of a wetting trend, particularly from the mid-1940s, followed by a general drying trend. This low-frequency fluctuation is generally consistent with the documented PDO shifts that occurred in the twentieth century.

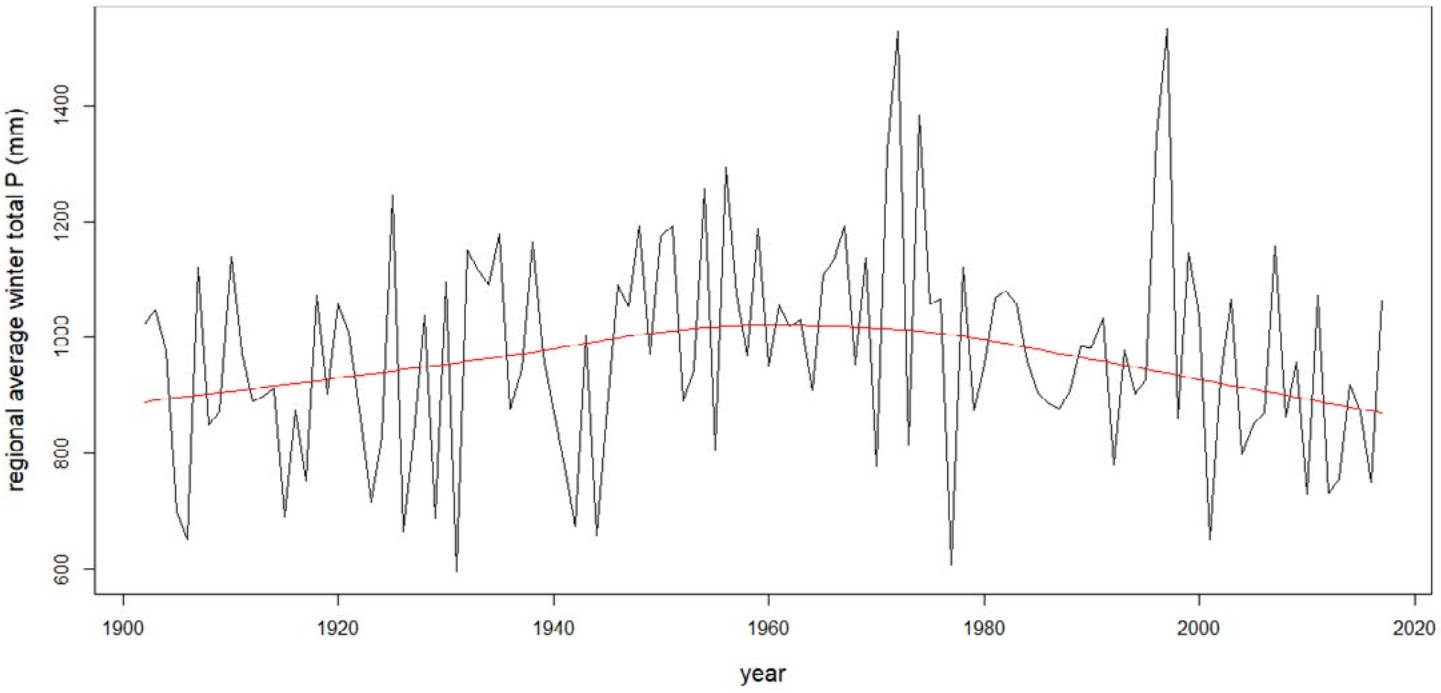

Figure 2.8 *Regional average of total wintertime precipitation across the seven supersites.*

Regional summer maximum temperature has shown some tendency to increase since the start of the record (Figure 2.9), presumably corresponding to global anthropogenic climate change. Recovery from Little Ice Age conditions near the start of the time series, and regional land use/land cover changes, such as forestry, urbanization, and reservoir construction, may conceivably influence these long-term trends as well. However, there was also an extended cooling period in the middle of the record that may again correspond to the strong PDO cool phase from 1947 to 1976. Correlations between T_{max} at individual supersites and year of observation are therefore modest, ranging roughly from 0.15 to 0.25.

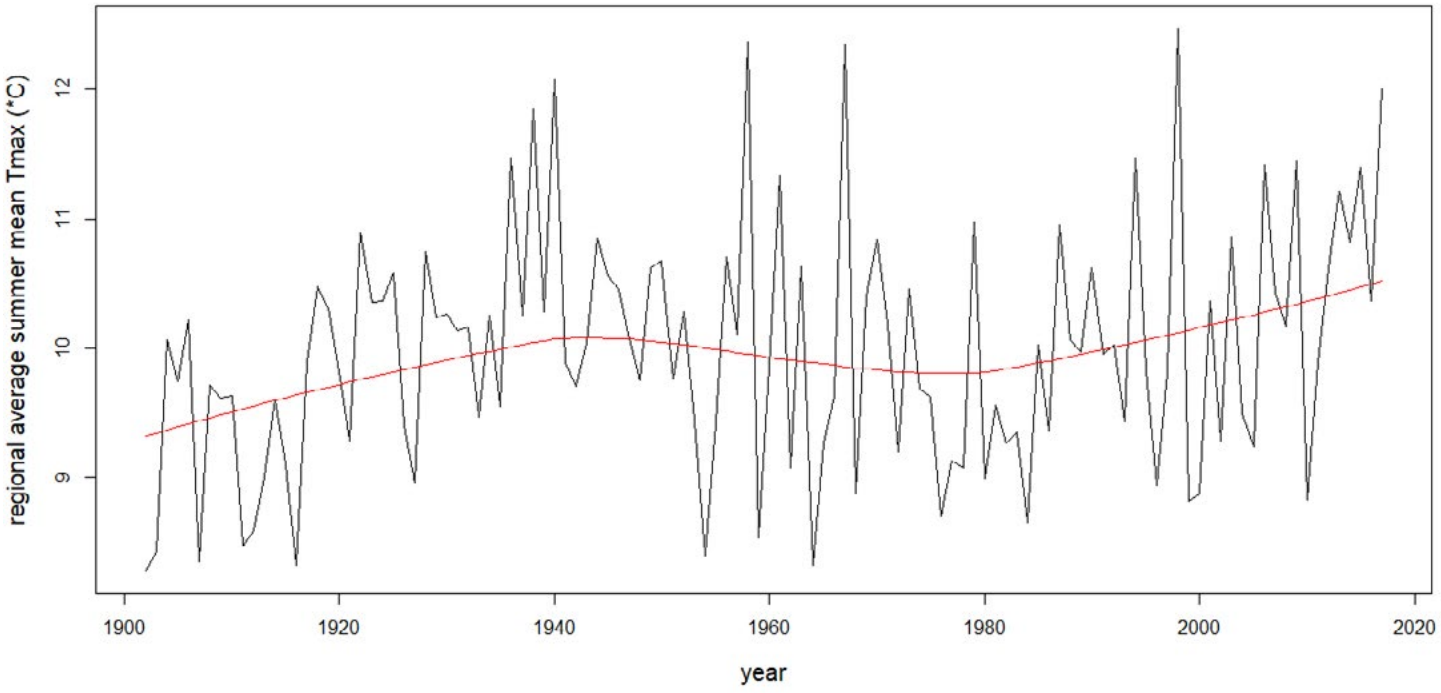

Figure 2.9 *Regional average of summertime mean maximum temperature across the seven supersites*

Of the three key climate variables considered, minimum summer temperature (Figure 2.10) demonstrates by far the most unambiguous long-term trend. Correlation coefficients between T_{min} at individual glaciers and the year of range from 0.70 and 0.73, indicating that a linear upward trend in temperature explains roughly 50% of the interannual variance in mean summer T_{min}.

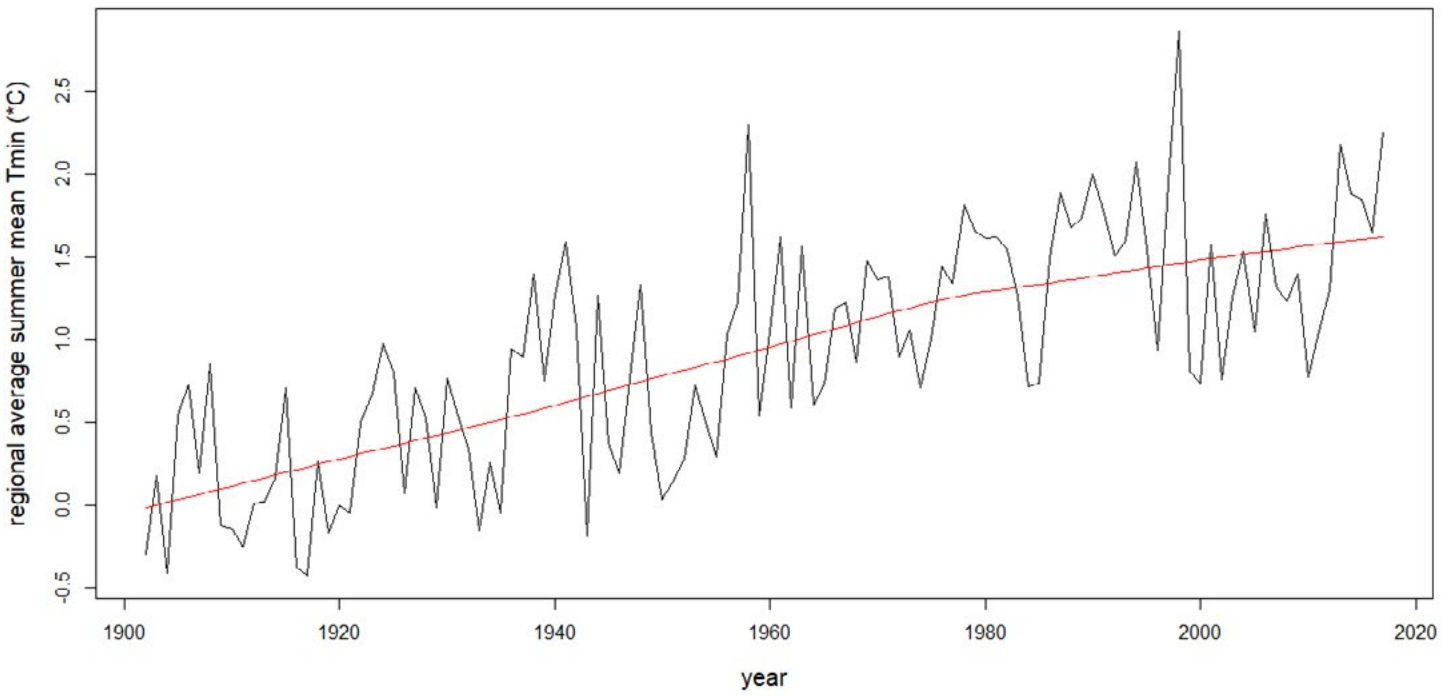

Figure 2.10 *Regional average of summertime mean minimum temperature across the seven supersites*

2.5 The intensive monitoring period in climatic context

The patterns documented above suggest an ongoing deterioration in climatic favourability for glaciers over the last three or four decades (from approximately 1980 onward), including both a general downturn in winter precipitation and increase in summer air temperature. Over the longer term, the last century has seen a general warming trend, which is again broadly conducive to gradual glacier mass loss and retreat, albeit with no clear monotonic trend in precipitation. Over the shorter term, the intensive monitoring period (2014 to 2018) appears to have sampled a particularly warm and dry period (although note that ClimateWNA data only extend through 2017). These climate patterns are broadly consistent with previous research in this region (Stahl and Moore 2006; Schiefer et al. 2007; Bolch et al. 2010; Gobena et al. 2013; Jost et al. 2012; Hamlet et al. 2013; Schnorbus et al. 2014b; Vincent et al. 2015; Clarke et al. 2015; Wan et al. 2019; Brahney et al. 2017a; Fleming and Dahlke 2014).

CHAPTER 3: SNOWPACK MONITORING

Authors: Frank Weber, Ben Pelto and Brian Menounos

3.1 Introduction

This chapter provides an overview of snowpack monitoring in British Columbia (BC) with a focus on the Canadian portion of the Columbia River Basin (the Basin). Snowpack is defined as snow on the ground.

The snowpack monitoring activities discussed here are for the purpose of quantifying the seasonal evolution, magnitude and spatial distribution of the snowpack. Several organizations collect snowpack data with a variety of instruments, guided by their respective standards and are organized into various station networks.

The snowpack variables most commonly used in water resource management include snow depth [cm], snow water equivalent [depth of water that would result by melting the snow at a specific point in mm], snow density [kg m^{-3}], snow covered area [km^2] and snow line elevation [m above sea level (asl)].

3.2 Monitoring networks

Instrumental snow records in BC started at Grouse Mountain (station number 3A01) on the Coast and Sinclair Pass (2C01) in the East Kootenays in 1935. Today, snow data are collected for various objectives that include: road safety management and snow plow scheduling; avalanche risk management for road and ski operations; estimation of snow loads on structure, water resource management for drinking water supply; hydropower generation and mining; flood forecasting and emergency management; climate change monitoring; hydrologic impact assessments and; wildlife habitat studies.

Snow monitoring networks in BC and in the vicinity of the Basin (Figures 3.1-3.3) are briefly described below.

3.2.1 BC Snow Survey Program

The primary public snow data collection network in BC is organized under the BC Snow Survey Program (https://www2.gov.bc.ca/gov/content/environment/air-land-water/water/water-science-data/water-data-tools/snow-survey-data). The objective of the BC Snow Survey Program is to collect long-term snow data, especially at higher elevations. The BC Ministry of Environment is the Program Coordinator, BC Hydro is a Program Partner, and Rio Tinto-Alcan and Metro Vancouver are Program Cooperators. The BC Snow

Survey Program operates 221 snow stations. In the vicinity of the Columbia River Basin BC Hydro and the BC Ministry of Environment, respectively, own or operate 65% and 35% of 56 manual and automated BC Snow Survey Program stations.

Nominal sampling dates of manual surveys are January 1, February 1, March 1, April 1, May 1, May 15, June 1 and June 15. For logistical reasons manual snow survey samples can be obtained six days before or after the nominal sampling date and still be included in the long term snow survey record. A manual snow survey station consists of five or ten fixed sampling locations which, in BC, can be located on sites with forest crown closures that range from very sparse to very dense. Snowpack parameters collected include snow depth, snow water equivalent, calculated snow density and snow line elevation.

Standard sensors at automated Snow Survey Program stations include snow water equivalent systems, all-season precipitation gauges and air temperature sensors. All BC Ministry of Environment-operated stations are equipped with snow depth sensors, whereas snow depth sensors do not exist for all BC Hydro and Alcan/Rio Tinto-operated stations. Select stations have real-time camera systems that transmit daily images of instrumentation and the landscape and which can be used to qualitatively infer snowline elevation.

3.2.2 Alberta Environment Snow Survey Program

Alberta Environment maintains automated and manual snow stations in the Rocky Mountains east of the Basin. Data collected at ten automated and 17 manual snow stations located just east of BC-Alberta border are close enough to the Columbia River Basin to infer snow conditions in the eastern part of the Basin.

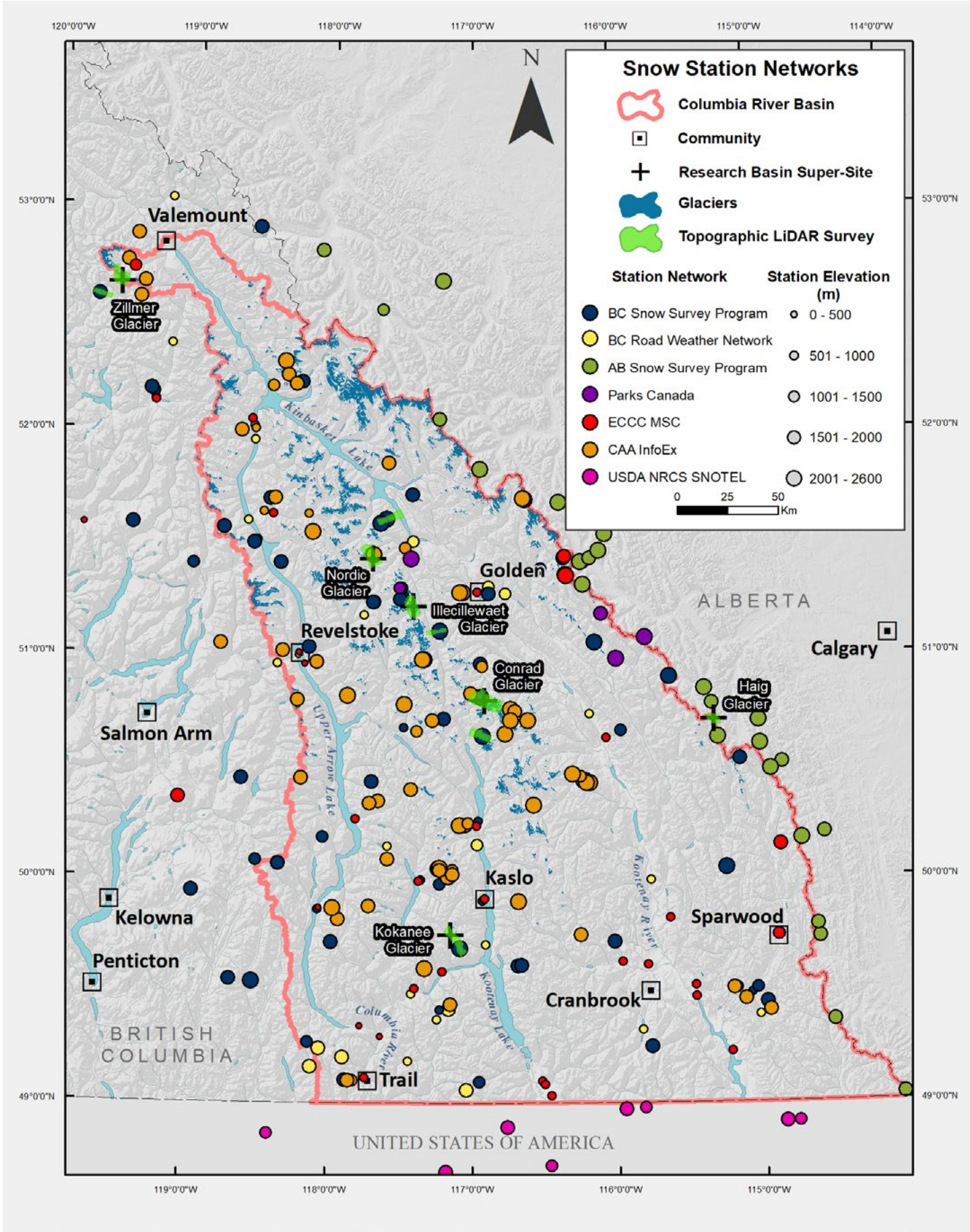

Figure 3.1 *Snow monitoring networks in and in the vicinity of the Canadian Columbia River Basin.*

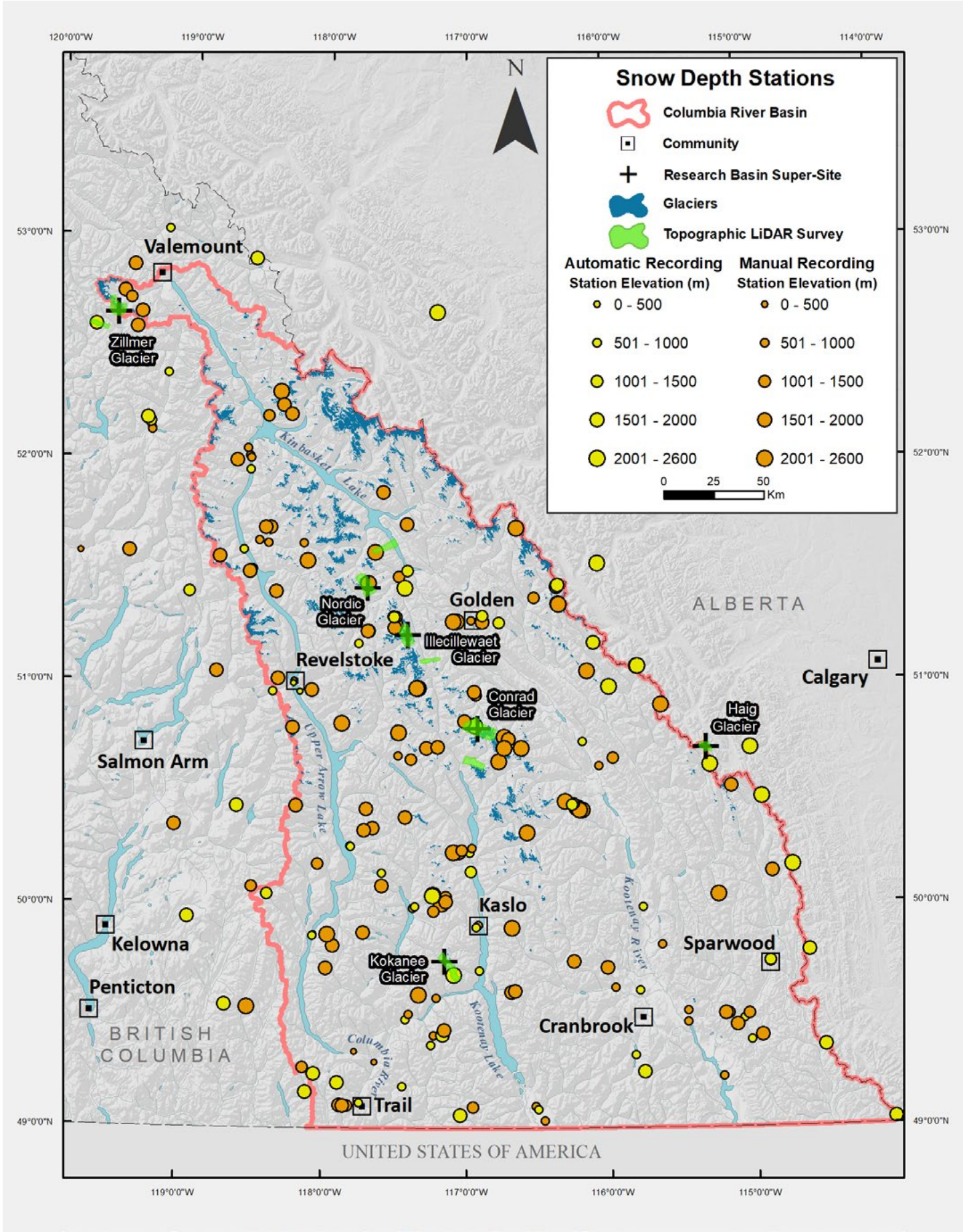

Figure 3.2 *Network of snow depth stations in and in the vicinity of the Canadian Columbia River Basin.*

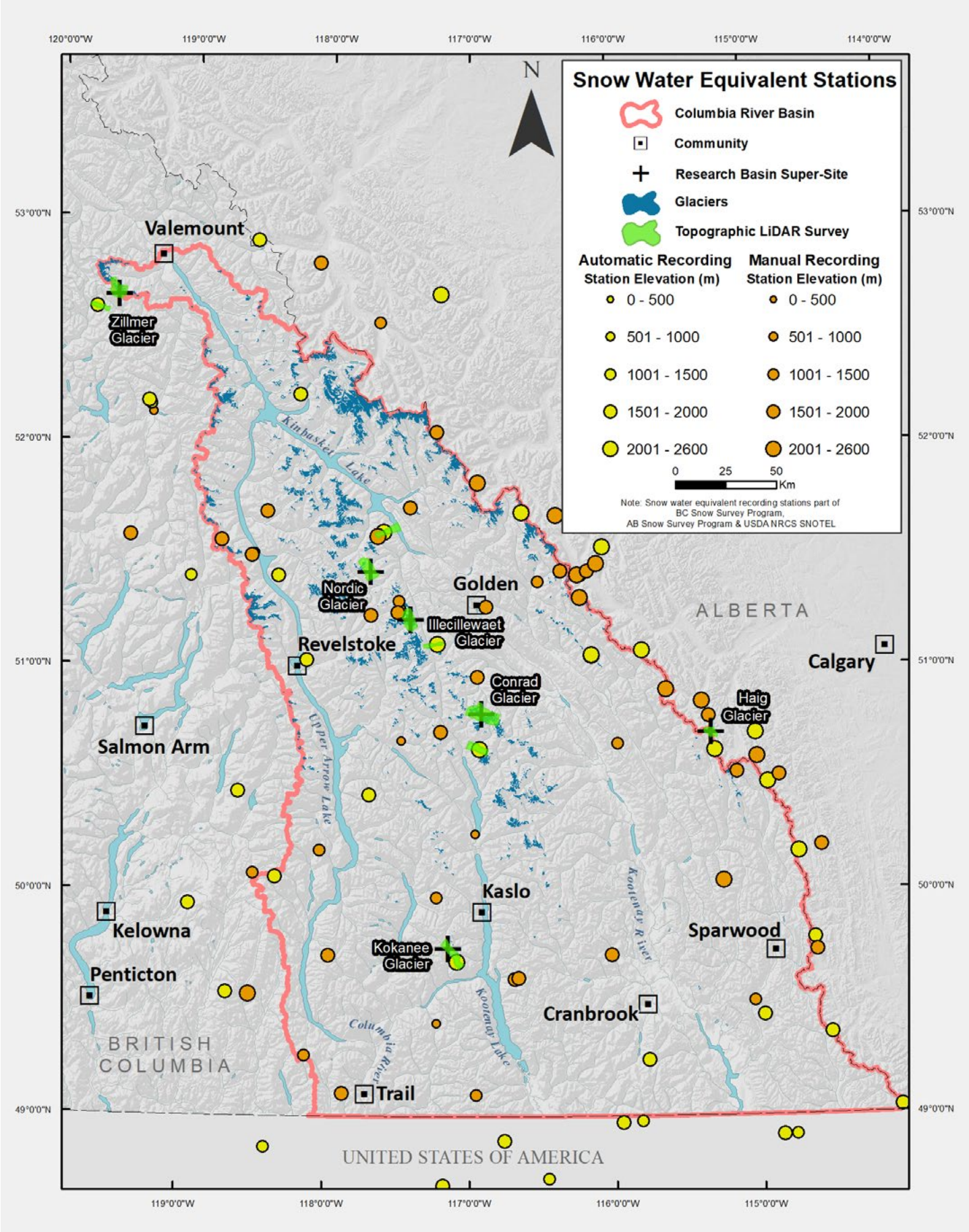

Figure 3.3 *Network of snow water equivalent stations in and in the vicinity of the Canadian Columbia River Basin*

3.2.3 US NRCS SNOTEL and Manual Snow Monitoring Program Network

Data collected at nine automated snow stations located just south of Canada-U.S. border can be likewise used to infer snow conditions in the Basin. The Snow Telemetry (SNOTEL) network is composed of automated data collection sites located in remote, high-elevation mountain watersheds in the western U.S. (https://www.wcc.nrcs.usda.gov/about/mon_automate.html). A standard sensor configuration includes a snow pillow, a storage precipitation gauge, and a temperature sensor. Similar to BC's Snow Survey Program, manual snow courses consist of five or ten sampling points. Unlike BC snow survey sites which can be located in dense forests, Natural Resources Conservation Service NRCS snow survey sites are typically situated in small open meadows protected from the wind.

3.2.4 Canadian Avalanche Association Industry Information Exchange database

The Canadian Avalanche Association (CAA) has been maintaining an Industry Information Exchange (InfoEx) database since 1991. InfoEx is used to share knowledge between subscribers about snow, weather, and avalanche conditions. Subscribers are organizations and commercial businesses employing CAA Professional Members and who actively manage avalanche hazards during the winter months (e.g., heli-skiing companies, BC Highways, ski areas, mountain parks). In the Basin there are approximately 70 subscribers who measure snow at 101 permanent locations. Snow at these locations is either manually measured (typically twice daily) or automatically recorded. Seventy-eight stations report long-term data records as defined by stations which were active at least for 50% of the last four years of the data analyzed (ie., 2014-17) and recorded data in 2017. Approximately 90% of the stations are at elevations below 2200 m asl.

The total depth of the snowpack (i.e., height of snow or HS) is a common variable measured at InfoEx contributing station operators. Total water equivalent of the snowpack is not measured. However, daily, half-daily (typically measured at 7:00 am and 4:00 pm) and/or storm snow water equivalent accumulations are obtained.

The observation period typically spans from early-October to mid-May, and the core observation period lasts from approximately the last week of December to mid-March. The record length of a third of the records is 12 years. Data entry of the manual observations into the InfoEx database occurs within 12 hours of the measurements.

3.2.5 Environment and Climate Change Canada surface weather and reference climate stations

Environment and Climate Change Canada (ECCC) operates a network of climate stations organized under the Surface Weather and Reference Climate Station networks (latter network is primarily intended for determining climate trends on regional and national scales) (https://climate.weather.gc.ca/). The stations are typically located near population centres and in valley bottoms. Select ECCC stations record snow depth. For automated snowfall observations, an ultrasonic snow depth sensor (Campbell Scientific SR50 and SR50A) is used. At manual observer stations snow depth data are taken once or twice daily using a snow ruler. According to a November 2017 inventory, ECCC operates 184 snow depth stations in BC.

3.2.6 BC Ministry of Transportation and Infrastructure, Road and Avalanche Weather Stations

Approximately 100 of the 135 automated road and avalanche weather stations operated by the BC Ministry of Transportation and Infrastructure (https://prdoas3.pub-apps.th.gov.bc.ca/saw-paws/weatherstation) are equipped with ultrasonic snow depth sensors (Campbell Scientific SR50 and SR50A). Twenty-seven stations are within or in close proximity to the Basin. Station locations range from valley bottom to mountain passes and higher elevations (at avalanche starting zones). Select stations collect and transmit hourly images of roads and the landscape, which can also be used to qualitatively infer snowline elevation.

3.2.7 Parks Canada

In Banff, Yoho, Kootenay, Glacier, Jasper and Little Yoho national parks, Parks Canada operates 23 automated, real-time reporting snow and/or climate stations (https://avalanche.pc.gc.ca/station-eng.aspx?d=TODAY&r=1). Some of these stations are equipped with snow depth sensors and record hourly snow depth data. These stations are not operated under BC Snow Survey Program.

3.2.8 UNBC LiDAR snow depth surveys

LiDAR (light detection and ranging) is a remote-sensing technique that is increasingly being used to obtain snow depth on watershed scales (Deems et al. 2013). Typically, LiDAR acquisitions are conducted using either airborne or ground-based instruments. Target positions are geolocated by coupling the LiDAR system with a high-precision GPS system. Differencing co-registered LiDAR maps from two dates, with one map being of the snow-free topography and the other of the snow surface, allows the calculation of snow depth with sub-decimeter vertical uncertainty and high horizontal spatial resolutions. Currently, LiDAR snow depth data are acquired over BC for research purposes only. Chapter 4 describes LiDAR surveys applied

to glaciers in the Basin. The University of Northern British Columbia (UNBC), funded by the Hakai Institute, BC Hydro and CBT, has been operating LiDAR equipment for the purpose of snow depth monitoring since 2014. As part of this project monitoring areas were chosen to be at and above treeline elevation and centred at the Zillmer, Nordic, Illecillewaet, Conrad, Haig and Kokanee glaciers. Snow data were acquired once per winter.

3.2.9 Other networks

Many local station networks collect short-term or long-term snow data but do not publicize their data. These include monitoring networks operated by municipalities, such as the North Kootenay Lake Water Monitoring Project, university research networks, such as UNBC Environmental Science and Engineering Program's Cariboo Alpine Mesonet and UBC glaciology, and the private industry, such as Independent Power Producers.

3.2.10 Monitoring network gap analysis

3.2.10.1 Review of the snowpack monitoring network in the Basin

Snow station density varies across the Basin; it is low in the northern tip and the south-eastern part of the Basin (Figure 3.1). The majority of the snow monitoring stations in the Basin are located at valley bottom and at an elevation of approximately 2000 m asl (Figure 3.4a). Installations of new stations should occur at elevations where station densities are low, which is – as can be gleaned from Figure 4 a, b and c – at around 1400 m and above 2300 m in the Basin. Installations of new monitoring stations should also focus on the two underrepresented regions of the Basin.

Valley bottom snow data are primarily collected by the BC Ministry of Transportation, ECCC MSC and BC Snow Survey Program stations (Figure 3.4 a). High elevation snow monitoring is conducted primarily by the BC and Alberta Snow Survey programs and the CAA InfoEx contributors. Without the CAA InfoEx network, the density of high elevation snow monitoring is greatly reduced (Figure 3.4b).

There are about twice as many manual stations as automated ones in the Basin (Figure 3.4a and 3.4c). This number is further reduced for automated snow water equivalent recording stations (Figure 3.4d). The number of automated snow water equivalent recording stations is low at valley bottom, increases up to an elevation of 2000 m and drops rapidly above that.

3.2.10.2 InfoEx snow data

CAA InfoEx monitoring stations complement other monitoring networks particularly at higher elevations and in the alpine and hence data could be useful for many applications. Two InfoEx stations, CMH Bobbie Burns' Rocky station and the Sorcerer Lodge Study Plot, were within the areas where snow depth is measured with LiDAR.

The relatively quick dissemination of the data – they are typically submitted within 12 hours to the database – makes the data attractive for operational water resource management applications. If an agreement with the CAA could be reached, public data access would have to be established.

3.2.10.3 In situ snow monitoring of alpine areas

The majority of snow and precipitation monitoring is limited to elevations at or below tree line. The primary reason for this upper elevation limit of the provincial snow monitoring network is the fact that snowpack in the alpine is affected by redistribution through wind. However, despite wind redistribution of snow, data from in situ alpine monitoring stations are expected to be a useful indicator of alpine snowpack. Seasonal snowpack development can be gleaned from the data despite wind caused, high-frequency snow depth variability (periods shorter than a few days).

To evaluate the representativeness of automated in situ snow data collection in the alpine and to collect data with which LiDAR snow depth data can be verified and to support glacier mass balance modelling, BC Hydro / Northwest Hydraulic Consultants installed an automated snow station in the Conrad Creek watershed.

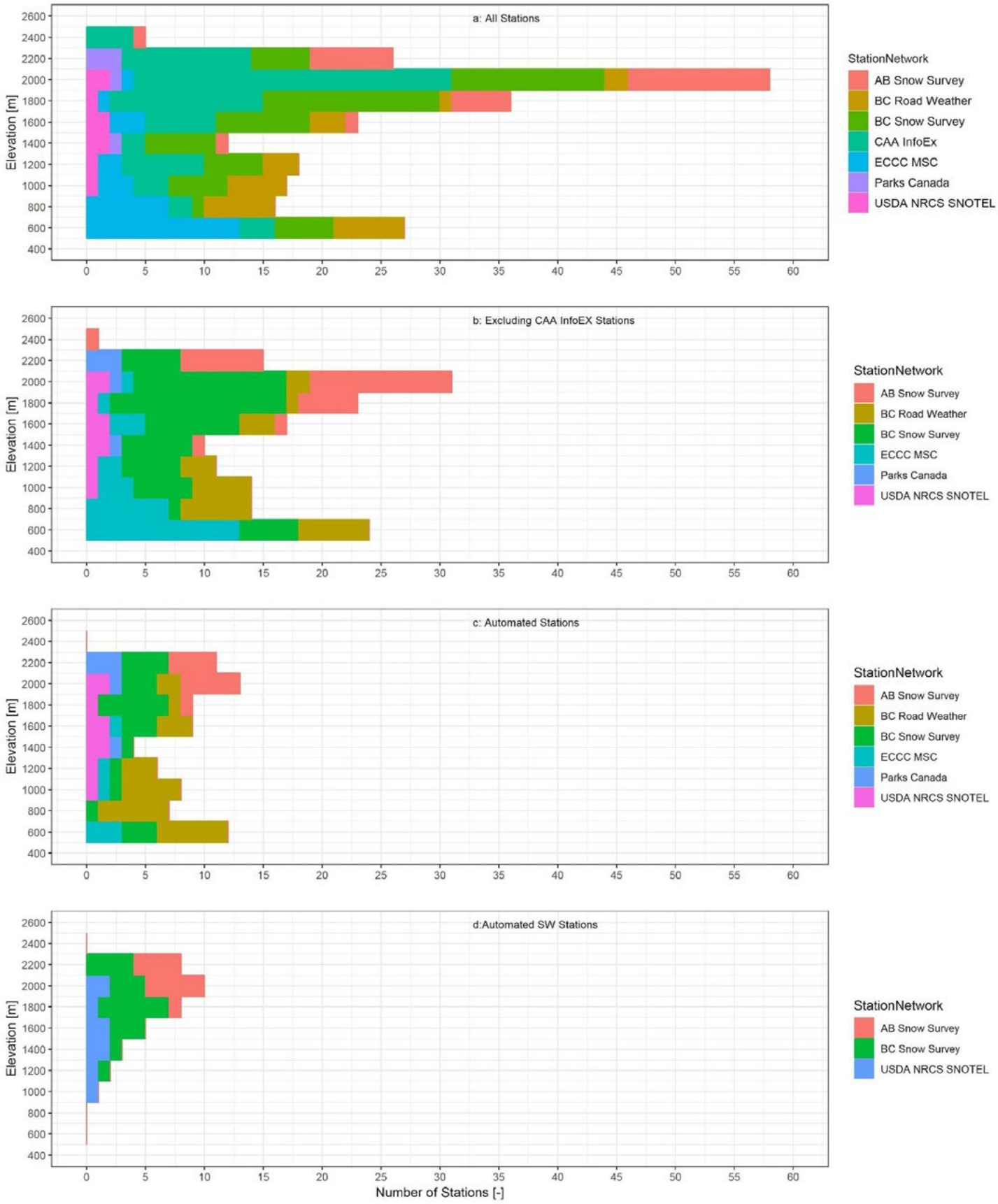

Figure 3.4 *Vertical distribution of snow stations in and in the vicinity of the Canadian Columbia River basin. A: all stations; B: all stations excluding CAA InfoEx stations; C: automated stations; D: automated snow water equivalent recording stations.*

The Conrad snow monitoring site selected for the installation is located on top of the ridge leading to the nunatuk in the centre of Conrad Glacier. It was selected due to the exposure of rock in the summer on which the instrumentation tower can be installed, avalanche safety and its high elevation. With an elevation of 2599 m asl, the Conrad Glacier station is the highest snow station operated in the BC Snow Survey Program.

The 3.5 m high instrumentation tower was installed in autumn, 2018. The station is currently equipped with an anemometer, and snow depth, air temperature and relative humidity sensors. A net radiation sensor is being tested and is scheduled to be added during autumn, 2019. The station is solar powered and data are transmitted in real-time via the Geostationary Operational Environmental Satellite (GOES).

3.3 Methods

3.3.1 Total depth of the snowpack

Depth of the snowpack is manually measured by: CAA InfoEX contributors using a permanently installed stake (Figures 3.7-3.8); volunteer ECCC observers with a ruler (Figure 3.8-3.9); or via technicians using a Federal Snow Sampler in the BC Snow Survey Program (Figure 3.9-3.10).

Automated sensors used in BC networks include Campbell Scientific's SR50 and SR50A (Figure 3.11-3.12), which are used by ECCC, BC TRAN and BC ENV, and Sommer's USH-8 and USH-9 ultrasonic sensors (Figure 3.12-3.13), which are used by BC Hydro. Ultrasonic technology relies on measurements of the travel time of sound pulses from the sensor to the ground/snow surface and back to the sensor to obtain snow depth.

The details of how a measurement is calculated vary by sensor and operator and range from SDI-12 sensor-specific averaging protocols to post-processing of samples in the datalogger to single samples.

In the Basin, data of total depth of snow are collected by the BC Snow Survey Program, standard as part of the manual snow survey network and at select automated snow weather stations, the BC Road Weather Station Network, ECCC's Cooperative Climate Network of manual observers as well as at selected ECCC automated stations, and the CAA's InfoEx network. Currently, 214 stations measure total snow depth; snow depth is continuously recorded at about one third (67) of those stations.

The Riegl VQ-780 instrument and the surveying aircraft are shown in Figure 3.16 and Figure 3.17. The methodology for calculating snow depth from LiDAR data is provided in Chapter 4 of this report. LiDAR snow depth monitoring was focused on Zillmer, Nordic, Illecillewaet, Haig, Conrad and Kokanee glaciers (Figure 1) and on alpine and subalpine terrain adjacent to these ice masses.

Figure 3.5 *Conrad Glacier station.*

Figure 3.6 *Conrad Glacier.*

3.3.2 Total snow water equivalent

Manual measurements of snow water equivalent of the snowpack at BC Snow Survey Program stations are obtained with the Federal Snow Sampler (Figure 3.9-3.10 and Figure 3.10-3.11). Federal Snow Samplers consist of an aluminum snow tube and a spring scale. At predetermined sampling stations, the tube is pushed through the snowpack to the ground, a core extracted, weighed and converted to mm water equivalent.

Automated systems to measure snow water equivalent in BC have relied primarily on snow pillows in open hydraulic systems and with shaft encoders (Figure 3.13-3.14). Those snow pillow systems are based on measurements of the displacement of the pillow fluid by the overlying weight of the snowpack into a vertical pipe (ie., manometer). Snow pillows that are equipped with submersible pressure transducers rather than shaft encoders (Figure 3.14-3.15) are in use in other jurisdictions such as Norway, New Zealand and the U.S., and are being tested by BC Hydro and the BC Ministry of Environment.

Unlike in Alberta's Snow Program, snow pillow snow water equivalent data in BC have historically not been corrected for the pillow fluid's density. In BC the conversion of the measured changes in manometer fluid level to mm snow water equivalent assume the fluid has the weight of water. However, the pillow fluid is a mixture of antifreeze and water (typically propylene glycol and water), which is denser and heavier than pure water. Since the density of the fluid column, which counter balances the weight of the snowpack on top of the fluid bladder, is greater than that of water, current snow pillow snow water equivalent data in BC underestimates snow water equivalent by about 5%.

Since 2012 Sommer Snow Scales (Figure 3.15) have been in use at selected station in the BC Snow Survey Program with variable success. Snow scales measure the weight of the overlying snowpack with load cells.

In the Basin, there are 97 active snow water equivalent data collecting stations, of which 57 are manual and 40 are automated, real-time reporting stations.

3.3.3 Average density of the total snowpack

The average density of the total snowpack above ground is obtained from manual snow surveys using the Federal Snow Sampler and from select automated snow stations equipped with collocated snow depth and water equivalent sensors. Currently only BC Ministry of Environment-operated snow stations are by default equipped with both snow water equivalent and depth instrumentation. BC Hydro-operated snow stations in north-eastern BC are equipped with both sensors, but currently not in the Basin.

Figure 3.7 *Snow stake.*

Figure 3.8 *Snow ruler.*

Figure 3.9 *Federal Snow Sampler (photo: Northwest Hydraulics Consultants).*

Figure 3.10 *Federal Snow Sampler.*

Figure 3.11 *Automated snow and climate station with Campbell Scientific SR50A snow depth sensor.*

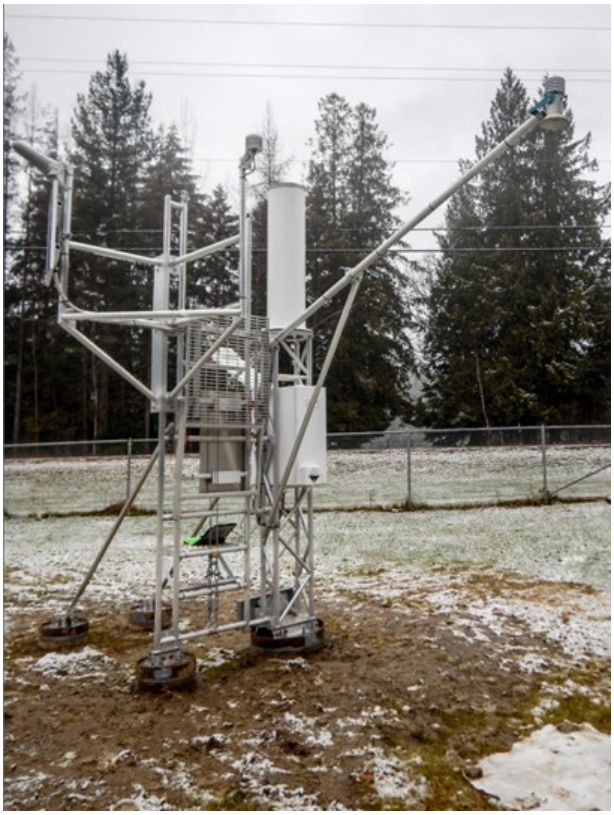

Figure 3.12 *Automated snow and climate station with Sommer GmbH USH-8 snow depth sensor.*

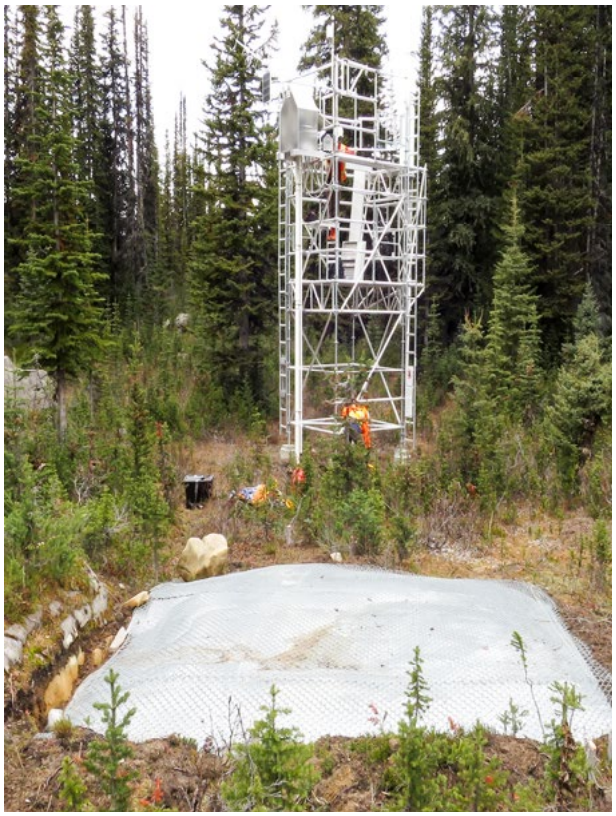

Figure 3.13 *Custom-built snow pillow with open hydraulic system and shaft encoder.*

Figure 3.14 *Custom-built snow pillow with open hydraulic system and submersible pressure transducer.*

Figure 3.15 *Sommer GmbH SSG1 snow scale.*

Figure 3.16 *Lidar sensor (on the left) mounted at the floor of the aircraft.*

Figure 3.17 *Aircraft used for LiDAR data acquisition.*

3.4 Results and discussion

3.4.1 Characterization of the 2015-2019 snowpack

With the exception of historical ECCC data and to some extent manual snow survey data, snow data available through the public data portals are not quality-controlled. The relatively poor quality of snow water equivalent data from automated BC Snow Survey Program stations limits their data use substantially. Table 3.1 summarizes the BC Snow Survey Program stations located near this project's monitoring areas.

Table 3.1 *In situ snow monitoring station near LiDAR monitoring areas.*

Station Name	Station ID	Station Type	Latitude	Longitude	Elevation [m]	Nearby LiDAR monitoring area
Azure River	1E08P	Auto	52.596	-119.724	1620	Zilllmer Glacier
Colpitti Creek	2A30P	Auto	51.608	-117.611	2131	Nordic Glacier
Sunbeam Lake	2A22	Manual	51.590	-117.653	2065	Nordic Glacier
Wildcat Creek	2A32P	Auto	51.696	-116.629	2122	Yoho-Peyto Glaciers
Mount Abbot	2A14	Manual	51.251	-117.509	1980	Illecillewaet Glacier
Glacier	2A02	Manual	51.263	-117.491	1250	Illecillewaet Glacier
Caribou Creek Upper	2A31P	Auto	51.109	-117.228	2201	Illecillewaet-Conrad Glaciers
Vermont Creek	2A19	Manual	50.963	-116.943	1538	Conrad Glacier
Mount Templeman	2D09	Manual	50.716	-117.202	1875	Conrad Glacier
East Creek	2D08P	Auto	50.640	-116.930	2030	Conrad Glacier
Redfish Creek	2D14P	Auto	49.690	-117.086	2106	Kokanee Glacier

Examples of continuous snow water equivalent data recorded in the vicinity of this project's monitoring areas and during the period 2015-2019 provide some information about the year-to-year variation in the magnitude and timing of snow accumulation and melt (Figure 3.18-3.19). Overall, 2015, 2016 and 2019 were low snowpack years in the Basin; 2017 and 2018 were relatively high snowpack years. In 2016 snowmelt started early.

Of the stations analyzed, the Redfish Creek station adjacent to Kokanee Glacier recorded the deepest snowpack. The second deepest snowpack was recorded in the north-western corner of the Basin in the Azure River – Zillmer Glacier area. Snowpack in the Nordic-Conrad glacier areas in the central Columbia Mountains as measured by the Colpitti Creek, Caribou Creek Upper and East Creek stations is similar and generally slightly lower than the Azure River snowpack. The Wildcat Creek station on the western slopes of the Rocky Mountains recorded the thinnest snowpack.

At the Conrad Glacier station, maximum snow depth (2.51 m) for water year 2019 occurred on May 2, 2019 (Figure 3.19). Snow depth data show periods of accumulation, followed by gradual snow densification and decreasing snow depth, as well as sudden changes as a result of snow redistribution by wind. While it is more difficult to detect wind-related deposition of snow during snowfall events, several sharp drops as a result of wind scouring can be observed. Examples include events during December 5, 2018, December 28-29, 2018 and March 7-9, 2019. Maximum wind gust of 125 km h^{-1} were measured on December 20, 2018.

3.4.2 LiDAR-based snow gradients

Due to the lack of in situ observations of the alpine snowpack it is currently challenging to accurately estimate and model seasonal catchment water supply. Specifically, data of vertical snowpack gradients are one important piece of information for developing well calibrated hydrologic models and for forecasting seasonal water supply.

On unglaciated terrain LiDAR technology provides spatially highly-resolved snow depth data. Over ice-covered terrain, glacier dynamics (horizontal and vertical ice velocity) preclude the analysis of snow depth versus elevation. When integrated over the entire glacier surface, the effects of ice dynamics cancel out so that reliable estimates of snow depth for a given glacier are possible.

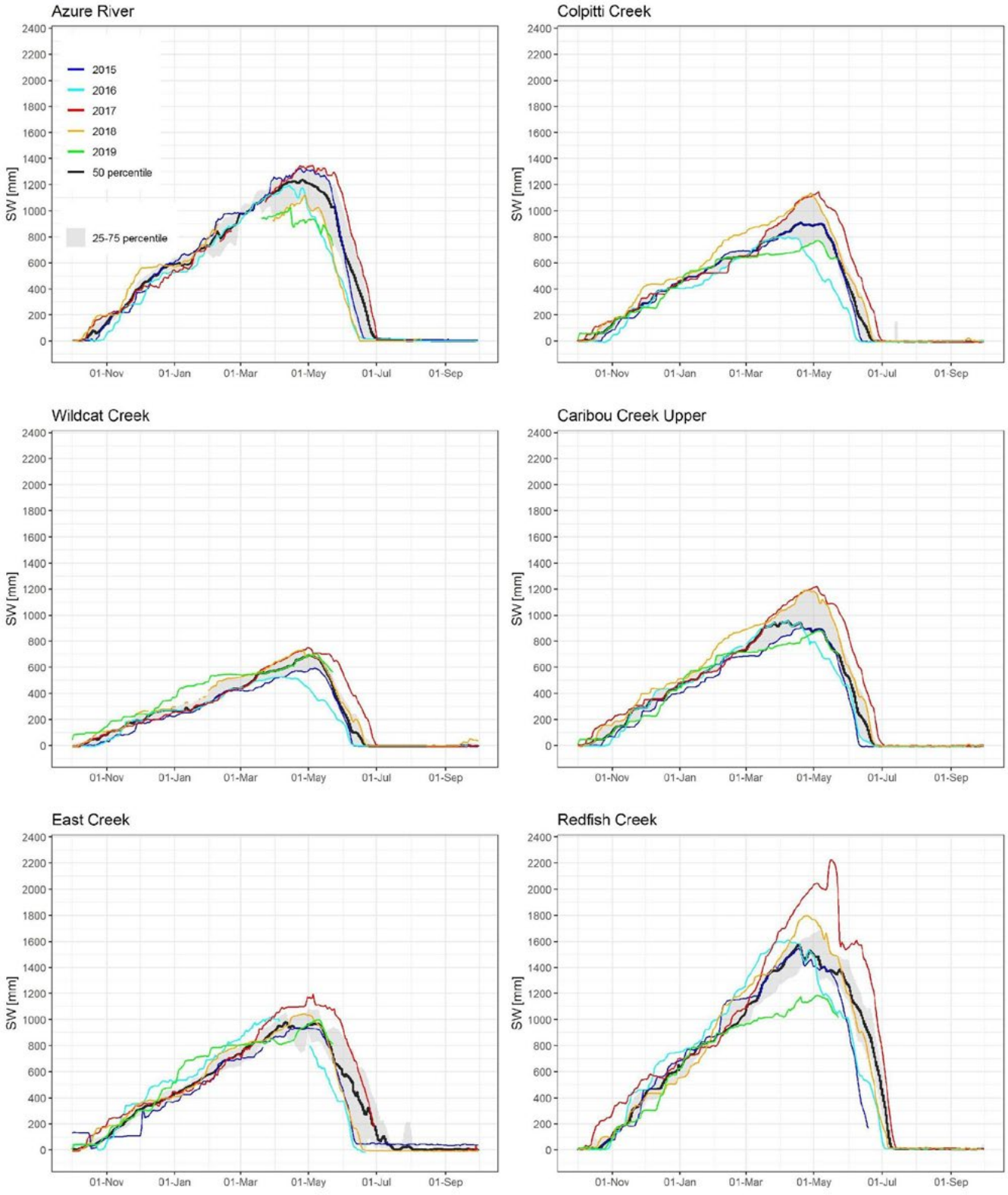

Figure 3.18 *Snowpack evolution near project supersites during the 2015-2019 project period and as measured by automated BC Snow Survey Program stations.*

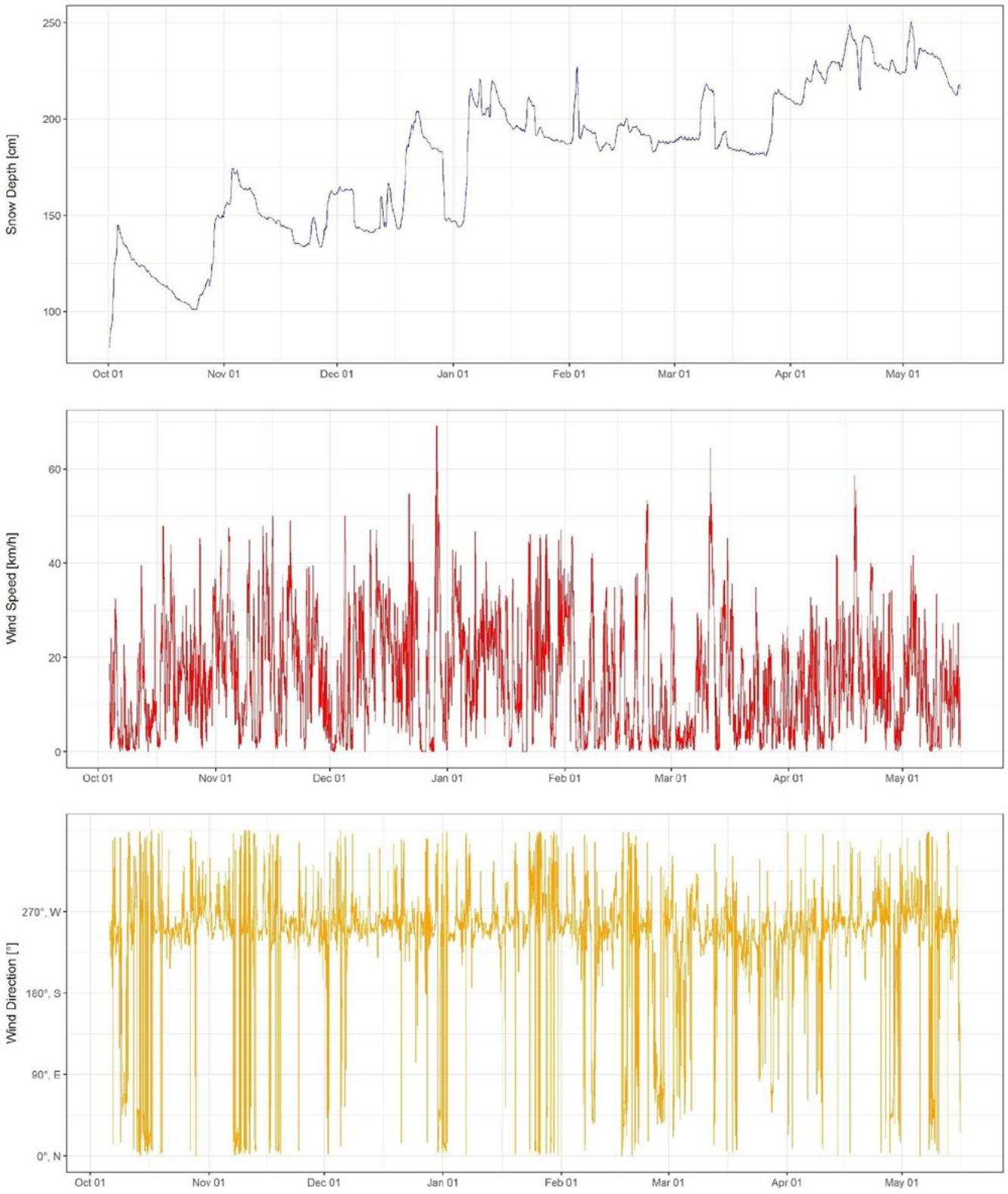

Figure 3.19 *Winter 2018-2019 Conrad Glacier snow depth and wind data. Examples of wind scouring reducing snow depth include events during December 5, 2018, December 28-29, 2018 and March 7-9, 2019. Maximum wind gust of 125 km h-1 were measured on December 20, 2018.*

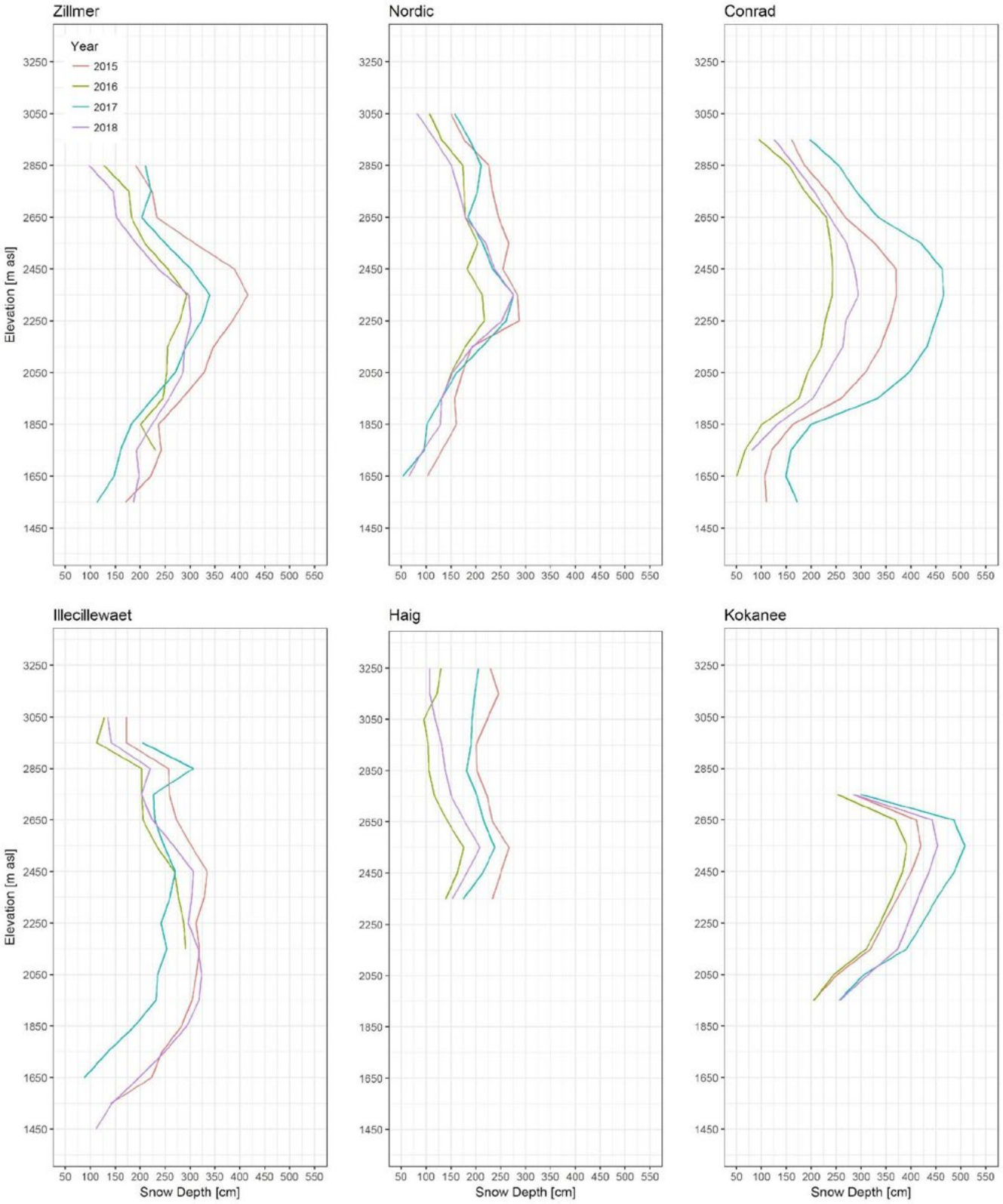

Figure 3.20 *Vertical LiDAR off-ice snow depth distribution in the six LiDAR monitoring areas binned at 100 m intervals. The surveys were conducted once per year during the time of maximum snow depth.*

While snow depth varies from year-to-year, a distinct elevation of maximum snow depth was found in most monitoring areas (Figure 3.20). The elevation of maximum snow depth ranges from 2250 – 2350 m asl in the northern monitoring areas to 2550 m in the south-eastern and southern monitoring area. Year-to-year variability of maximum snow depth elevation in the Illecillewaet Glacier area was higher and ranged from 2050 – 2450 m asl.

In some monitoring areas or in some years only secondary snow depth maxima were recorded at the lowest or highest elevations. For example, the data show an increase in snow depth at Conrad below 1600 m asl. Field observations suggest that the increase in snow depth at Conrad below 1600 m asl is likely due to avalanches that contribute to snow accumulation at this elevation band. The effect of avalanches on snow depth is amplified by the fact that the footprint of this elevation band is small and a small number of avalanche deposits at valley bottom have a significant effect on snow depth.

Snow depth gradients for each monitoring area (Equation 1) were calculated for elevations below and above the maximum snow depth. The gradients were calculated from LiDAR data according to:

$$[3.1] \qquad gradient_{snow} = \frac{(d_{max} - d_{min})}{(z_{snowmax} \; z_{snowmin})}$$

Where d_{max}, d_{min} respectively denote maximum and minimum snow depths and $z_{snowmax}$, $z_{snowmin}$ refer to the maximum and minimum elevations over which snow is observed. These data were averaged over the four years in which surveys were conducted (Table 3.2).

LiDAR gradients of increasing snow depth are similar in the six monitoring areas and average to about 30 cm per 100 m elevation. The decreasing gradients above the elevation of maximum snow depth vary substantially between the monitoring areas. They range from -16 cm to -82 cm per 100 m elevation.

Gradients derived from in situ measurements differ from LiDAR gradients and are steeper at elevations below the elevation of the maximum snow depth and shallower at elevations above the maximum snow depth. They differ by 17% and 64%, respectively, for areas below and above the maximum snow depth elevation. The differences may stem from different accumulation and ablation patterns over glaciated and non-glaciated terrain, limited representativeness of in situ measurements and/or data acquisition errors.

Table 3.2 *Snow depth gradients averaged over four years and representative of the time of maximum snowpack for elevations below and above the maximum snow depth estimated from off-glacier LiDAR data and on-glacier in situ measurements.*

Monitoring areas	Gradients for elevations below the elevation of maximum snow depth Off-glacier LiDAR	Gradients for elevations below the elevation of maximum snow depth On-glacier in situ	Gradients for elevations above the elevation of maximum snow depth Off-glacier LiDAR	Gradients for elevations above the elevation of maximum snow depth On-glacier in situ
	[cm / 100 m elevation]	[cm / 100 m elevation]	[cm / 100 m elevation]	[cm / 100 m elevation]
Zillmer	29	43	-38	-31
Nordic	30	23	-19	-3
Illecillewaet	29	46	-25	no data
Conrad	36	36	-32	-16
Haig	23	no data	-16	no data
Kokanee	35	31	-82	-23
Average	30	36	-35	-18
Standard deviation	5	9	24	12

Vertical snow gradients are the result of the interaction of processes controlling orographic precipitation and the redistribution of snow (Grünewald et al. 2014). The hypothesis is that for larger scales and with sufficient moisture supply, precipitation increases with elevation because condensation increases as a result of decreasing air temperatures, specifically on the windward side of mountain ranges. However, limited moisture supply can lead to decreasing precipitation below the highest elevations (Sevruk 2004). On the lee side rain shadow effects or local winds can cause deviations from the general pattern. Differences between precipitation gradients and snowpack gradients are attributed to the erosion of snow at higher elevations and deposition of snow at sheltered locations, avalanches, sloughing, snow creep, snowmelt and sublimation (Grünewald et al. 2014).

3.4.3 Comparison of in situ and LiDAR snow depth

LiDAR-derived snow depth was compared with in situ data of snow depth data collected by the BC Snow Survey and the CAA InfoEx programs. The 1 m resolution LiDAR snow depth data were averaged over an approximately 100 m^2 area (ie., 100 data points) centered on the location of an in situ station to account for the uncertainty in the in situ snow depth monitoring location and the geo-referencing of the LiDAR data. In some cases averaging areas of less than 100 m^2 were used to minimize the influence of large vegetation.

The in situ snow depth data used to ground truth, or verify, LiDAR data include the BC Snow Survey Program Azure River (1E08P) and Redfish Creek (2D14P) stations and the CAA InfoEX Sorcerer Lodge Study Plot for the 2015 to 2018 period. Figure 3.21 (a) shows the comparisons of LiDAR-based and in situ snow depth data. For a perfect agreement between LiDAR-based and in situ data, data points would have to lie on the 1-to-1 line (red lines of Figures 3.21 (a) and (b)). Figure 3.21 (a) shows that, with the exception of the Redfish Creek data point, LiDAR data underestimate snow depth. Based on the small sample of 6 data pairs, the average LiDAR bias is -28 cm, i.e., LiDAR underestimates snow depth on average by 12%.

The underestimation of snow depth by LiDAR data is consistent with other studies. Broxton et al. (2019) attributed the underestimation to low and dense vegetation that is misclassified as ground when the signal cloud density is too low. In comparison, manual in situ snow measurements, used to verify LiDAR data, penetrate to the ground. This shows that it is important that LiDAR snow depth is based on the bare earth signal return as opposed to the non-base earth signal returns. Lower flight altitudes which result in denser point clouds and/or bias correction of LiDAR data with in situ data would improve LiDAR snow depth estimates in areas near and below treeline.

Some of the differences might stem from inaccuracies in the in situ station geolocations as the data are typically obtained from handheld GPS units with low accuracies of about 3-10 m. Further, the geographic location provided by field staff is thought to be most representative for the instrumentation tower that supports the precipitation gauge and/or snow pillow standpipe and data logger and not the snow depth and snow water equivalent monitoring site, which can be up to 50 m away.

Differencing of temporal sequences of snow surface data with snow free-ground surface data requires that all datasets are perfectly georeferenced. However, winter data are difficult to co-register with snow free data, because potential reference points disappear under the snow.

Data differences could theoretically arise from different observation dates, particularly if manually collected data are used. For this reason paired observations with different observation dates were removed from analysis. Since LiDAR flights occurred on days without cloud cover and therefore precipitation, different acquisition times of day are assumed to be negligible.

Meaningful verification of spatial data with in situ point data is labour intensive. This study relied on snow depth data collected by existing monitoring networks and the number of samples was low. Future work should aim at both increasing the spatial distribution of in situ point observations at individual monitoring sites (eg., by monitoring of a fine scale grid) and increasing sampling locations. It is essential that the location of the sampling locations is highly accurate.

LiDAR monitoring for this project was optimized for glacier areas and not for the swaths flown over treed areas. Data accuracies for forested areas can be improved and data gaps reduced by increasing the number of swaths and lower flight altitudes (if possible). Also, wet snow surfaces can absorb the light pulses emitted by the LiDAR and reduce the strength of the reflected signal which in turn can lead to a loss of data.

Throughout the course of the project the LiDAR system was upgraded from the Riegl VQ580 to the Riegl VQ780. The new sensor is stronger and the data cloud denser thereby minimizing the likelihood of unsurveyed areas.

3.4.4 Comparison of in situ and LiDAR snow water equivalent

To compare in situ snow water equivalent data with LiDAR-based snow water equivalent estimates, LiDAR snow depth was converted to snow water equivalent with snow densities observed at nearby BC Snow Survey Program stations. The estimated snow densities are shown in Table 3.3. In situ snow water equivalent data analyzed include the BC Snow Survey Program Colpitti Creek (2A30P), East Creek (2D08P), Caribou Creek Upper (2A31P) and Redfish Creek (2D14P) stations for the 2017 to 2018 period.

LiDAR-based snow water equivalent estimates generally overestimate snow and are positively biased by 14% (Figure 3.21). The mean absolute error is 14%. The maximum error is 33%. The disagreement decreases when the negative bias of approximately 5% of snow pillow based snow water equivalent data in BC is accounted for.

The data clearly show that uncertainties in the snow densities used to convert snow depth to snow water equivalent greatly affect snow water equivalent estimates and better methods for modelling snow densities need to be applied.

Table 3.3 *Snow density estimates used to convert LiDAR snow depth to snow water equivalent.*

Snow monitoring station	In situ data measurement date	Measured snow density [kg m^{-3}]	Comments	LiDAR data acquisition date	Snow density used to convert LiDAR data [kg m^{-3}]
Sunbeam Lake (2A22)	April 29, 2017	390		May 21, 2017	400
Mt. Templeman (2D09)	April 28, 2017	400			400
Redfish Creek (2D14P)	May 1, 2017	540	Last plausible value that season		540
Sunbeam Lake (2A22)	April 26, 2018	400		April 26, 2018	400
Mt. Templeman (2D09)	Not measured	380	Estimate based on Sunbeam Lake trend		380

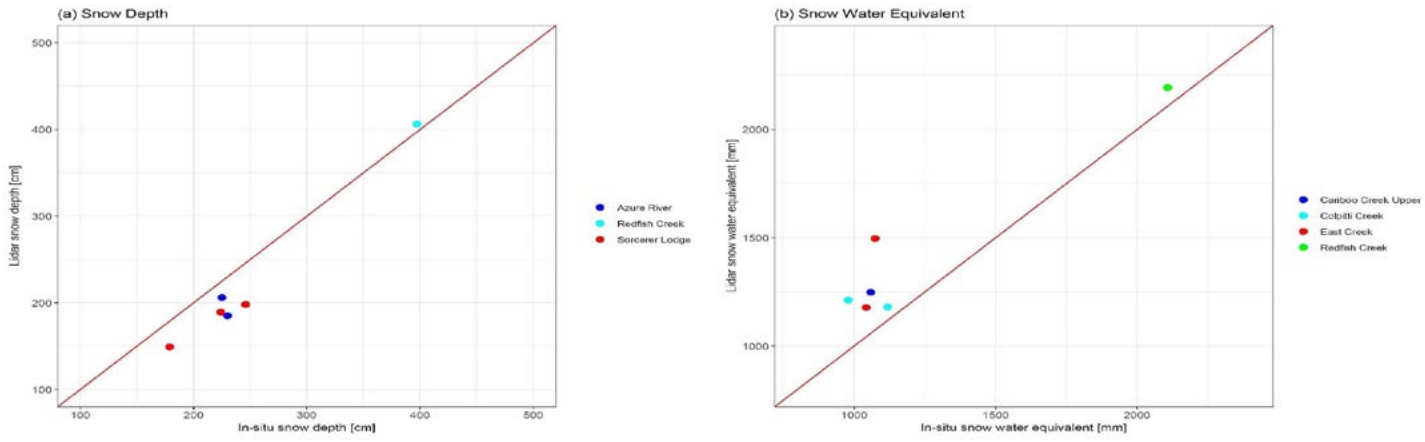

Figure 3.21 *Comparison of LiDAR and in situ measurements of (a) snow depth and (b) snow water equivalent with the 1-to-1 line shown in red.*

3.5 Summary

This chapter provides an overview of snowpack monitoring in BC with focus on the Canadian portion of the Columbia River Basin (the Basin). Snowpack data are collected by several agencies and organizations. Not all data become publicly available and few datasets are quality-controlled.

The authors counted a total of 245 snow monitoring stations in and in the vicinity of the Basin, 214 and 97 of which measure snow depth and snow water equivalent, respectively.

The spatial distribution of stations suggests that the installation of new monitoring stations should focus on the northern tip and the south-eastern part of the Basin. Also, snow monitoring in the Basin is concentrated at valley bottom and at treeline. The vertical distribution of the monitoring network could be improved by adding stations at elevations between 1200 and 1600 m and above 2200 m.

If made publicly available, CAA InfoEx snow data have the potential to significantly complement existing public monitoring networks. For example, the near real-time availability of the data makes the data attractive for operational water resource management applications.

Automated snow water equivalent systems are expensive and fickle to operate. To maximize seasonal data collection, automated snow water equivalent–recording stations are concentrated at treeline. We, recommend improvement of snow water equivalent monitoring at lower elevations. Further, the quality of raw snow water equivalent data from automated BC Snow Survey Program stations is poor. The availability of a provincial quality-controlled dataset would significantly improve data analysis efforts.

Automated monitoring and real-time reporting of snowpack data are preferable over manual snow data collection. For operational decision-making, such as required for avalanche hazard forecasting, snow removal, flood forecasting and water supply forecasting, timeliness of the information greatly improves decision-making quality. Further, to compare data sets, such as comparisons of sporadic LiDAR data with in situ station data, coinciding continuous records are critical.

In situ snow density data are fundamental for developing snow density models. We therefore recommended that all BC Snow Survey Program stations are upgraded to collected co-located snow depth and snow water equivalent data, from which density can be calculated.

While snow depth varies from year-to-year, a distinct elevation of maximum snow depth was found in almost all cases followed by a decrease in snow depth to the highest elevations. The elevation of maximum snow depth ranges from 2250 – 2350 m in the northern monitoring areas to 2550 m in the south-eastern

and southern monitoring area. More broadly, vertical snow gradients are the result of the interaction of processes controlling orographic precipitation and the redistribution of snow. No analysis was conducted to quantify the relative contributions of each process.

On average LiDAR data underestimate snow depth by approximately 30 cm or 12%, possibly caused by low lying and dense vegetation which was misclassified as snow free ground and inaccurate geolocation of in situ data.

LiDAR-based snow water equivalent estimates on average overestimate snow by 14%. The conversions from snow depth to water equivalent were based on sparse snow density observations. Snow water equivalent estimates calculated from snow depth data would greatly benefit from temporally and spatially higher resolution snow density data, specifically outside of the January to May manual snow survey period.

CHAPTER 4: GLACIER CHANGE

Authors: Ben Pelto and Brian Menounos

4.1 Introduction

Glacier mass balance is a function of accumulation and ablation processes, responding directly to meteorological forcing (Oerlemans et al. 1998). Mass balance observations provide glacier mass change, which can be used to calculate glacier runoff (Jost et al. 2012; Ragettli et al. 2016; Stahl and Moore 2006), contributions of glacier mass loss to sea level rise (Huss and Hock 2015), and improve projections of glacier response to climate change (Clarke et al. 2015). Since annual mass balance is the sum of mass gain and loss for a given year, seasonal balance measurements can provide insight into meteorological conditions responsible for glacier nourishment and melt.

Seasonal balance programs are logistically and financially difficult, which likely explains why there are few existing records at the global scale (Cogley et al. 2011); western Canada currently reports no seasonal balance observations to the global community (WGMS 2018). Seasonal snowpack forms a critical component of glacier mass balance (Machguth et al. 2006). Knowledge of the high elevation snowpack and its change through time is limited or non-existent for most alpine regions (Barnett et al. 2005; Hamlet et al. 2005), including within the Canadian Columbia River Basin (Brahney et al. 2017b). A better understanding of the alpine snowpack and meteorological conditions that control its extent and amount would help to assess its fate under future climate.

Geodetic methods, which utilize measurements of the Earth's surface, offer the ability to greatly expand the number of glaciers over which these measurements can occur (Berthier et al. 2014; Nolan et al. 2015). Geodetic mass balance studies have been predominantly multi-annual studies. Recently, geodetic techniques are being used to measure seasonal snow depth on glaciers (Sold et al. 2014; McGrath et al. 2015; Machguth et al. 2006; Helfricht et al. 2014a; Dadic et al. 2010), to measure annual mass balance (Klug et al. 2018), and to estimate seasonal mass balance (Belart et al. 2017; Sold et al. 2013). However, no prior study estimated seasonal mass change over a series of glaciers, for multiple years. As part of this project (Pelto et al. 2019) evaluated the reliability of using geodetic surveys to estimate seasonal mass change for several alpine glaciers across a series of mountain ranges, over multiple years.

In this chapter, we quantify the current rate of mass change for glaciers in the Basin and describe the seasonal mass balance of these glaciers. We also evaluate the reliability of airborne LiDAR to produce glacier mass balance estimates.

4.1.1 Previous work

Glacier research within the Columbia Mountains to-date has been limited (DeBeer et al. 2016).

Tennant and Menounos (2013) examined the volume and area loss of the Columbia Icefield over most of the twentieth century. The area of the icefield shrank by 23% over the period 1919-2009, and glaciers thinned by nearly -50 m w.e. on average (Tennant and Menounos 2013). However, only 3 of the 25 glaciers of the Columbia Icefield contribute meltwater to the Basin.

Jost et al., (2012) found that while glaciers in the Mica Basin (NE Columbia Basin) only cover 5% of the watershed, glacier ice melt contributes up to 25 and 35% of streamflow in August and September, respectively. Contribution of glacier melt to mean annual runoff from the Mica varied between 3 and 9% and averaged 6%.

Between the 1951-1965 and 2001-2002, the area of glaciers in the Columbia and Rocky mountains decreased by 5 and 15% respectively (Debeer and Sharp 2007), with largest glaciers losing most area. From 1985 to 2005 glaciers in the Columbia Mountains and southern Rocky Mountains experienced a similar rate of area loss -15.2 and -14.8%, respectively (Bolch et al. 2010). While area loss is a valuable measure of glacier change, glaciers respond differently to climate change based upon their morphometry, hypsometry, and balance gradient (Schiefer et al. 2008). Many glaciers are thinning with little retreat or area change (Paul et al. 2004). Area change is a valuable metric, but caution is required when making inferences about glacier mass change from changes in area (Arendt et al. 2002).

4.1.2 Glacier monitoring

The glacier mass balance monitoring program measured the seasonal mass balance of six primary supersite glaciers (Table 2.1) that lie within the headwaters of the Columbia River Basin (Figure 4.1). Between 2014 and 2018, these glaciers were visited twice annually for field-based glaciological measurements. In concert with the field-based measurements, bi-annual airborne light detection and ranging LiDAR surveys were conducted to measure height change (a geodetic measurement) over the supersite glaciers, as well as additional 74 glaciers proximal to each supersite. In measuring these additional glaciers remotely, we were able to increase our sample size to 6% of the glacier area in the Basin, better enabling confidence in the observations to be applicable across the Basin. In total, our LiDAR surveys captured 80 glaciers covering 101 km^2.

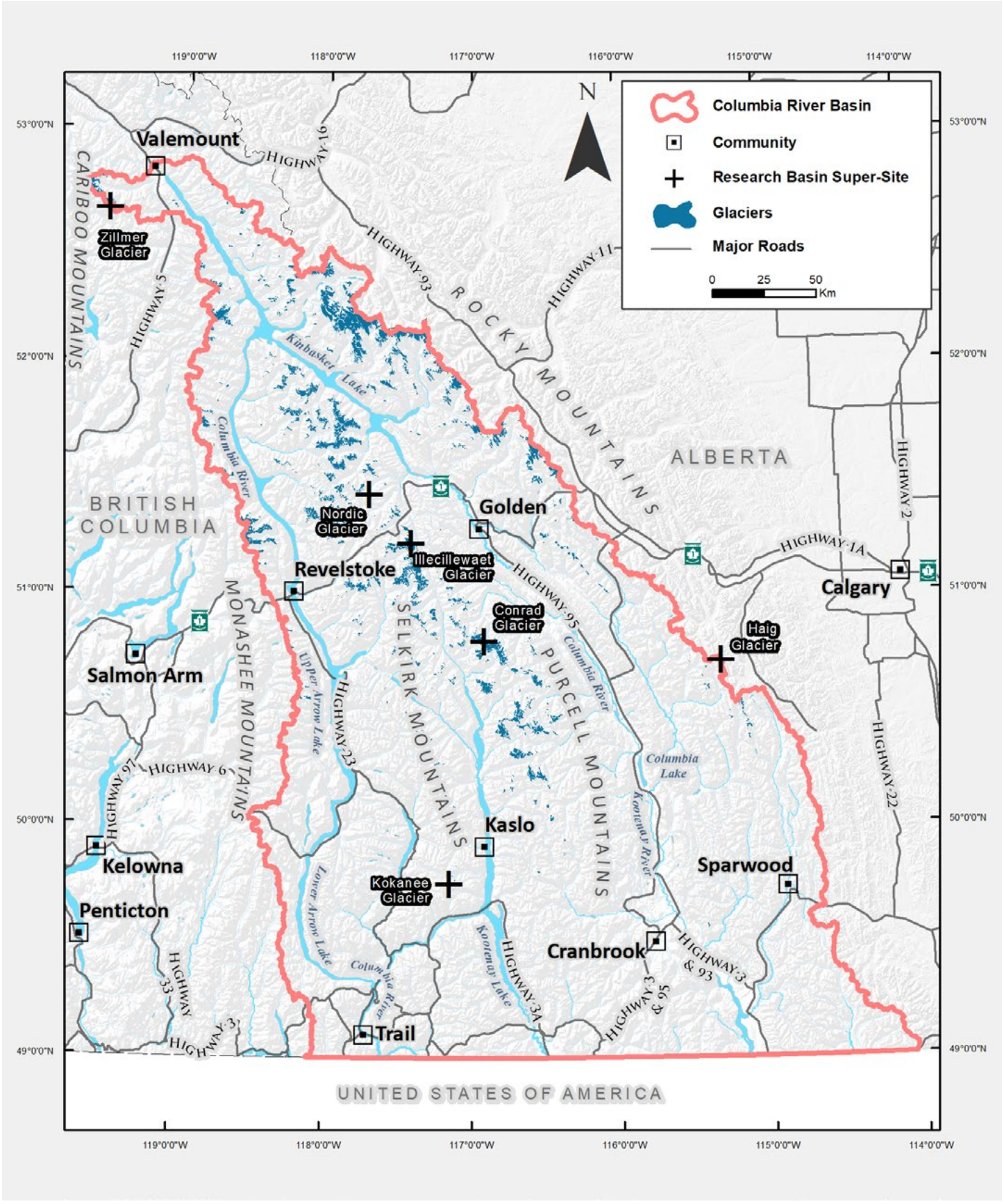

Figure 4.1 *Glacier study sites in the Columbia River Basin.*

The University of Northern British Columbia (UNBC) was responsible for data collection on the Kokanee, Conrad, Nordic and Zillmer glaciers, and both acquisition and processing of all LiDAR surveys. Parks Canada conducted mass balance measurements on the Illecillewaet Glacier in Glacier National Park (Hirose and Marshall 2013), and the University of Calgary monitors the Haig Glacier (Marshall 2014). Ice thickness data was also collected by UNBC on the supersite glaciers in the Columbia Mountains.

All data will be made publicly available through the World Glacier Monitoring Service (WGMS) and can also be found in Pelto et al. (2019).

4.2 Methods

We here present an overview of the methods used to calculate seasonal mass change from glaciological and geodetic methods, collection and processing of ice thickness data, and glacier area change. Additional details can be found elsewhere (Pelto et al. 2019).

4.2.1 Glaciological mass balance

We collected glacier mass balance measurements using the glaciological method (Cogley et al. 2011). Our winter glaciological field campaigns typically occurred between mid-April and mid-May, and the summer/annual balance visits took place between mid-August and mid-September (Table 4.1). Annual glacier mass balance is defined as the sum of accumulation and ablation throughout the balance year (Cuffey and Paterson 2010), which can be expressed as the sum of winter and summer balance:

[4.2] $B_a = B_w + B_s$

For glaciological and geodetic mass balance, by rearrangement of equation 2, the point measurements of B_a and B_w allow the calculation of summer balance B_s:

[4.3] $B_s = B_a — B_w$

Glacier mass balance measurements included snow depth, snow density, ablation, and kinematic GPS surveys of the glacier surface.

Glaciological methods that we describe apply to the glaciers studied by UNBC. For Haig Glacier, mass balance is derived from a combination of point observations and a distributed model of glacier melt (Marshall 2014; Samimi and Marshall 2017). The glacier melt model has 30-m resolution and uses a surface energy balance scheme, driven by automatic weather station data collected on the upper glacier and the

glacier forefield. Mass balance measurements for Illecillewaet Glacier have been made by Parks Canada since 2009 (Hirose and Marshall 2013).

We used G3 industrial aluminum probes to collect over 1,700 estimates of snow depth over the period of study. Snow depths ranged from tens of centimeters to 8 m. We measured snow density with a 100 cm^3 box cutter in snow pits and from snow cores using a 7.25 cm-diameter Kovacs corer. Spring snow density was measured at low, middle and upper locations for each glacier, and we used ablation stakes to record ice and firn ablation (Figure 4.2).

To calculate mass balance, we used the profile method (Escher-Vetter et al. 2009), applied over 100 m hypsometric elevation bins. The area-altitude distribution of a given glacier was obtained using our annual late-summer LiDAR digital elevation models (DEM). For Zillmer, Nordic and Conrad glaciers, we separately considered the measurements from two distinct branches or sides of each glacier. We used the contour method for Illecillewaet Glacier as there were insufficient point measurements to apply the profile method.

To account for elevation change between a given field visit and the associated LiDAR survey, we completed kinematic GPS surveys using a Topcon GB-1000 receiver as a rover and a second receiver as a base station. Height change observed between the LiDAR DEM surface and survey points were binned by elevation (Pelto et al. 2019), and assigned a density based upon surface classification as determined from satellite imagery. Since LiDAR surveys were essentially synchronous (typically flown over two to three days), we chose to apply the correction to the glaciological estimates of mass balance. We surveyed 2-6 control points at each site to determine the survey reliability and found that horizontal and vertical uncertainties respectively averaged ±0.04 m and ±0.06 m. Additional details about our methods, sources of uncertainty and error propagation can be found in (Pelto et al. 2019).

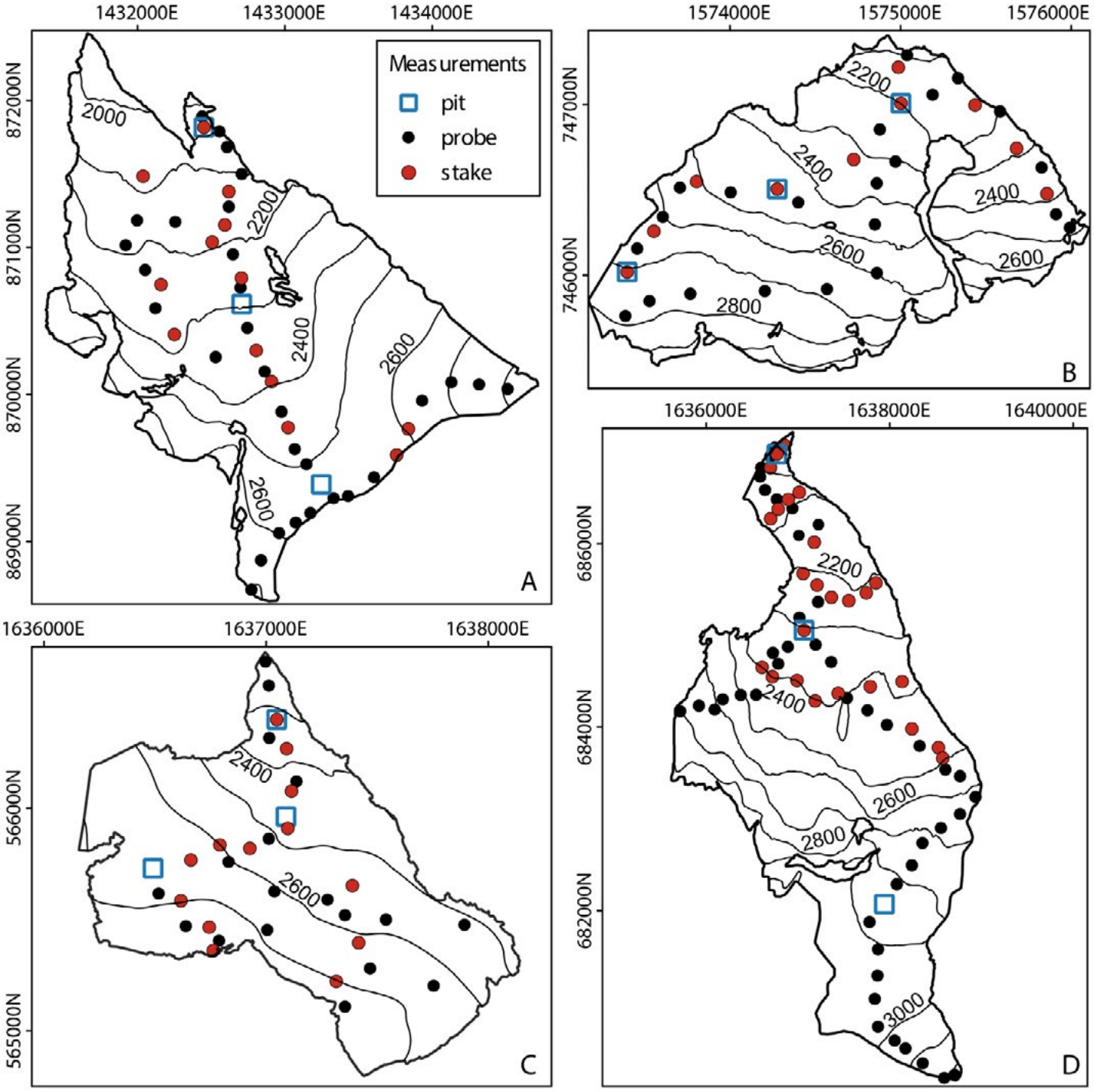

Figure 4.2 *Measurement networks for the A) Zillmer, B) Nordic, C) Kokanee, and D) Conrad glaciers. Snow depth measurement locations, ablation stakes, and snow pit/core locations are pictured. Refer to Marshall et al. (2014) for the Haig Glacier, and Hirose and Marshall (2013) for the Illecillewaet Glacier. Map coordinates are in WGS84/UTM11N.*

4.2.2 Geodetic mass balance

We performed repeat fixed wing LiDAR surveys from late-summer 2014 to late-summer 2018 (Table 4.1) using a Riegl VQ-580 infrared (1024 micron) laser scanner with dedicated Applanix POS AV Global Navigation Satellite System (GNSS) Inertial Measurement Unit (IMU). Later surveys used the same GNSS IMU and a Riegl Q-780 infrared (1024 micron) laser scanner. We planned the airborne surveys to yield return point densities that averaged 2 laser shots m^{-2} with an effective sampling diameter of 10-20 cm per laser shot.

Year	Glacier	Late-summer Glac.	n	Late-summer LiDAR	Cover (%)	Points (m^{-2})	Winter Glac.	n	Winter LiDAR	Cover (%)	Points (m^{-2})
2015	Zillmer	8/23/2015	23	10/3/2015	100	2.75	5/30/2015	20	4/19/2015	100	3.34
2016	Zillmer	8/15/2016	23	9/14/2016	100	2.44	4/14/2016	46	4/18/2016	100	3.69
2017	Zillmer	8/22/2017	26	11/3/2017	100	1.49	4/13/2017	31	5/20/2017	100	0.80
2018	Zillmer	—	—	—	—	—	5/19/2018	42	4/29/2018	100	4.37
2014	Nordic	8/29/2014	8	9/11/2014	100	8.71	4/27/2014	16	—	—	—
2015	Nordic	8/31/2015	11	9/11/2015	99	1.99	5/1/2015	20	4/19/2015	100	3.04
2016	Nordic	8/21/2016	21	9/12/2016	99	3.27	5/2/2016	28	4/17/2016	100	3.21
2017	Nordic	9/14/2017	18	9/27/2017	100	2.35	5/1/2017	21	5/21/2017	100	0.96
2018	Nordic	—	—	—	—	—	5/1/2018	21	4/26/2018	100	1.84
2015	Illecillewaet	9/24/2015	9	9/11/2015	97	1.02	—	—	4/19/2015	100	2.31
2016	Illecillewaet	9/13/2016	7	9/12/2016	100	1.37	—	—	4/17/2016	100	2.50
2017	Illecillewaet	9/27/2017	7	9/17/2017	100	2.59	5/19/2017	3	5/21/2017	100	1.22
2018	Illecillewaet	—	—	—	—	—	—	—	4/26/2018	100	1.64
2015	Haig	9/12/2015	2	9/12/2015	100	0.93	5/12/2015	33	4/20/2015	100	2.89
2016	Haig	9/13/2016	1	9/13/2016	100	1.85	5/18/2016	33	4/17/2016	100	2.64
2017	Haig	9/16/2017	1	9/16/2017	97	4.82	5/12/2017	33	5/21/2017	100	1.09
2018	Haig	—	—	—	—	—	—	—	4/27/2018	100	3.23
2014	Conrad	9/4/2014	7	9/11/2014	100	10.38	—	—	—	—	—
2015	Conrad	9/5/2015	9	9/12/2015	92	1.35	4/23/2015	38	4/20/2015	100	3.58
2016	Conrad	8/28/2016	31	9/12/2016	100	2.45	4/26/2016	44	4/17/2016	100	2.45
2017	Conrad	9/10/2017	42	9/17/2017	94	3.70	5/15/2017	59	5/21/2017	100	1.29
2018	Conrad	—	—	—	—	—	4/24/2018	56	4/26/2018	100	1.84
2015	Kokanee	8/27/2015	11	9/12/2015	100	1.04	4/20/2015	20	4/19/2015	100	2.99
2016	Kokanee	9/5/2016	23	9/13/2016	100	2.07	4/19/2016	33	4/17/2016	100	2.77
2017	Kokanee	9/19/2017	15	9/16/2017	83	2.63	4/17/2017	23	5/21/2017	100	0.92
2018	Kokanee	—	—	—	—	—	4/18/2018	21	4/26/2018	100	1.33

Table 4.1 *Date and number of observation locations (n) for glaciological visits and geodetic acquisition dates and point density. Field dates are median date of glacier visit.*

4.2.2.1 LiDAR post-processing

Post-processing of the LiDAR survey flight trajectory data used the PosPac Mobile Mapping Suite (Applanix), with Trimble CenterPoint RTX with vertical and horizontal positional uncertainties that were typically better than ±15 cm (1σ). We cleaned point clouds and exported finished LAS files into LAStools (https://rapidlasso.com/lastools/) where we created 1-m DEMs from each survey. We co-registered all DEMs following the method detailed in Nuth and Kääb (2011). For late-summer surveys, one master DEM was chosen and all other late-summer DEMs were co-registered to that DEM for stable surfaces only (ice and snow-covered areas, forests and lakes identified in satellite imagery were excluded).

For winter DEMs, the previous late-summer DEM was used as the master DEM to mitigate any surface height changes in areas defined as stable terrain such as rockfall and vegetation cover change. There was no snow-free terrain, except rocky features with extreme slopes which are not used in the co-registration (slope >40 ° excluded). We thus did not apply any vertical shift during co-registration of winter DEMs.

We utilized satellite imagery from Landsat 7 and 8, Sentinel-2, and Planet Scope at 30, 10, and 3-5 m resolution respectively (Bevington et al. 2018), to guide surface classification used to co-register DEMs and calculate geodetic mass change. We selected the latest snow-free imagery from September or late-August, and used a band-ratio and threshold method (Kääb 2005) to classify areas of snow, firn, and ice.

Table 4.2 *Seasonal balance and uncertainty estimates for geodetic (geod) and glaciological mass balance (glac) in m w.e. Kinematic GPS survey-derived corrections applied to glaciological data (surv.corr). Bias correction applied over the glacier (Bias$_{\Delta h}$) to geodetic height change. Statistical analysis of the DEMs over stable terrain can be found in Pelto et al. (2019). Mean density of Ba$_{geod}$ is ρ. Average values include only cases where both geodetic and glaciological data were collected. Bw$_{geod.gl}$ is calculated using glaciological densities (Table 4.4), and Bw$_{geod.ss}$ is calculated using snow survey data (Figure 4.2). Listed Bs$_{geod}$ is derived using Bw$_{geod.ss}$. Regional late summer snow density was used to calculate Ba$_{geod}$.*

Year	Glacier	$Bw_{geod.gl} \pm \sigma_{geod.bw}$	$Bw_{geod.sc} \pm \sigma_{geod.bw}$	$Bs_{geod} \pm \sigma_{geod.bs}$	$Ba_{geod} \pm \sigma_{geod.ba}$	$Bw_{glac} \pm \sigma_{glac.bw}$	$Bs_{glac} \pm \sigma_{glac.bs}$	$Ba_{glac} \pm \sigma_{glac.ba}$	$Bw_{surv.corr}$	$Ba_{surv.corr}$	AAR	ELA (m)	NMAD Ba (m)	NMAD Bw (m)	Median $Ba_{\Delta h}$ (m)	$Bias_{\Delta h}$ (m)	$\bar{\rho}$ (kg m^{-3})
2018	Zillmer	1.70 ± 0.19	1.75 ± 0.20	-2.69 ± 0.23	-0.94 ± 0.12	1.65 ± 0.17	-2.41 ± 0.46	-0.76 ± 0.37	-0.15	-0.28	0.40	2470	0.15	1.40	0.00	0.06	737 ± 45
2018	Nordic	1.87 ± 0.26	2.07 ± 0.27	-2.50 ± 0.28	-0.43 ± 0.07	2.18 ± 0.14	-2.67 ± 0.32	-0.49 ± 0.25	-0.04	-0.52	0.32	2600	0.30	1.76	-0.02	0.01	735 ± 40
2018	Illecillewaet	1.61 ± 0.17	1.65 ± 0.18	-2.57 ± 0.21	-0.92 ± 0.10	—	—	—	—	—	0.36	—	0.38	2.26	-0.04	0.00	894 ± 10
2018	Haig	1.25 ± 0.15	1.31 ± 0.19	-2.57 ± 0.22	-1.26 ± 0.16	1.42 ± 0.15	-2.78 ± 0.28	-1.36 ± 0.24	—	—	0.00	—	0.42	1.83	0.10	-0.24	762 ± 50
2018	Conrad	1.62 ± 0.21	1.84 ± 0.23	—	—	1.83 ± 0.12	—	-0.60 ± 0.25	0.00	—	0.42	2645	—	2.34	—	—	—
2018	Kokanee	2.07 ± 0.25	2.31 ± 0.26	-2.70 ± 0.26	-0.29 ± 0.12	2.25 ± 0.13	-2.39 ± 0.31	-0.14 ± 0.25	0.01	—	0.62	2580	0.28	1.76	0.00	0.02	698 ± 50
2017	Zillmer	2.12 ± 0.24	2.03 ± 0.25	-2.70 ± 0.27	-0.67 ± 0.10	1.93 ± 0.26	-2.44 ± 0.35	-0.51 ± 0.23	0.15	-0.31	0.48	2440	0.60	1.83	-0.10	-0.05	729 ± 45
2017	Nordic	2.14 ± 0.29	2.18 ± 0.30	-2.77 ± 0.31	-0.59 ± 0.09	2.03 ± 0.22	-2.78 ± 0.32	-0.75 ± 0.23	-0.04	-0.10	0.39	2540	0.28	1.80	0.01	-0.09	732 ± 43
2017	Illecillewaet	1.47 ± 0.19	1.54 ± 0.20	-2.55 ± 0.27	-1.01 ± 0.18	2.00 ± 0.16	-2.84 ± 0.32	-0.84 ± 0.28	—	—	0.36	2615	0.32	2.19	0.01	0.00	718 ± 49
2017	Haig	1.58 ± 0.20	1.65 ± 0.23	-3.56 ± 0.31	-1.91 ± 0.21	1.50 ± 0.17	-3.43 ± 0.29	-1.93 ± 0.24	—	—	0.04	—	0.31	1.62	0.01	0.04	885 ± 10
2017	Conrad	2.10 ± 0.22	1.91 ± 0.23	-2.97 ± 0.26	-1.06 ± 0.13	2.17 ± 0.17	-3.12 ± 0.29	-0.95 ± 0.24	-0.16	-0.16	0.48	2600	0.31	2.68	0.00	-0.01	730 ± 45
2017	Kokanee	3.15 ± 0.32	2.86 ± 0.33	-3.14 ± 0.34	-0.28 ± 0.08	2.84 ± 0.25	-2.87 ± 0.34	-0.03 ± 0.23	0.00	0.01	0.62	2560	0.34	1.99	-0.08	-0.01	711 ± 55
2016	Zillmer	1.68 ± 0.19	1.72 ± 0.20	-2.27 ± 0.22	-0.55 ± 0.07	1.99 ± 0.23	-2.61 ± 0.33	-0.62 ± 0.24	0.02	-0.38	0.49	2410	0.21	1.76	0.01	-0.02	726 ± 46
2016	Nordic	1.79 ± 0.22	1.70 ± 0.23	-1.85 ± 0.24	-0.15 ± 0.08	1.79 ± 0.14	-1.90 ± 0.21	-0.11 ± 0.16	-0.08	0.01	0.43	2555	0.16	1.63	0.00	-0.04	727 ± 40
2016	Illecillewaet	1.41 ± 0.17	1.46 ± 0.18	-1.73 ± 0.18	-0.27 ± 0.05	—	—	-0.19 ± 0.28	—	—	0.60	2550	0.45	1.90	-0.01	0.05	718 ± 54
2016	Haig	1.15 ± 0.15	1.21 ± 0.17	-2.27 ± 0.20	-1.06 ± 0.11	1.34 ± 0.17	-2.49 ± 0.29	-1.15 ± 0.24	—	—	0.03	—	0.38	1.24	-0.01	-0.04	893 ± 10
2016	Conrad	1.40 ± 0.18	1.47 ± 0.19	-1.74 ± 0.20	-0.27 ± 0.06	1.88 ± 0.12	-2.08 ± 0.20	-0.20 ± 0.16	0.11	-0.13	0.55	2530	0.14	2.1	0.00	-0.02	734 ± 50
2016	Kokanee	1.98 ± 0.22	2.05 ± 0.23	-1.93 ± 0.23	+0.12 ± 0.05	2.07 ± 0.13	-1.94 ± 0.26	+0.13 ± 0.22	-0.05	0.12	0.72	2545	0.15	1.67	0.00	0.00	681 ± 64
2015	Zillmer	—	—	—	—	2.06 ± 0.30	-2.82 ± 0.40	-0.76 ± 0.27	0.00	-0.32	0.30	2500	—	—	—	—	—
2015	Nordic	1.74 ± 0.22	1.81 ± 0.23	-2.81 ± 0.28	-1.27 ± 0.16	1.83 ± 0.19	-3.02 ± 0.31	-1.19 ± 0.24	-0.16	0.06	0.32	2610	0.26	1.76	0.00	0.02	744 ± 42
2015	Illecillewaet	—	—	—	—	—	—	-1.17 ± 0.47	—	—	0.30	2600	—	—	—	—	—
2015	Haig	—	—	—	—	1.23 ± 0.25	-3.02 ± 0.25	-1.79 ± 0.25	—	—	0.00	—	—	—	—	—	—
2015	Conrad	1.65 ± 0.17	1.64 ± 0.18	-3.06 ± 0.24	-1.42 ± 0.16	1.80 ± 0.13	-3.20 ± 0.35	-1.40 ± 0.32	-0.02	-0.31	0.44	2685	0.21	2.2	-0.01	-0.03	736 ± 43
2015	Kokanee	—	—	—	—	2.18 ± 0.29	-3.38 ± 0.40	-1.20 ± 0.28	0.00	—	0.20	2680	—	—	—	—	—
All	Average	1.87 ± 0.11	1.88 ± 0.09	-2.59 ± 0.16	-0.76 ± 0.16	1.95 ± 0.08	-2.67 ± 0.13	-0.73 ± 0.15	-0.04	-0.14	0.38	2553	0.29	1.89	-0.01	-0.01	748 ± 62

Table 4.3 *Density values used for geodetic and glaciological balance. Glaciological values are average values. *Geodetic spring snow density (ρ_{spring}) is 440 ± 50 kg m^{-3} for Haig Glacier and glaciological is 420 ± 45 kg m^{-3} (n = 46).*

Location	Mean ρ_{snow} (kg m^{-3})	Range ρ_{snow} (kg m^{-3})	References
South Cascade Gl., WA, US	580	530 – 600	(Bidlake et al., 2010; Krimmel, 1996)
Juneau Icefield, AK, USA	560	540 – 580	(Miller and Pelto, 1999; Pelto and Miller, 1990)
Castle Creek Gl., BC, CA	600	—	(Beedle et al., 2014)
North Cascades, WA, USA	600	590 – 630	(Pelto and Riedel, 2001)
Haig Glacier, AB, CA	545	530 – 570	(Marshall, S.J., 2012)
Columbia Basin, BC, CA	570	535 – 615	This study

Figure 4.3 *Snow depth versus snow water equivalent from May 1 provincial snow course data. The mean date of our spring field seasons was May 1, and so we chose May 1 BC snow course data (left) to derive a SWE/snow depth regression from which we determined the average May 1 snow density.*

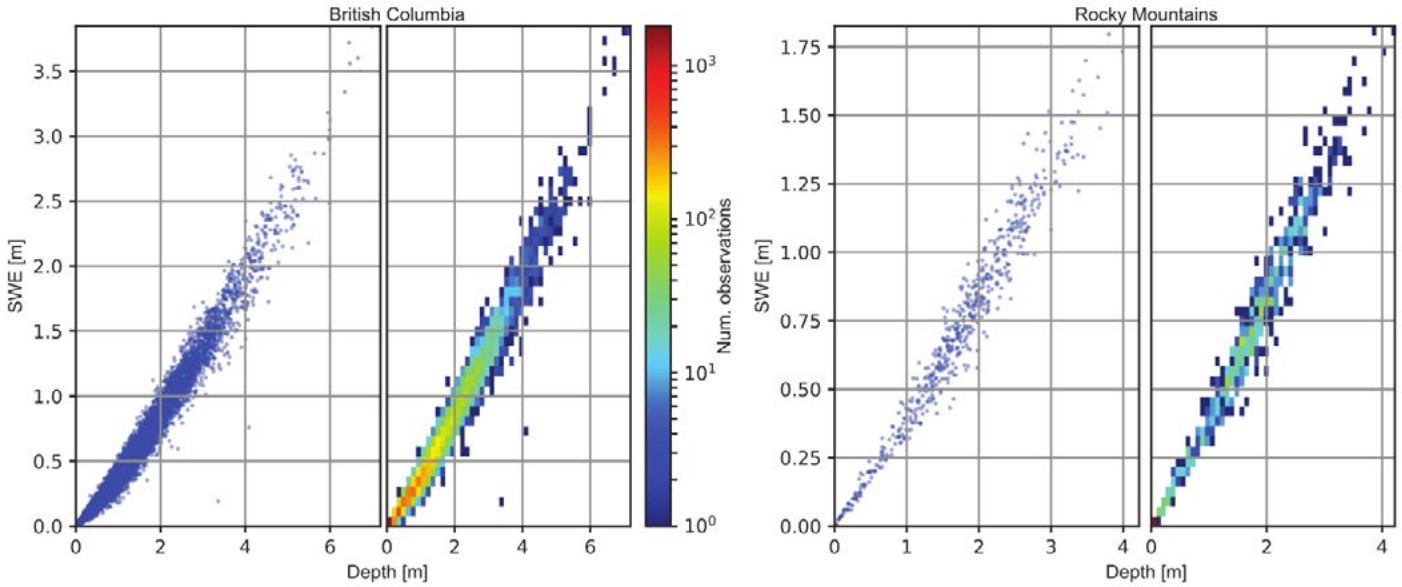

To calculate annual mass change (B_a), we: (1) difference two DEMs to create a height change DEM (ΔDEM); (2) determine the mean difference between the two DEMs in stable terrain ($Bias_{\Delta h}$, Table 4.2) to bias-correct the observed height change by any systematic elevation difference between the DEMs after co-registration; (3) derive a mask based on surface classification of ice, firn and snow from satellite imagery (Pelto et al. 2019); and (4) apply the density of each respective surface type (Table 4.3) to the ΔDEM to calculate mass balance.

4.2.2.2 *Density estimates*

While LiDAR provides an accurate estimate of snow depth with vertical uncertainties of ±0.1–0.3 m (Joerg et al. 2012), it provides no information regarding snow density. We use snow course measurements available from the British Columbia River Forecast Center (BCRFC) as independent data to estimate spring snow density and compare with our measured glaciological snow densities. We use these BCRFC data to evaluate whether reliable estimates of snow density can be obtained for regions where no snow observations over glaciers exist.

The mean date of our spring field visits was May 1st (Table 4.1), so we chose May 1st snow course data (n = 10,169) to derive a relation between SWE (kg m^{-2}) and snow depth (m) (Figure 4.3). The linear relation (regression fit) yields a slope of 470 ± 70 kg m^{-3} (r^2 = 0.97), which we use as the average May 1st snow density which we applied for our geodetic Bw calculations. For Haig Glacier, we chose only snow course measurements from the Rocky Mountains for a linear relation yielding 440 ± 50 kg m^{-3} (n = 629). We use the standard deviation (σ) of the snow course data as an estimate of the uncertainty in bulk snow density. For our glaciological density-informed Bw_geod, we use the observed glacier-wide snow density (Table 4.4) and a linear regression of density versus day and used the slope (3.0 kg m^{-3} day^{-1}, r^2 = 0.43) and days between the survey and the observations to adjust for change in snow density (Figure 4.4). The lack of an altitudinal trend in snow density observed on many glaciers (Fausto et al. 2018; McGrath et al. 2015, 2018; Sold et al. 2016) and those of this study, coupled with the absence of high-elevation snow density measurements and the annual variability of snow density evolution, required the use of a single value for spring snow density.

Figure 4.4 *Snow density versus Julian day for all discrete snow pit and snow core locations (n = 46). For our glaciological density-informed estimates, we use the observed glacier-wide snow density and a linear regression of density versus day and used the slope (3.0 kg m^{-3} day^{-1} (r^2 = 0.43)) and days between the survey and the observations to adjust for change in snow density (Table 4.4).*

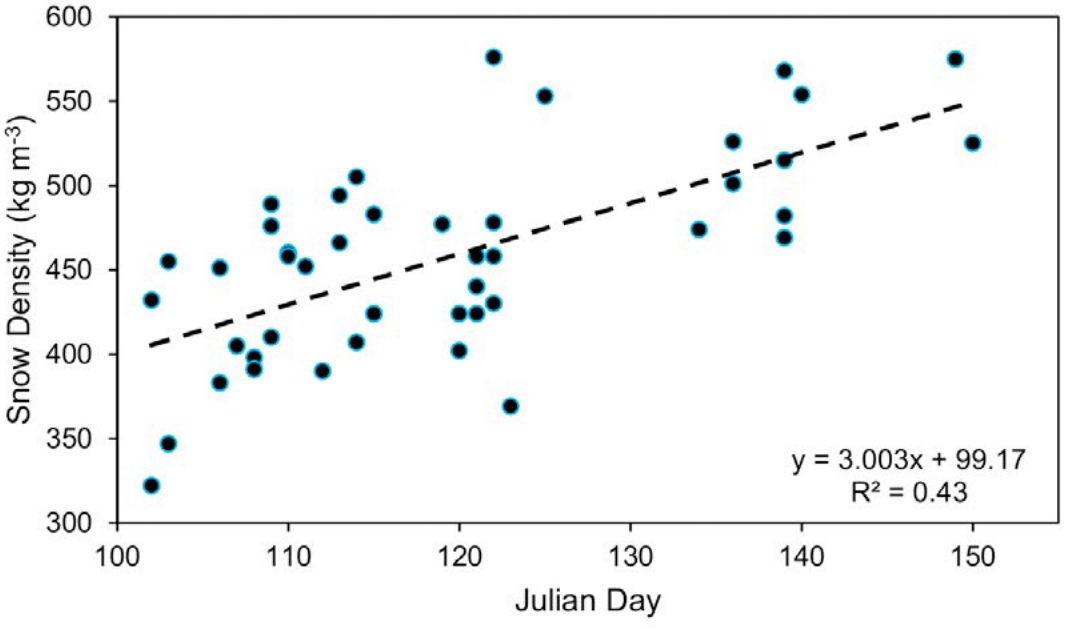

Table 4.4 *Glacier-wide spring snow density from glaciological observations ($\rho_{spring.obs}$), and updated spring snow density using the linear relation ($\rho_{spring.lin}$) of Julian day versus snow density (Figure 4.3). No observed density implies no winter balance trip occurred, and no data in the $\rho_{spring.lin}$ column implies no B_{w_geod} was derived. When no spring glaciological visit occurred, the average spring snow density for the sites' available record was used.*

Year	Glacier	$\rho_{spring.obs}$ (kg m^{-3})	$\rho_{spring.lin}$ (kg m^{-3})
2018	Zillmer	517	457
2018	Nordic	426	411
2018	Illecillewaet	—	461
2018	Haig	—	420
2018	Conrad	407	413
2018	Kokanee	395	419
2017	Zillmer	381	492
2017	Nordic	403	463
2017	Illecillewaet	443	449
2017	Haig	420	420
2017	Conrad	500	518
2017	Kokanee	415	517
2016	Zillmer	447	459
2016	Nordic	541	496
2016	Illecillewaet	456	456
2016	Haig	420	420
2016	Conrad	480	453
2016	Kokanee	459	459
2015	Zillmer	554	—
2015	Nordic	452	416
2015	Illecillewaet	—	—
2015	Haig	420	—
2015	Conrad	481	472
2015	Kokanee	466	—

Regional observations of late-summer snow density are consistent; ranging from 530-630 kg m^{-3} for glaciers across the Pacific Northwest (Pelto et al. 2019). Since we independently evaluate glaciological vs. geodetic estimates of mass change, we compare application of our late-summer glaciological snow density measurements to calculate net balance with estimates based on average observations from four regional sources (590 ± 60 kg m^{-3}) (Pelto et al. 2019), to test the impact of uncertainties of up to 10% in this parameter. Firn density has not been reported for the study area, so we estimate 700 ± 100 kg m^{-3} for multi-year firn based on our firn core measurements for firn two or more years old (average density of 703 ± 65 kg m^{-3}, n=4) (Pelto et al. 2019). Measurements of one-year-old firn averaged 619 ± 47 kg m^{-3} (n=8). Given the sustained mass loss of Pacific Northwest glaciers (Bolch et al. 2010; Pelto 2006; Menounos et al. 2018), exposed firn is generally more than one year old. After performing a pixel-based surface classification for each late-summer, we used these classification masks to assign a density (Table 4.3) to each pixel (snow/firn/ice).

4.2.3 Ice thickness data

To obtain the ice thickness, we conducted GPR surveys in April-May 2015, 2016, 2017, and 2018. We used a Blue Systems Integration radar system, employing 10MHz center frequency antennas with a 1100V transmitter (Mingo and Flowers 2010). Antenna separation was set to 15 m, and the step size was typically 5 m, dependent upon travel speed. Data were collected along longitudinal and cross-profiles. Location of profiles was highly dependent upon slope and safety concerns. We extracted ice thickness using IcePick assuming a typical homogeneous propagation velocity of 168 m μs^{-1} (Glen and Paren 1975; Kovacs et al. 1995; Wilson et al. 09/2013).

Each radar trace had an associated geographical position recorded with a Garmin NMEA GPS18x Global Positioning System (GPS) receiver with an estimated positional accuracy of ~3 m. In total, 189 km of data were collected by UNBC (Table 4.5) across five glaciers. Of these transects, actual bedrock reflections were detected for 175 km of data and over 34,000-point measurements of ice thickness.

Table 4.5 *Acquired and utilized GPR measurements for Conrad, Nordic, Zillmer, Kokanee, Illecillewaet and Haig glaciers. Number of measurements (n) indicates the number of point observations for which the bed (ice thickness) was successfully picked. Distance represents the number of kilometers represented by the point measurements, which are collected along transects across and up glacier (e.g. Figure 4.14).*

Glacier	Total acquired [km]	Total used [km]	n
Conrad	97	85	13,769
Nordic	15	14	3,178
Zillmer	25	23	4,410
Kokanee	12	11	2,175
Illecillewaet	41	36	8,171
Haig	13	10	2,770
Total	203	179	34,473

4.2.4 Glacier mass change

We also report an estimate of glacier mass change for all Canadian glaciers in the Columbia Basin based on the results of Menounos et al., (2018). Mass change data in that study was summarized on both a 1x1 degree grid and for glaciological regions originally defined by Schiefer et al., (2007). Estimates of glacier mass change are provided for the period 2000-2018.

4.3 Results

4.3.1 Mass change observations (5 year period)

4.3.1.1 Glaciological vs. geodetic mass balance

Comparison of seasonal balance from glaciological and geodetic methods showed strong overall agreement (Figure 4.5), with glaciological winter balance (B_{w_glac}) averaging 1.95 ± 0.08 m w.e., 4% greater than our geodetic estimate. Average summer and annual glaciological balance estimates were 3% smaller and 3% larger, respectively, than our geodetic measurements (Figure 4.6). For individual glaciers, average difference between B_{a_glac} and B_{a_geod} was in excellent agreement (-0.03 m w.e. relative to B_{a_glac}), with an average absolute deviation of 0.10 ± 0.07 m w.e. a^{-1} between estimates (Figure 4.6). B_{w_glac} was 5% greater relative to B_{w_geod}, and B_{s_glac} was 4% more positive relative to B_{s_geod} when considering individual glaciers. For B_w and B_s, geodetic and glaciological balance were within 20% for over 85% of cases.

Figure 4.5 *Geodetic versus glaciological mass balance estimates from 2015 through 2018 for all six study glaciers with a one-to-one line and 1σ uncertainties. Blue shows the winter balance covering the accumulation season from mid-September to late April; red shows the summer balance spanning the remaining months; gray shows the annual balance. Average B_{w_glac} was 4% greater than B_{w_geod}, and B_{s_glac} and B_{a_glac} were 3% smaller and 3% smaller, respectively, than our geodetic estimates.*

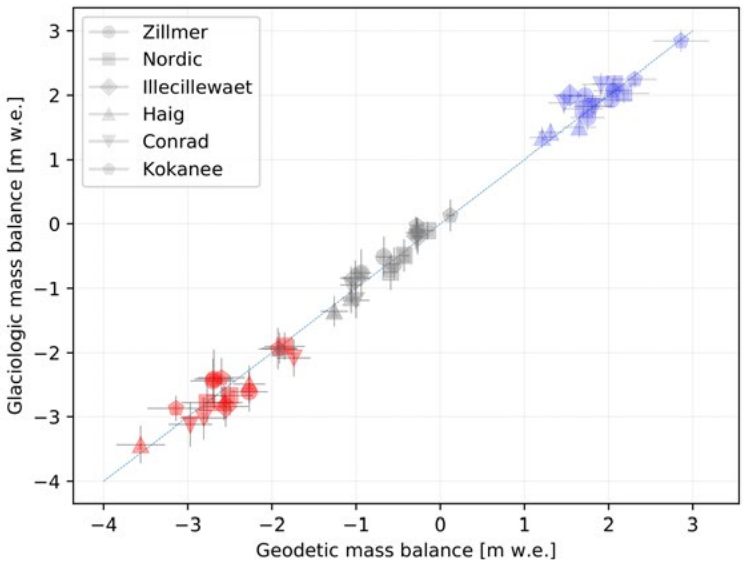

Average mean annual balance from 2015–2018 was -0.73 ± 0.15 m w.e. and -0.76 ± 0.16 m w.e. for glaciological and geodetic methods respectively (Table 4.2). Mean B_{s_glac} was -2.67 ± 0.13 m w.e. All individual estimates of seasonal and annual balance are within 2σ uncertainties, and only in three instances are outside 1σ uncertainties (Figure 4.6).

Figure 4.6 *Seasonal and annual mass balance for all study glaciers from both geodetic and glaciological measurements for each balance year from 2014 to 2018 with 1σ uncertainties. A) 2014 to 2015 balance year, B) 2015 to 2016 balance year, C) 2016 to 2017 balance year, D) 2017 to 2018 balance year.*

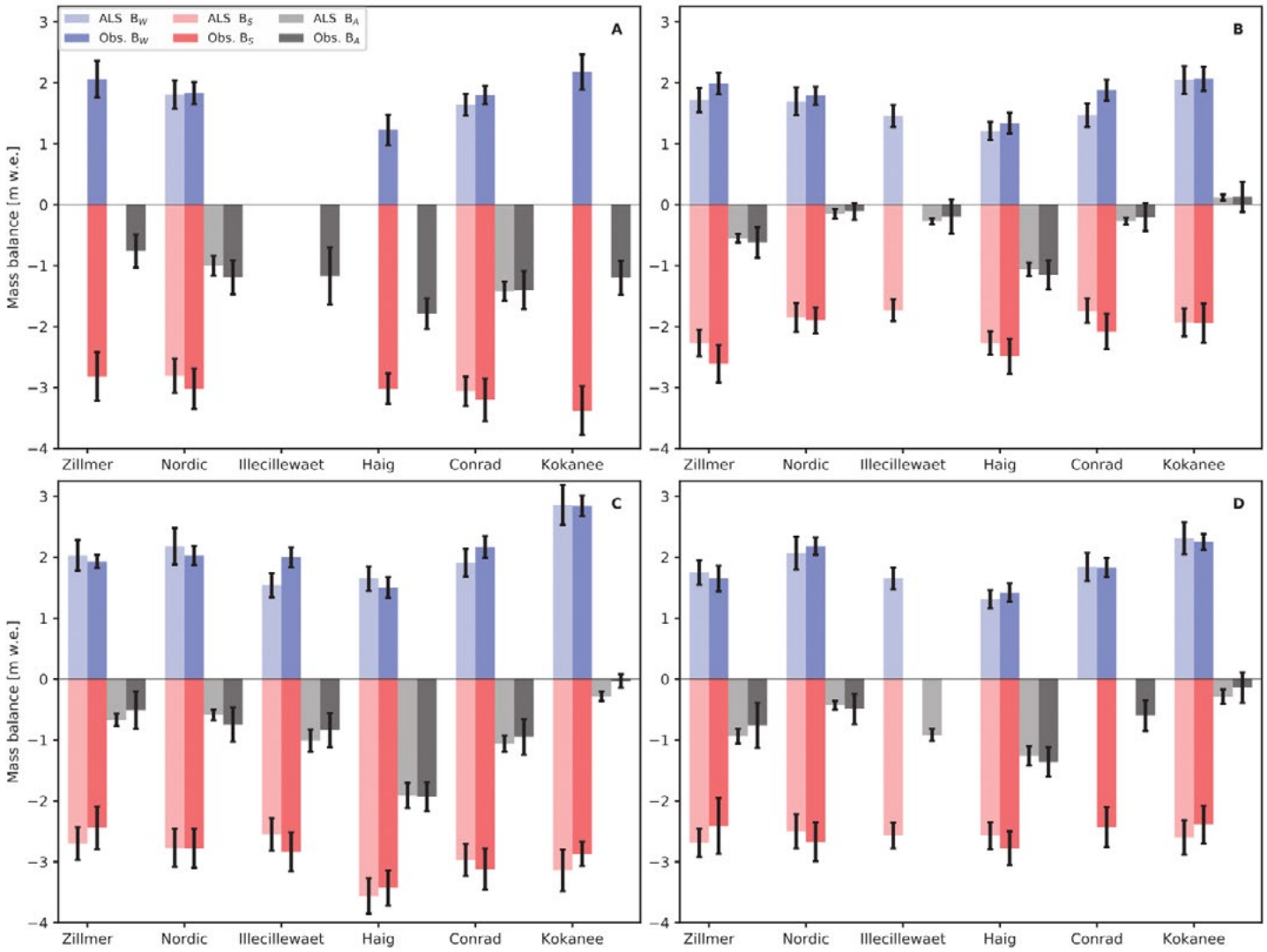

We created a ΔDEM from the last and first late summer DEM for each site (Figure 4.7) and compared the calculated mass change from this ΔDEM to the sum of the individual balance years that comprised that given period (Figure 4.8). We found that all cumulative seasonal B_a estimates from glaciological and geodetic balance were within uncertainty (2σ) of the last-first change approach (Figure 4.8). Glaciological balance was in net more positive (average +0.09 m w.e.) and had an average absolute difference of ±0.20 m w.e. from the last-first ΔDEM. Summed B_{a_geod} agree with our last-first estimates, with an average deviation of only 0.03 m w.e.

4.3.1.2 Glaciological observations

Average glacier spring snow density from snow pits and cores was 457 ± 48 kg m^{-3}, within uncertainty of our snow course estimate. Average probe depth for spring was 4.20 ± 0.06 m (n=1,754). Average probe depth in late-summer is 1.85 ± 0.10 m. Observed average spring glacier snow depths are typically between 3.4 and 6.9

m, and average 4.56 ± 0.21 m. While spring snow density showed greater variability than late-summer snow density, snow depth is far more variable than snow density in both seasons.

4.3.1.3 Interannual and spatial variability

Varied meteorological conditions affected the glaciers over the period of study. The lowest average B_{w_glac} of the four studied winters (1.81 ± 0.12 m w.e.) occurred in 2016 (Figure 4.9), yet was also the year with the least mass loss (Figure 4.6). The 2016-2017 winter brought deepest snow cover of our study period, 2.08 ± 0.18 m w.e., yet substantial mass loss was still observed (average B_{a_glac}: -0.84 ± 0.23 m w.e.). The balance year of 2014-2015 saw high sustained mass loss (average B_{a_glac} of -1.30 ± 0.13 m w.e.), despite having a near-identical B_{w_glac} to 2016.

The standard deviation between the seasonal and annual balances for each glacier reveals that B_w (σ = 0.14 m w.e., 7%) experienced lower interannual variability than B_s (σ = 0.38 m w.e., 14%). Kokanee Glacier experienced the highest B_w in all four years 2015-2018 averaging 2.34 ± 0.30 m w.e. (Figure 4.6), while Haig Glacier's B_w was lowest, averaging 1.37 ± 0.11 m w.e., and the highest mass loss, averaging B_{a_glac} = -1.62 ± 0.34 m w.e.

Figure 4.7 *Surface height change for the Zillmer, Nordic, Haig, Illecillewaet, Conrad, and Kokanee glaciers from the first late-summer DEM (2014 or 2015) until late-summer 2017. Study glaciers are outlined with thick black line and other glaciers with a thin black line. Off-ice areas deemed stable terrain were used for error analysis and co-registration.*

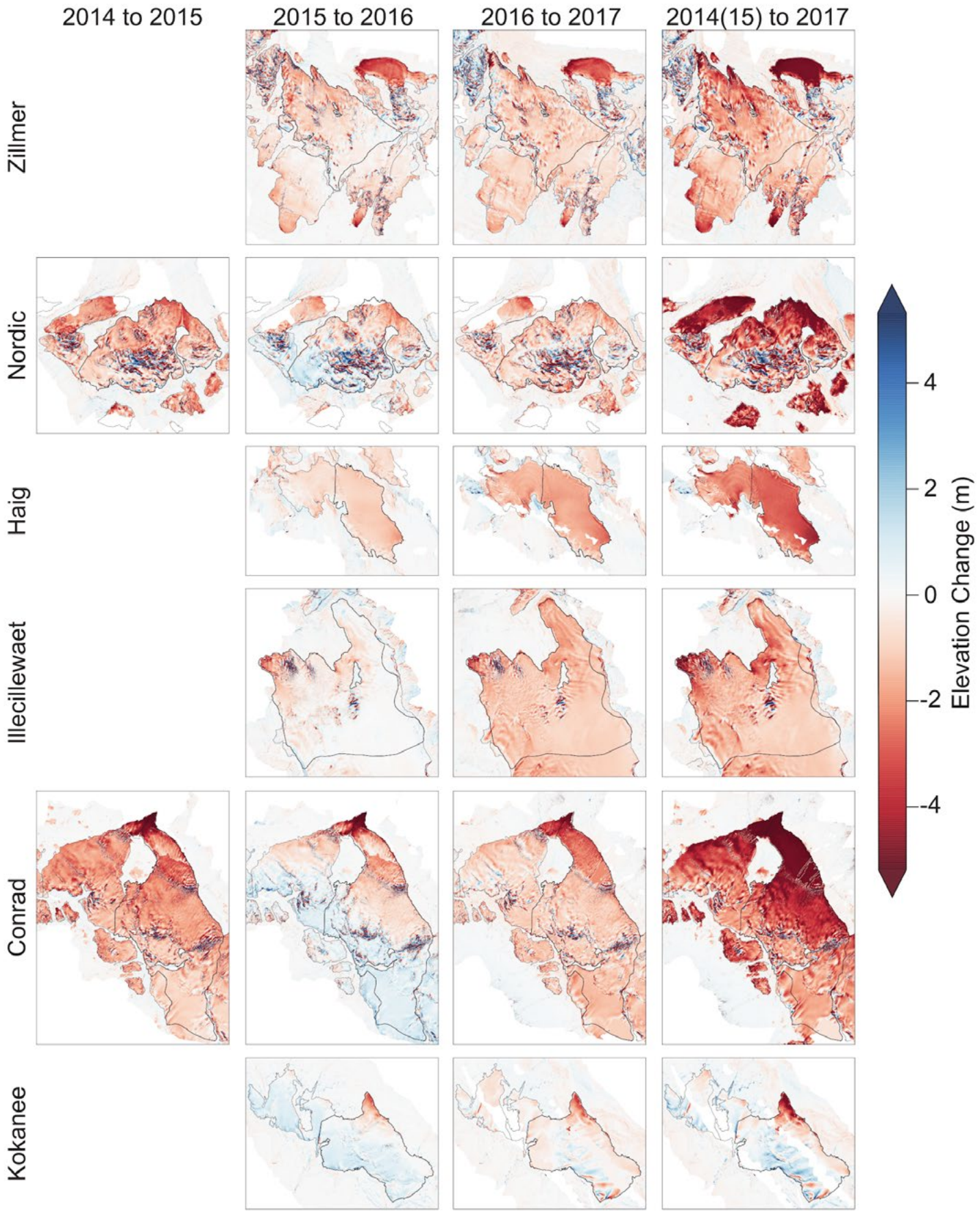

Figure 4.8 *Summed annual mass balance from glaciological data (∑glac), geodetic data (∑geod), and last-first ΔDEM. Last-first ΔDEMs were created by differencing the first available DEM (2014 or 2015 late summer) from the last available DEM (2017) for each site (Table 4.1). Errors denote 2σ uncertainties.*

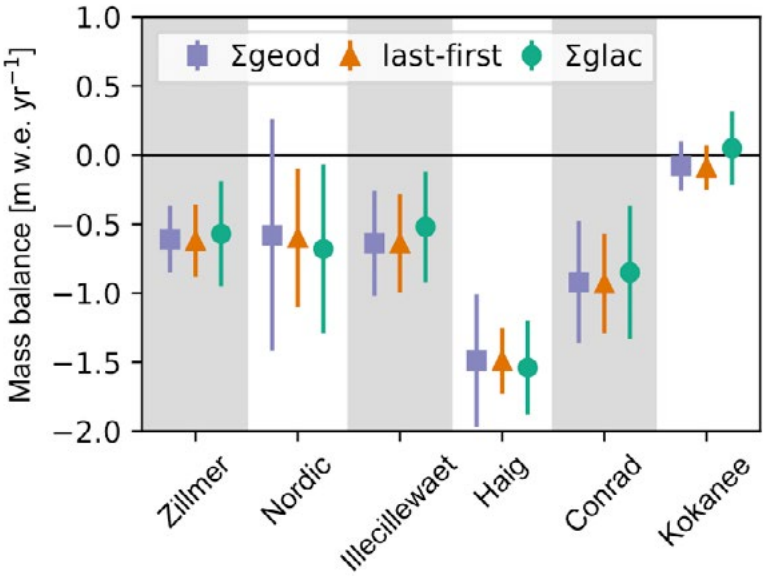

Over the period 2014-2018, our glaciers had an average AAR of 38% (Table 4.2), with multi-year firn exposed over 13% of the glacier surface, leaving the remaining 49% of glacier area as bare ice. Haig Glacier is the easternmost site in our study and experiences less winter precipitation than the glaciers in the Columbia Mountains (Figure 2.1) (Marshall 2014). The glacier lost nearly all its firn cover over the last 20 years, with firn area reduced to 6% in 2015. Excluding this site, the remaining study glaciers in the Columbia Mountains had an AAR of 45% with 15% exposed multi-year firn cover and 40% bare glacier ice.

4.3.1.4 Balance gradients

Between 1800 and 2600 m asl, the average winter balance gradient is 1.55 ± 0.14 mm w.e. m^{-1} for Zillmer, Nordic, Conrad, and Kokanee glaciers, with all glaciers falling between 1.22 and 1.98 mm w.e. m^{-1} (Figure 4.10). Average balance gradients observed for all glaciers 2014 through 2018 show a maximum snow depth around 2600 m asl. Maximum snow depth on Conrad Glacier, which is 400 m higher than the other sites, occurs between 2800-3000 m asl. The elevation of maximum snow depth occurs about two-thirds of the elevation range up-glacier from the terminus, with an average elevation of maximum SWE within 100 m of the two-thirds mark for all four UNBC study sites terminus: $SWE_{max} = (z_{range} * 0.65) + Z_{min}$. The Kokanee Glacier has the lowest balance gradient (Figure 4.10), and smallest elevation range (Table 2.1), with the weakest relationship between elevation and snow depth ($r^2 = 0.15$).

Figure 4.9 *Winter surface height change for the Zillmer, Nordic, Illecillewaet, Haig, Conrad, and Kokanee glaciers for between 2014 and 2018. Study glaciers are outlined with thick black line and other glaciers with a thin black line.*

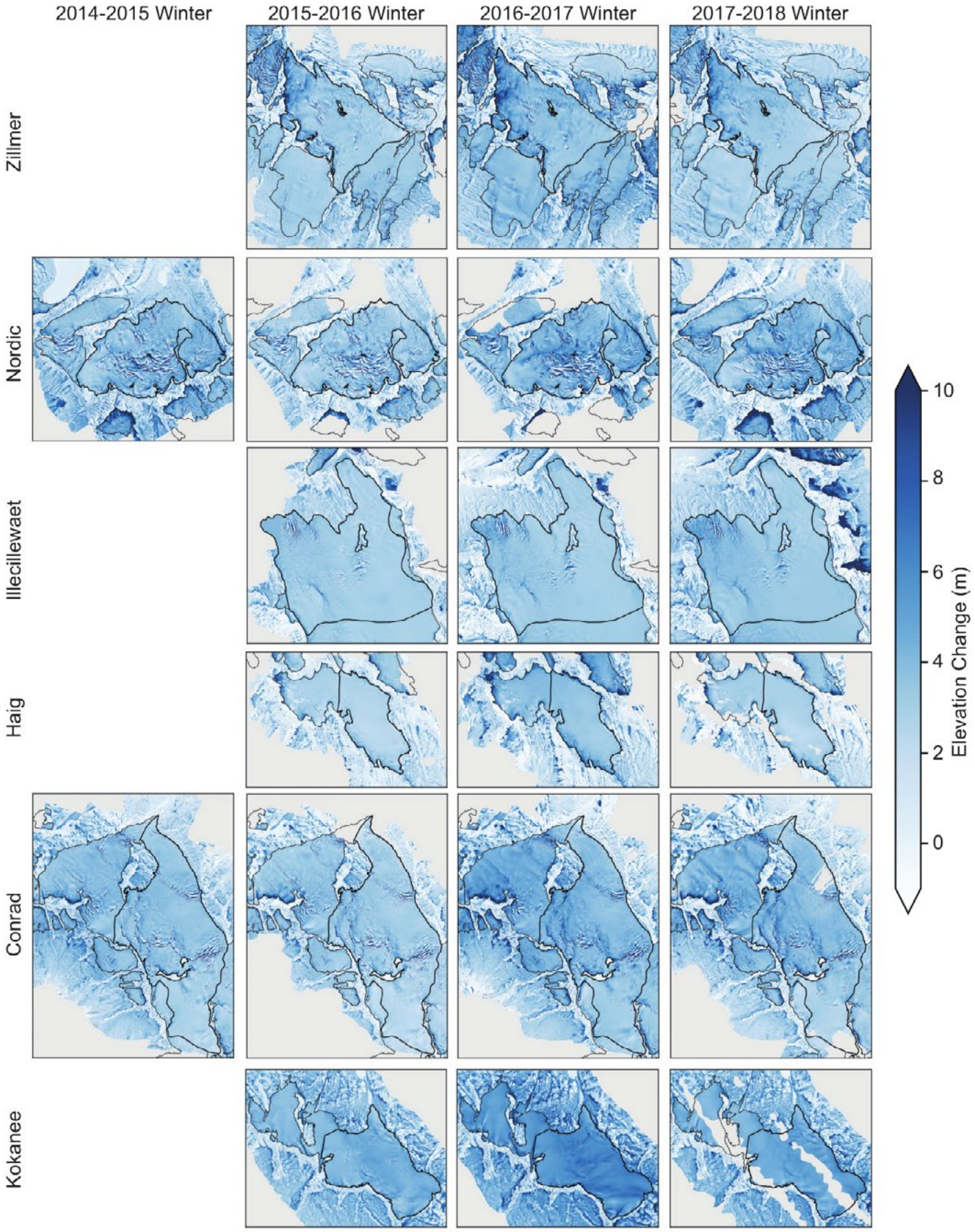

Figure 4.10 *Summer (red), winter (blue), and annual (black) glaciological balance gradients for: (clockwise from top left) A) Zillmer, B) Nordic, C) Conrad and D) Kokanee glaciers from 2015 to 2018.*

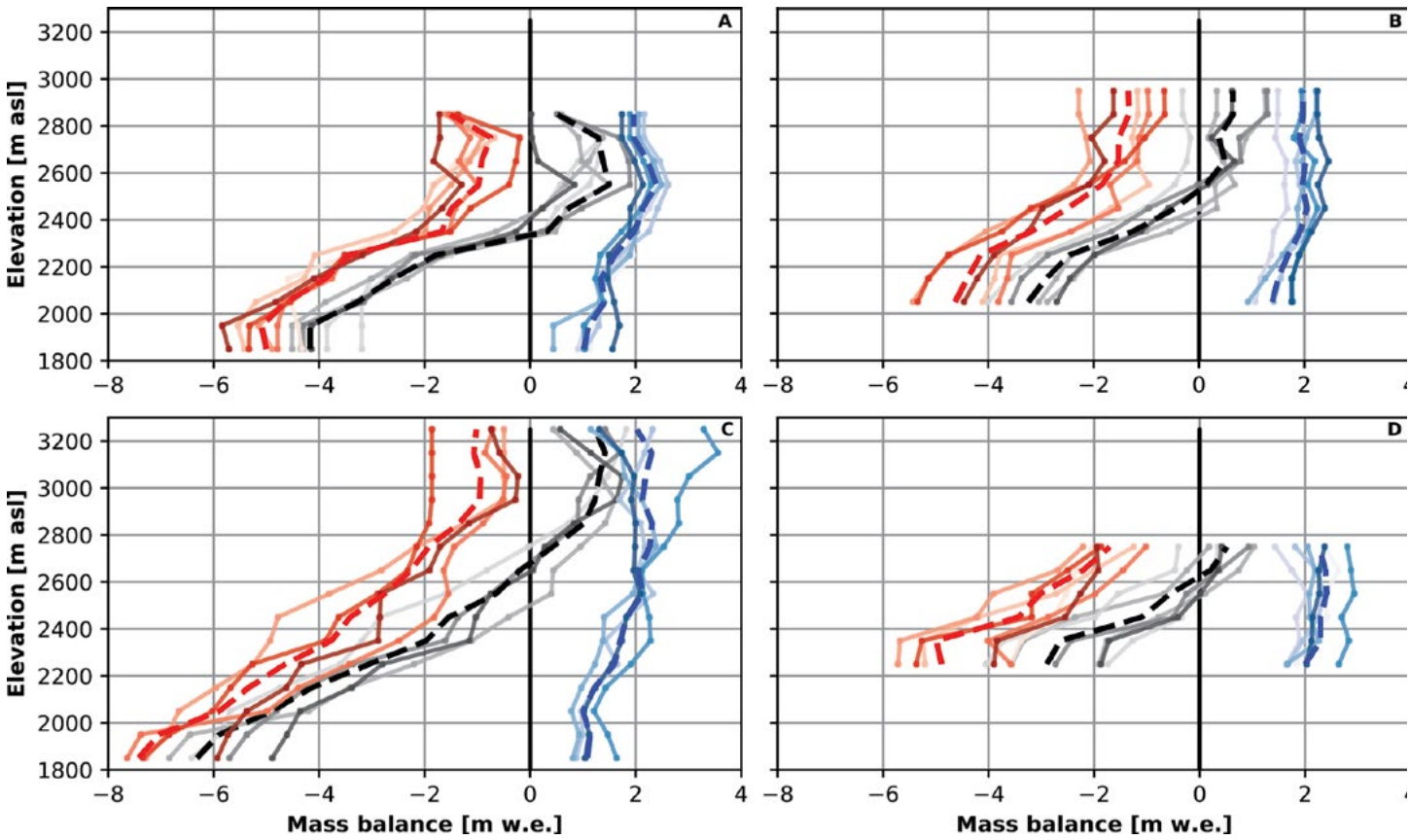

4.3.1.5 Study glaciers vs. proximal glaciers

In addition to the six primary glaciers where we directly measure surface mass balance, our LiDAR surveys also covered an additional 74 glaciers covering 69 km^2 near our primary glaciers (Figure 4.7). Geodetic balance for these proximal glaciers relative to the primary study glaciers is 6% greater on average in winter, identical in summer, and 14% (0.09 m w.e.) less negative in Ba (Figures 4.11 and 4.12). Our six comparison glaciers have 8% more of their relative area at lower elevations (1800-2500 m), 13% less at mid-elevations (2500-2900 m), and 4% more at altitude (2900-3300 m) relative to the additional proximal glaciers (Figure 4.13). The average size of proximal glaciers (0.88 km^2) is six times less than that of our study glaciers, (5.4 km^2), with median size of 0.24 km^2 and a range from 0.03 to 11.81 km^2. The Illecillewaet and Conrad glaciers had the largest discrepancy in Bw at 18% and 15% more snow on proximal glaciers to each respectively (Figures 4.8 and 4.12). Interestingly, the Illecillewaet Glacier also had the least disagreement between Ba estimates at 3%. The largest net differences in Ba was that of the Nordic Glacier, which experienced 0.42 m w.e. less mass loss than its proximal glaciers. For Nordic Glacier, 12 of its 17 proximal glaciers are south facing (Figure 4.7). In all but four instances, individual comparisons were within 2σ uncertainties (Figure 4.12).

Figure 4.11 *Geodetic balance for the six study glaciers plotted against geodetic balance for the glaciers near each study glacier which are also captured during each LiDAR survey. E.g. when flying the Conrad Glacier LiDAR survey, 31 glaciers in addition to the Conrad are captured; here their average mass change is plotted against that of Conrad Glacier. Proximal glaciers have a 3% percent greater snowpack (p-value 0.02), 2% less summer mass loss and 16% (0.10 m w.e.) less annual mass loss.*

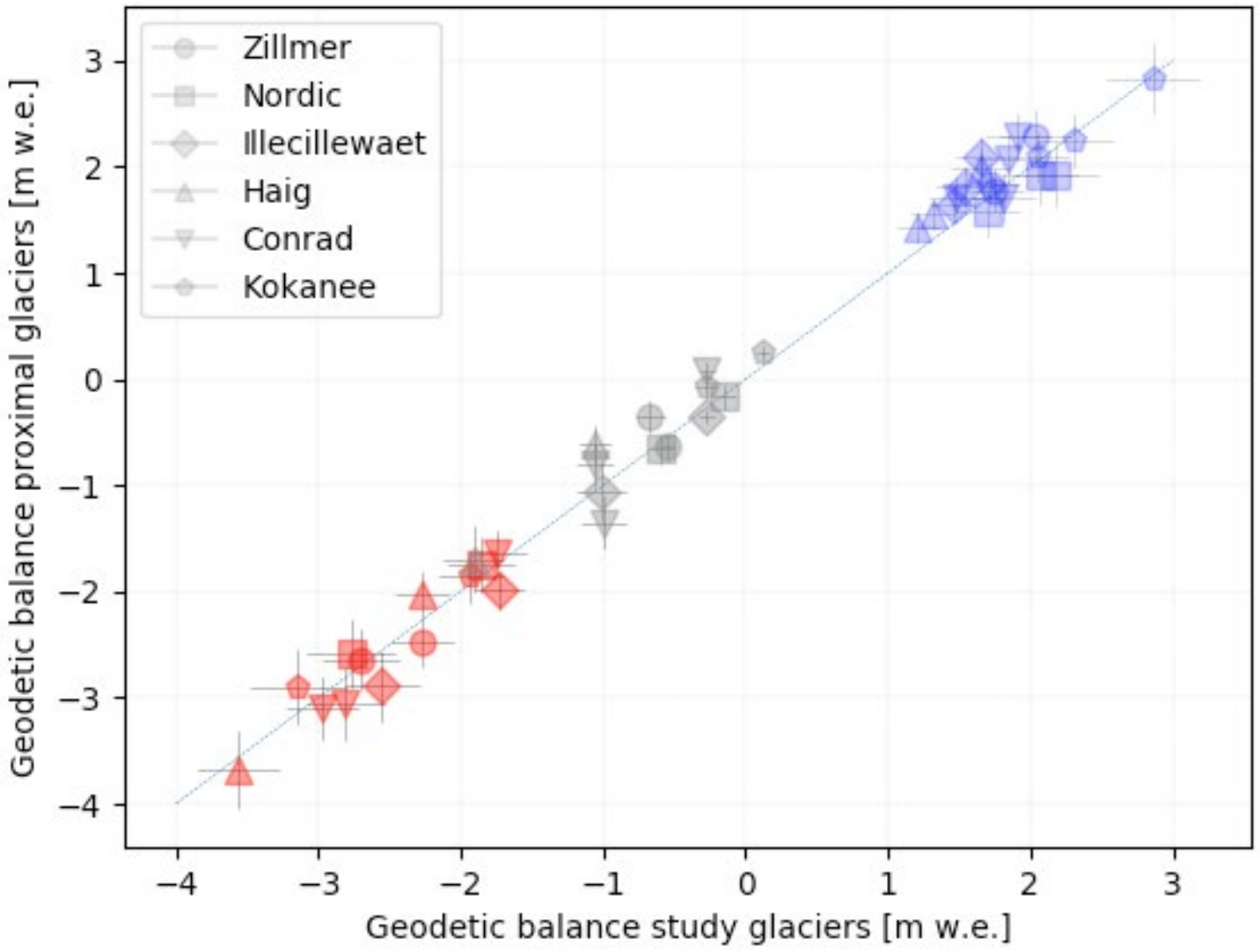

4.3.1.6 Glacier hypsometry

Our study glaciers were selected as representative glaciers for ice in the Basin. The glaciers cover 32.5 km^2 (2% of Basin ice), whereas our LiDAR data surveys cover 101 km^2, or 6% of Basin ice. The mean elevation of our study glaciers is 2530 m asl, 20 m higher than the average elevation of glaciers in the Basin (Figure 4.13). In the Basin, 47% of ice exists between 2400-2700 meters, outside of these mid-elevations, 19% exist below 2400 m, and 21% above 2700 m. The six glaciers chosen for glaciological measurements have a very similar distribution to basin-wide ice, with 2% less area above 2700 m, 4% more elevation between 2400-2700 m and 1% less below 2400 m. Our total LiDAR survey ice footprint has relatively more ice at mid-elevations (58%) and less ice at low elevations (13%). Unlike basin-wide ice, our study glaciers do not extend below 1700 m, yet there is only 3.1 km^2 ice in this 1300-1700 m range, less than 0.2% of ice area in the Basin.

Our study glaciers sample the north-south range of the Basin, with the Zillmer in the far north, and Kokanee to the far south. With the Haig Glacier, we capture the eastern edge of the Basin, however we do not have mass balance estimates from the Clemenceau Icefield area, home to the largest concentration of ice in the Basin, nor in the Monashee Mountains, at the eastern edge of the Basin, home to around one-fifth of glacier area in the Basin.

Figure 4.12 *Geodetic seasonal and annual mass balance for the six study glaciers versus the other surveyed glaciers proximal to each for every balance year from 2014 to 2018 with 1σ uncertainties. A) 2014 to 2015 balance year, B) 2015 to 2016 balance year, C) 2016 to 2017 balance year, D) 2017 to 2018 balance year.*

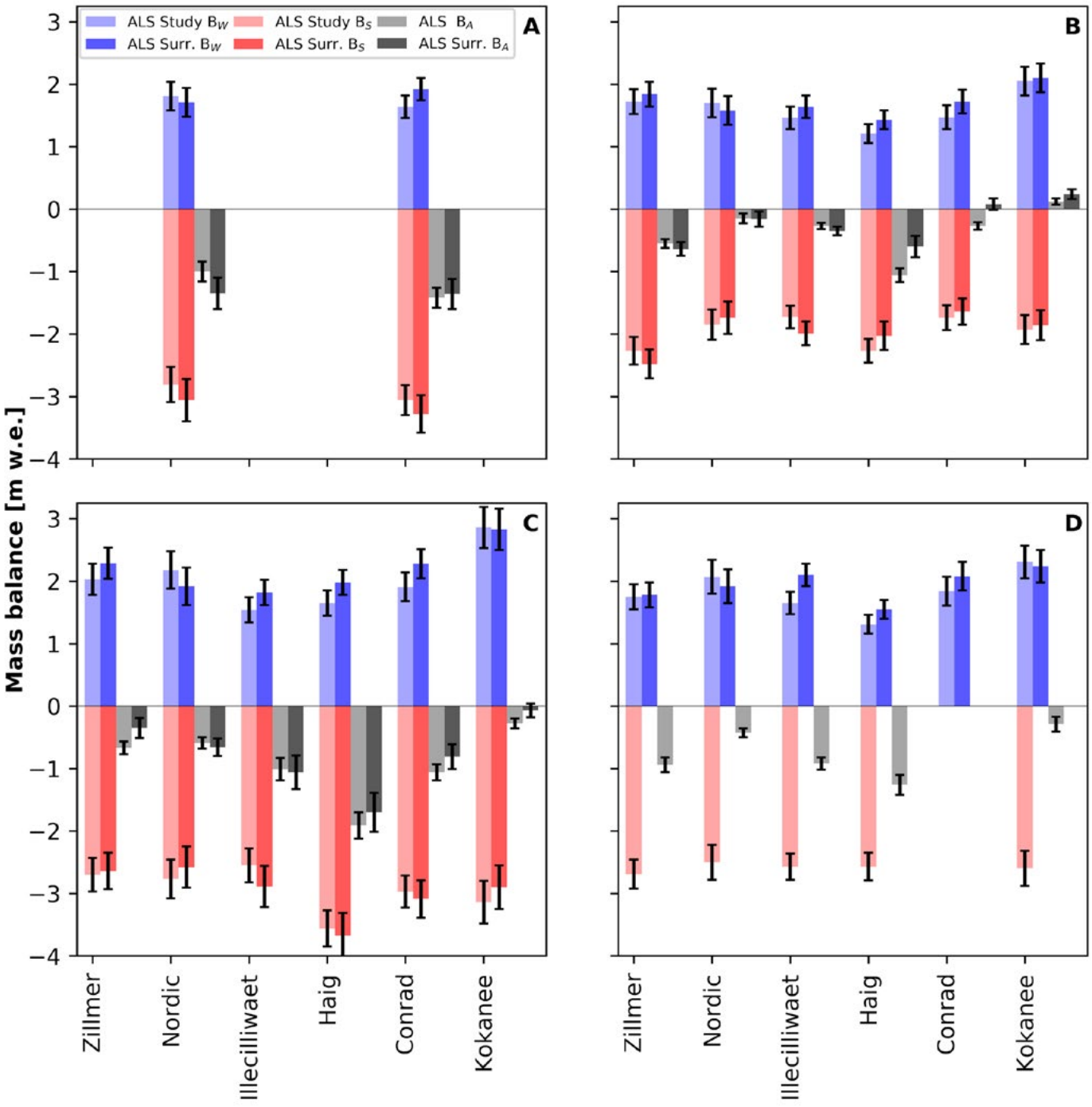

Figure 4.13 *Area altitude distribution for all glaciers in the Columbia Basin (1752 km2), the six study glaciers (32.5 km²), and all glaciers captured by the LiDAR surveys (101.6 km²). Mean elevations are 2509, 2533, and 2527 m, respectively. Lower mean basin elevation is in part due to the glaciers of the Clemenceau Icefield and Columbia Icefield area which extend to lower elevations, but primarily due to the nature of the LiDAR surveys. The surveys are targeted to capture our study glaciers, and often miss the termini of other proximal glaciers. Glaciers with incomplete coverage are not used in our surrounding glacier analyses, which preferentially removes around 20-30 glaciers which extend to lower elevations.*

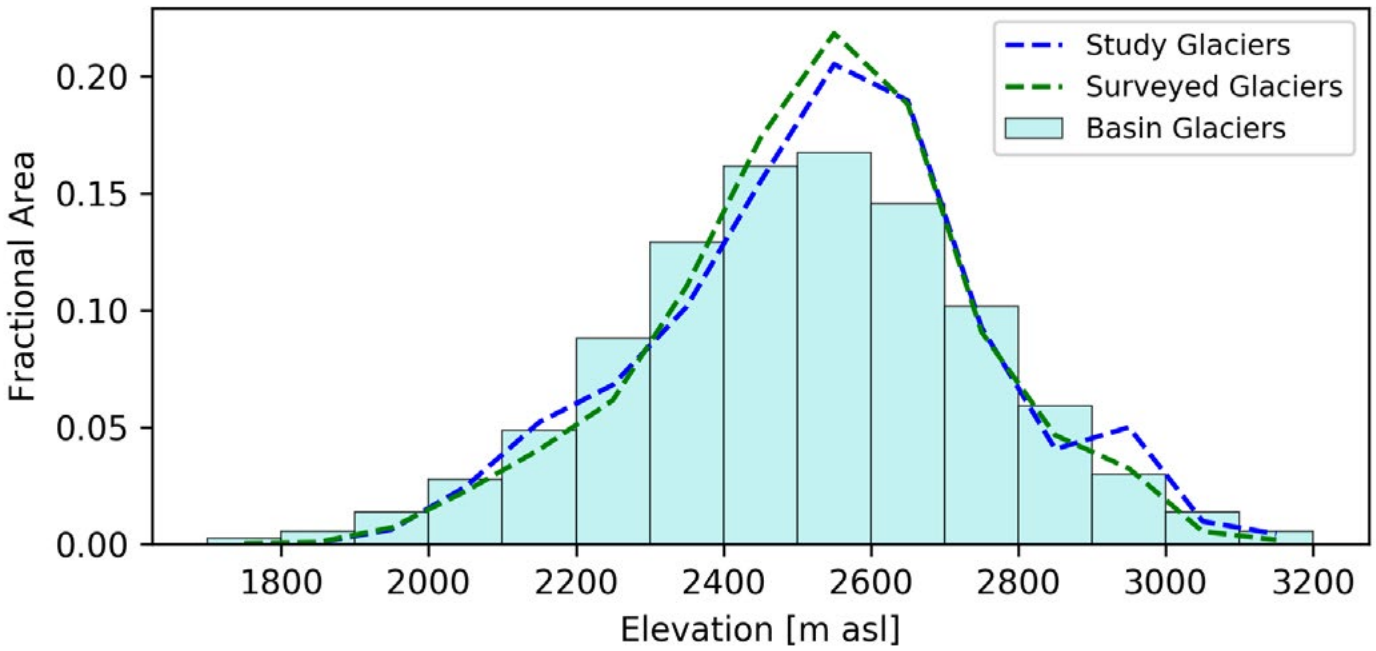

4.3.2 Ice thickness observations

Our ice thickness measurements provide a new dataset of ice thickness in the Columbia River Basin. In total, 189 km of data were collected by UNBC (Table 4.5) across five glaciers. Of these transects, bedrock reflections (Figure 4.14) were detected for 175 km of data and over 34,000-point measurements of ice thickness. We observe that the Conrad Glacier is the thickest of our study glaciers at 135 ± 5 m, and Kokanee Glacier is the thinnest at 46 ± 4 m. Our maximum observed depth is 318 m on the Conrad Glacier. We compared our ice thickness estimates against thickness estimates derived through surface inversion methods (Huss and Farinotti 2012; Farinotti et al. 2019; Clarke et al. 2013) and found that measured ice was about 20% thicker relative to modeled estimates of ice thickness.

Figure 4.14 *Ice thickness of Illecillewaet Glacier as measured by ground penetrating radar. Maximum ice thickness is 260 m and average ice thickness is 107 m. Data collected in May 2018.*

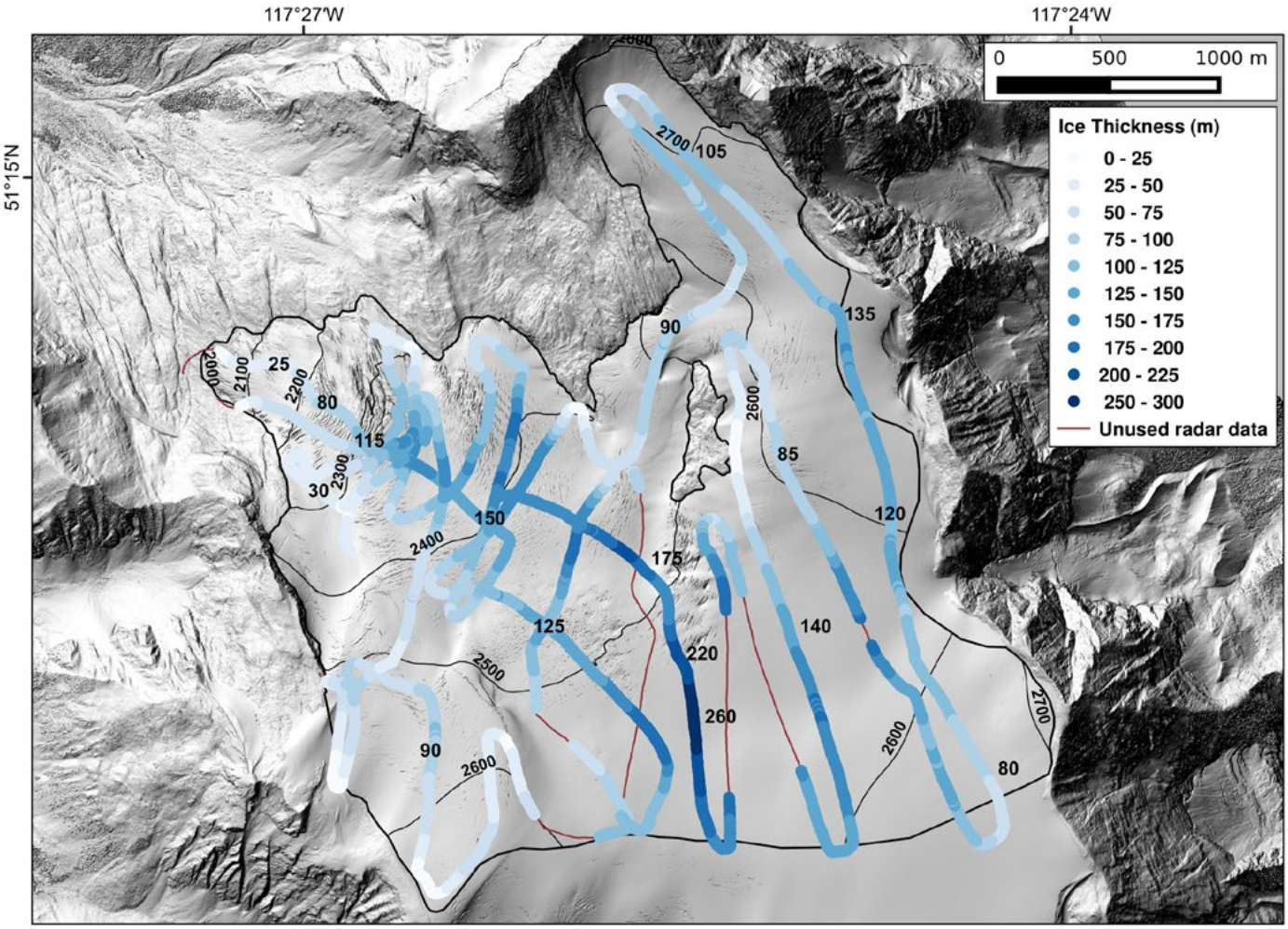

4.3.3 Area change

Trend analysis of glacier area using Landsat imagery over the period 2000–2018 reveals that the total glacier area in the Columbia Basin, on average, shrunk by 0.47% per year. Total area in the Basin in 2018 was 1749 ± 50 km^2, down from 2252 km^2 in 1985, a loss of 20.5%.

4.3.4 Regional mass change

Trend analysis of elevation change using ASTER imagery over the period 2000–2018 (Menounos et al. 2018) reveals that glaciers in the Columbia Basin, on average, thinned annually by -0.42 m. When multiplied by the total surface area of ice in watershed (1,750 km^2) and ice density (850 kg m^{-3}), this thinning corresponds to a basin-wide annual estimate of mass loss of -0.36 ± 0.19 m w.e. Over the period 2000–2018, glaciers in the Basin lost 11.34 gigatons.

4.4 Discussion

4.4.1 Mass change observations (5 year)

4.4.1.1 Glaciological vs. geodetic balance

The consistency between our geodetic and glaciological seasonal balance estimates for six glaciers over multiple years implies that high-resolution geodetic surveys can be used to reliably measure both winter and summer mass balance. Our study builds upon previous work, which established the feasibility of geodetic methods to accurately produce B_w (Belart et al. 2017; Sold et al. 2013), and B_a (Klug et al. 2018). While others have shown that geodetic surveys can be applied for a single winter (Belart et al. 2017; Sold et al. 2013) or for one glacier over a number of years (Klug et al. 2018), our study showed that remotely-measured seasonal balance is possible for multiple glaciers across entire mountain ranges (Figure 4.1). Though only spanning five balance years, our records captured a wide-range of variability in accumulation and ablation rates. Rather than rely on our glaciological data to inform our geodetic estimates, we instead produced independent estimates of density, and used our glaciological data to better constrain the uncertainty on, and compare against, geodetic seasonal balance.

4.4.1.2 Glaciological observations

We notice that particularly at high elevation (2500–3300 m), different areas of the glacier occupying the same elevation bands experience greatly differing snow depths (Figure 4.9) (Machguth et al. 2006). These differences were relatively consistent year to year (Helfricht et al. 2014b; McGrath et al. 2018, 2015), and are primarily due to preferential deposition of snow (Dadic et al. 2010) and snow redistribution (Grünewald et al. 2013). Our glaciological observations and balance gradients (Figure 4.10) thus illustrate that the spatial pattern of seasonal snow depth is similar from year to year, a finding that accords with other studies (McGrath et al. 2018; Sold et al. 2016).

The greater B_{w_glac} of 2016 on Conrad Glacier is likely due to both snow accumulation between the glaciological visit and LiDAR survey, and to the late summer 2015 LiDAR survey missing the lowest reaches of the glacier. We estimated the snow depth for the lower reaches of the glacier based upon the ratio of snow depth observed there for other years relative to the rest of the glacier, and snow depths along the cut-off margin. The B_w discrepancy for Zillmer Glacier in 2016 is likely due to a bias in our glaciological sampling, as the east transect (Figure 4.2), which has a shallow snowpack (Figure 4.9), was not sampled, and the 30-day difference between field and LiDAR survey date (Table 4.1) may not be fully resolved by the GPS survey correction.

As described in Pelto et al., (2019) we utilized in situ GPS surveys of the glacier height which were then compared with LiDAR DEMs. Challenges in using this method include: 1) fresh snowfall in spring or late-

summer, between the GPS and LiDAR surveys; and 2) significant densification of the snowpack in spring.

4.4.1.3 Geodetic observations

The small values of elevation uncertainty and bias (Table 4.2) indicates that these error sources are minor, but they still require quantification (Joerg et al. 2012; Klug et al. 2018). As described below, density distribution and conversion factors comprise a large portion of total mass change uncertainty, with firn compaction, fresh snow at the time of LiDAR acquisition, and changing crevasse bridging also contributing.

The spatial coverage of LiDAR is superior to glaciological observations; however, isolating the snow-depth portion of surface height change at a given location requires estimates of dynamical influences on elevation: vertical ice velocity and firnification (Belart et al. 2017; Sold et al. 2013). To date, studies have differenced glaciological and geodetic surface height change and assigned the difference to these processes (Belart et al. 2017; Sold et al. 2013; Beedle et al. 2014). Future efforts will use an ice dynamics model to account for these processes.

Converting volume change to mass change is a major challenge for geodetic studies (Huss 2013; Moholdt et al. 2010). Over multiple years to decades, a constant value of density can produce tolerable uncertainty in mass change (Huss 2013). For shorter timescales, and particularly for seasonal balance, a careful consideration of density is necessary (Klug et al. 2018). Klug et al (2018) used LiDAR intensity data and satellite imagery for a pixel-based classification the glacier surface as firn and ice. Our mapping built on this work and mapped areas of ice, but also distinguished between snow and firn (Pelto et al. 2019).

4.4.1.4 Interannual and spatial variability

Our study captured variable accumulation and ablation rates. We observe that the magnitude of B_s is consistently greater than B_w, leading to mass loss over the period of study (Figure 4.6).

Observed mass loss over this three-year period is consistent with that observed in the North Cascades, Canadian Rockies, BC southern coast mountains, and Juneau Icefield of southeast Alaska (Pelto 2018; WGMS 2018). The 2015-2016 winter season had the thinnest snowpack (Figure 4.9), yet the least mass loss (Figure 4.7), while the snowpack of winter of 2016-2017 delivered the greatest snowpack but featured heavy mass loss. The northeast pacific high-pressure ridge was positioned far from the coast, limiting the intensity of hot days and the duration of hot stretches. July 2016 was cooler than average and was a major departure from July 2015 which was abnormally hot (normal data are from the 30-year climatological baseline period 1981 to 2010 from Environment Canada, Water Survey of Canada, and BC Hydro data). Together a cool July and wet September 2016 limited ablation despite a hot and dry August. The 2015 balance year featured record mass loss for western North America for most reporting glaciers (Pelto 2018; WGMS 2018), and was

the year of greatest mass loss for our sites, yet had a winter balance within 0.01 m w.e. of 2016, our year of least mass loss. Winters 2015 and 2016 had around 62% of May 1st SWE for the Columbia Basin, with a record low SWE for two of the three catchments of the Basin in 2015, only to have the East Kootenay record broken in 2016 (May 1st snow survey, 1985–2015, BC River Forecast Center). Winter 2017 brought 129% of average annual snowpack to the Basin, yet the balance year went on to produce strong mass loss (Figure 4.6). The Columbia Basin was severely hot and dry throughout summer 2017, caused by strong high-pressure ridging, and the worst fire season on record, erasing the strong winter balance. Winter balance is clearly a critical component of annual balance, but under the current climate, only the ablation season can be deemed predictive of whether a given year will be a positive or negative balance year.

Kokanee Glacier, our southernmost site (Figure 4.1), was observed to have the greatest snowpack in all four years averaging 2.34 ± 0.30 m w.e (Table 4.2 and Figure 4.6). Haig Glacier had the lowest Bw, averaging 1.37 ± 0.11 m w.e., and the highest mass loss (average B_{a_glac}: -1:62 ± 0.34 m w.e.).

The lowest observed winter accumulation per our results and the BCRFC occurred in the 2014–2015 and 2015–2016 winters. Following these winters we had both our year of least mass loss (2016), and our record for negative mass balance (2015) as seen across western North America (Pelto 2018; WGMS 2018). The record winter snowpack of 2017 in southeastern BC was also followed by heavy mass loss (Figure 4.6).

4.4.1.5 Balance gradients

Balance gradients, observed from glaciological data, indicate relative stable gradients for both winter accumulation and summer ablation. In specific years, however, the accumulation gradient deviates from the norm at high or low elevations. In 2017, for example, snow depth on Conrad Glacier reached a maximum below the head of the glacier, likely due to decreased wind redistribution or wind velocity during precipitation (Grünewald et al. 2013, 2014; Dadic et al. 2010). Snow depth on the terminus of each glacier was commonly thinnest. However, some years defy this trend, where on Zillmer Glacier in 2017 snow depth there was 3 m, an increase over the elevation bands immediately above, compared to 2016 when the terminus had a thin snowpack of ~1m (Figures 4.8 and 4.10). While such variability is of interest in terms of physical processes that control glacier mass balance, most of the area, and thus the mass of the glacier, is at the middle elevations. Over the main body of the glaciers, winter balance gradients were remarkably consistent. The elevation of maximum SWE occurs about two-thirds of the elevation range up-glacier from the terminus.

4.4.1.6 Study glaciers vs. proximal glaciers

In measuring 101 km^2 of glaciers, we sample 6% of the total glaciated terrain of the Columbia Mountains. The greater winter balance recorded for the six glaciers relative to those sampled with our LiDAR surveys

(Figure 4.11) likely arose from differences in elevation (Figure 4.13), aspect and morphometry. That our study glaciers were on average six times larger than the proximal glaciers may also impact snow retention and ablation. Discrepancies in annual balance may be due to density assumptions; the ratio of glacier covered by snow, firn and ice of the study glacier is taken as that of the surrounding glaciers. Agreement between mass balance estimates from our study glaciers compared to their proximal glaciers (Figures 4.11 and 4.12), suggests that our study sites are a reasonable proxy for nearby glaciers despite these differences. Such accord holds promise for extrapolating the mass change and runoff for all glaciers of the Basin but is beyond the scope of this report. Additional analysis could assess the relation between elevation change and morphometric characteristics of the glaciers (Schiefer et al. 2008).

4.4.2 Ice thickness

Our ice thickness data reveals that glaciers are around 45-135 m thick on average, about 20% thicker than estimates provided through surface inversion methods. These thickness data (Figure 4.14) and our mass balance observations are currently being used to help improve modeled estimates of ice volume for the Columbia River Basin. That our measurements were consistently thicker than previously modeled (Huss and Farinotti 2012; Farinotti et al. 2019; Clarke et al. 2013) suggests current estimates of total ice volume are an underestimate. This suggests Basin glaciers will provide a slightly greater runoff than based on current ice volume, but this additional thickness may not impact the ultimate survival of glaciers in the Basin (Clarke et al. 2015).

4.5 Conclusions

Estimates of seasonal mass balance presented here show strong agreement between glaciological and geodetic estimates on a glacier-by-glacier basis. The agreement and the similarity between glaciological estimates of mass change for the benchmark glaciers and those estimates of mass change captured in the LiDAR surveys suggest that geodetic methods could be reliably used to sample seasonal balance for many hundreds of glaciers within the Basin. This approach, however, cannot estimate snow density without ground-based measurements, and cannot be used to produce mass balance gradients, an important dataset to help improve regionally distributed mass balance models. Expenses incurred for glaciological versus geodetic surveys were similar. Our field surveys covered six glaciers (32 km^2) whereas the LiDAR surveys sampled 101 km^2 of terrain, thus a three-fold increase in glacier area studied.

The hydrologic cycle of western North America is dominated by snowfall in the mountains, however, observations of alpine snowpack above 2000 m are sparse. As climate continues to change, there is a growing need for a more detailed understanding of seasonal balance of glaciers and snowpack. Across

the vast landscapes of western North America, geodetic methods are needed to supplement in situ observations, to meet this knowledge gap and improve our understanding of mountain snowpack and glacier response to climate change. To date, most high-resolution geodetic balance studies of seasonal or annual balance have been conducted in regions such as the European Alps, where extensive glaciological data exist and have a long history (Zemp et al. 2009). Our study provides further evidence that geodetic methods can be used to assess seasonal balance of glaciers, even in mountain ranges lacking long-term records of mass balance, as long as density is carefully considered (Belart et al. 2017). Recent advances in satellite technology (Marti et al. 2016; Berthier et al. 2014) suggest that such efforts can be made with increasing spatial and temporal coverage, greatly adding to our understanding of mountain hydrology, on which so much depends, but so little is known.

4.5.1 Glacier mass balance conclusions

While short in duration, our mass balance measurements over the five-year study captured a wide array of balance conditions. Melt seasons exhibited great variability, from the anomalously warm summer of 2015, to the cool summer of 2016, and smoky, hot 2017 and 2018 summers. From 2014-2018, negative mass balance dominated, however, we documented a wide array of accumulation and ablation rates. The lowest observed winter accumulation per our results and BCRFC observations occurred in the 2014-2015 and 2015-2016 winters. Following these winters, was the year of least mass loss (2016), and our record for negative mass balance (2015) as seen across western North America (Pelto 2018; WGMS 2018). The record winter snowpack of 2017 in southeastern BC was also followed by heavy mass loss (Figure 4.6). This indicates the propensity for melt-season conditions to overwhelm accumulation variability; an above average winter snowpack does not equate to positive mass balance in the Columbia Mountains.

We find that our glaciers lost an average of 0.73 m w.e. a-1 from 2014-2018. Menounos et al. (2018) found that glaciers lost an average of -0.65 m w.e. from 2009-2018 across the Basin. Agreement between our data and Menounos et al. (2018), suggest that our glaciers are representative of the entire Basin, and that the current rate of mass loss is a four-fold increase in mass loss relative to 2000-2009.

The Columbia Mountains are characterized by high winter balance (Table 4.2) and steep balance gradients (Figure 4.10). Maximum accumulation was observed around 2600 m, close to the observed average ELA during this study (Table 4.2), with snow depth levelling off before slightly decreasing at the highest elevations (Figure 4.10). More precisely, maximum snow depth occurred within 50 m of two-thirds of the elevation range up-glacier from the terminus. Snow density was consistent in the late-summer, with spring density showing far greater variability, partly dependent on the time of the field visit (mid-April vs mid-May), and whether a significant period of warmth had occurred prior to the visit. Snow depth was far more variable than snow density in both seasons, consistent with many studies (Elder et al. 1991).

CHAPTER 5: STREAMFLOW

Authors: R.D. (Dan) Moore, Dave Hutchinson, Ben Pelto and Brian Menounos

5.1 Introduction

This chapter has the following objectives to:

- Characterize the hydrologic regimes in the Canadian Columbia River Basin (the Basin) (Basin), with a focus on the contrast between glacier-fed and non-glacier-fed streams,
- Depict historical variation and trends in August streamflow, which can include significant contributions from glacier melt,
- Quantify vulnerability of water supply from glacier loss, including the contribution to flow from glacial wastage at Nordic Creek and Canoe River, and
- Assess the representativeness of the five-year enhanced monitoring period in the broader context of the last four decades.

This chapter begins by providing an overview of streamflow data in the Basin in relation to the characteristics of the gauged catchments. This overview is followed by four chapters that present the results of data analyses to address the key objectives, followed by a discussion and a summary of key results. All analyses were performed using the R programming language (R Development Core Team 2013).

5.2 Streamflow data sources in the Basin

This study used long-term records of streamflow at gauges operated by the Water Survey of Canada (WSC) and obtained through Environment and Climate Change Canada's National Water Archive (Environment And Climate 2018) (Environment and Climate Change Canada, 2018). Hydrometric data were accessed using the R package *tidyhydat*. Catchment characteristics were generated by intersecting catchment boundary polygons with other spatial layers, including a raster map of the Biogeoclimatic Ecological Classification (BEC) zones and polygons of glacier cover for 1985 and 2005, using functions in the *sf* package. Catchment polygons were accessed via Government of Canada (2019), while the BEC zone data were extracted using the *bcmaps* package (Teucher, A., Hazlitt, S., & Albers, S. 2018).

Analyses focused on the period from 1977 to present to avoid potential complications associated with the 1976–1977 shift in the Pacific Decadal Oscillation, which influenced streamflow throughout western North America (Whitfield et al. 2010). Stations were selected based on the following criteria: (1) currently active, (2) established prior to 1977, (3) unregulated flow, (4) drainage area less than 10,000 km^2, and (5) at least 36 years of record from 1977 to present to maximize statistical power and ensure the stations represent a common period of record. In addition, this record length permits the application of multiple regression models with three predictor variables. A total of 35 stations met all the criteria.

The subset of hydrometric gauges selected for analysis monitor varying contributions from glaciers, from non-glacierized to a maximum of 18% glacier cover (for Canoe River, WSC station number 08NC004) (Figure 5.2). Generally, gauges on non-glacierized catchments are located in the southwestern portion of the Columbia Basin and have lower median elevations (Figures 5.1 and 5.2). Catchments with more than 2% glacier cover are generally greater than 100 km^2 in area and have median elevations greater than 1700 m (Figure 5.2). Glacier-fed catchments with areas under 100 km^2 are not represented in the selected subset. The Water Survey of Canada commenced operation of Nordic Creek at the outlet of Nordic Glacier (WSC station number 08NB020) in June 2015 to help address this gap in monitoring of small glacier-fed basins.

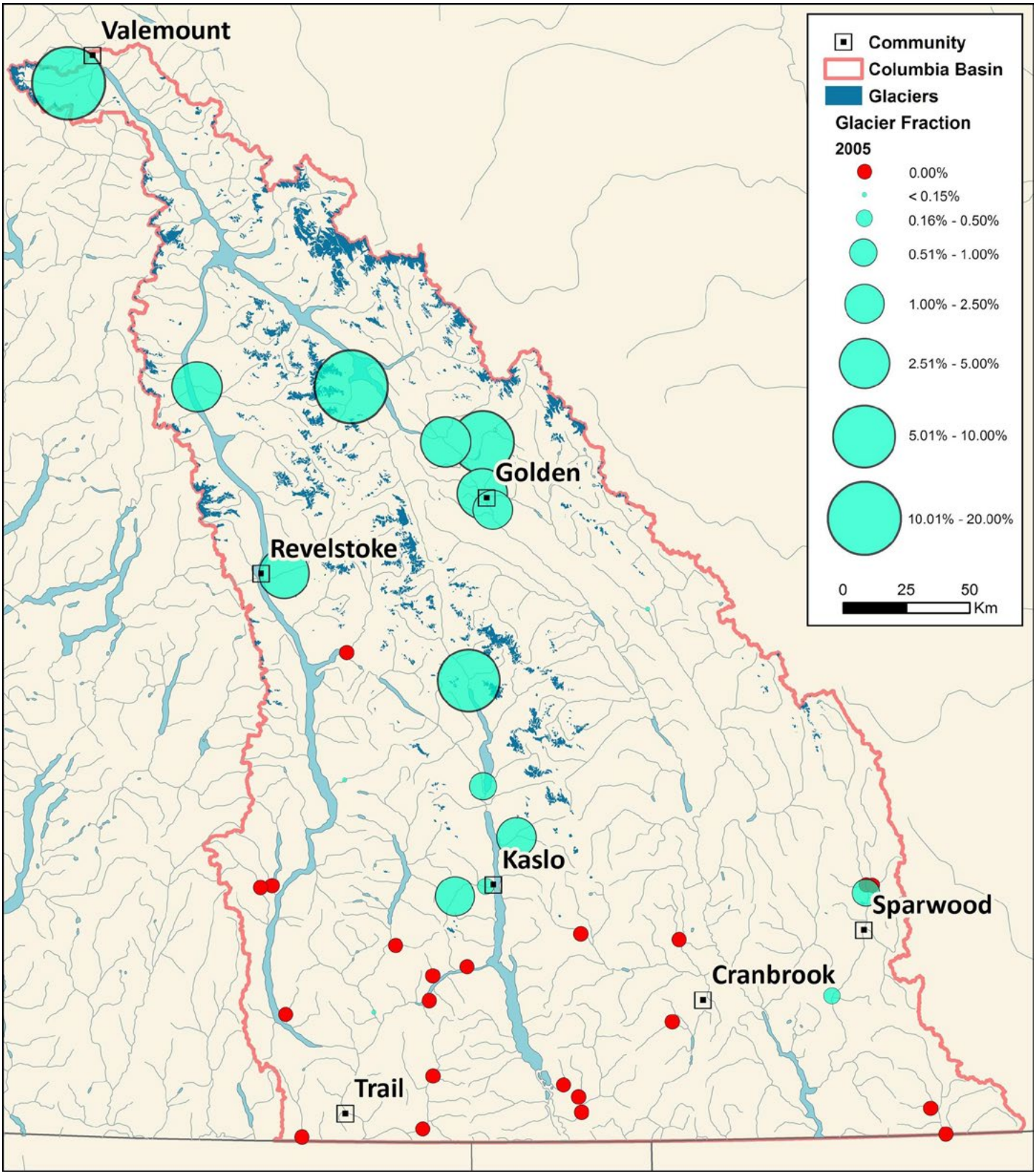

Figure 5.1 *Map of subset of hydrometric gauges operated by Water Survey of Canada (WSC) that were used in this analysis.*

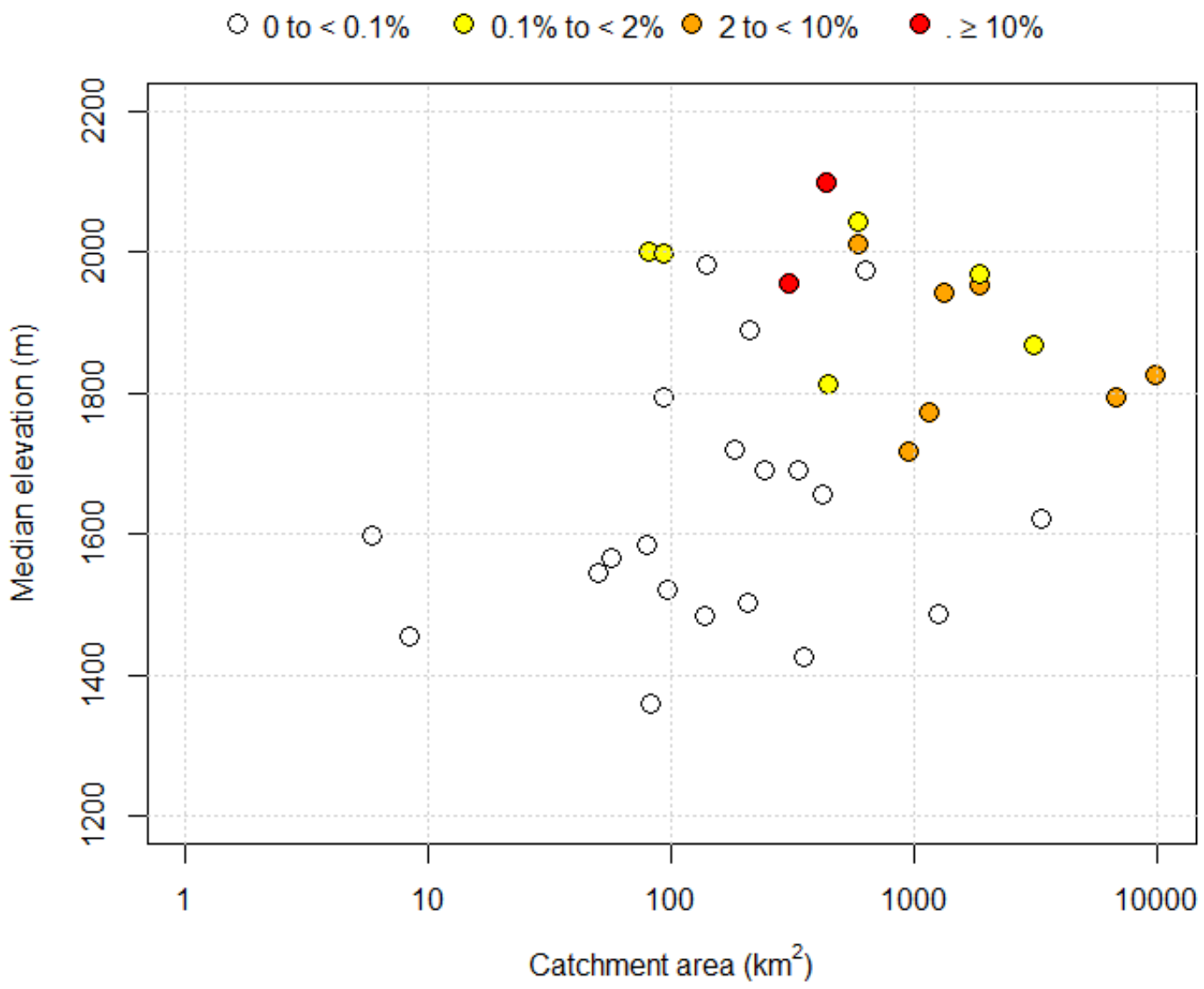

Figure 5.2 *Scatterplot of median catchment elevation vs drainage area for the subset of catchments used in this analysis. Symbol colour indicates catchment glacier cover.*

In 1985, the fraction of catchment glacier cover ranged from 0 to 0.19. Figure 5.3 presents the magnitude of the change in glacier cover in 2005 and 2013, relative to 1985. Although one glacier appeared to advance slightly from 1985 to 2005 ($f_g > 0$), the rest retreated. By 2013, all glaciers retreated, with all showing a net negative change relative to 1985. With the exception of the most heavily glacierized catchment, the amount of change in glacier cover generally varied linearly with the glacier cover in 1985, representing about a 20% decrease in glacier coverage between 1985 and 2013.

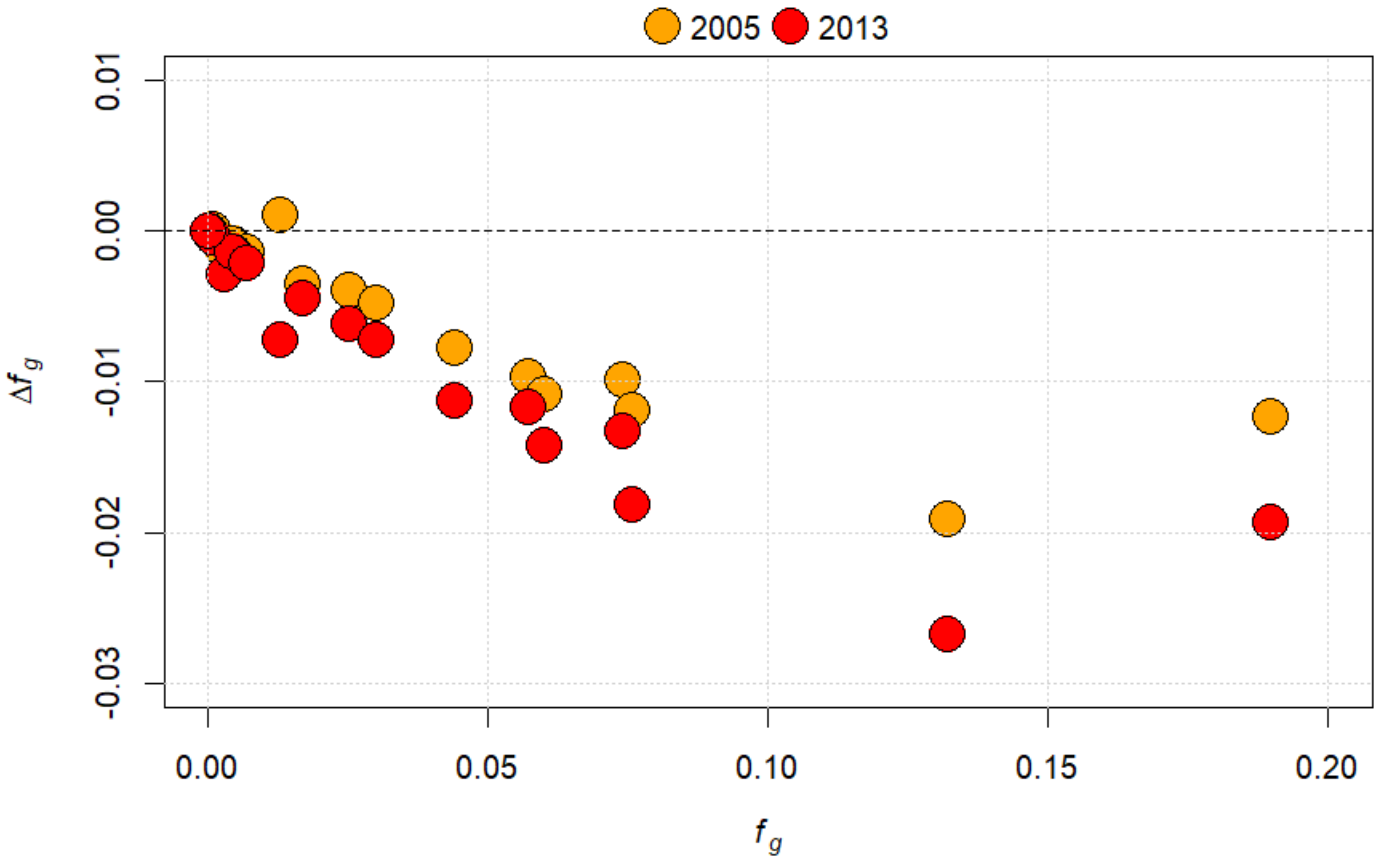

Figure 5.3 *Changes in glacier cover Δf_g between 1985 and 2005 and 1985 and 2013, plotted against glacier cover in 1985.*

5.3 Streamflow regimes in the Columbia River Basin

5.3.1 Introduction

"Streamflow regime" refers to the typical pattern of streamflow magnitude and timing over an annual cycle. It is commonly characterized by computing long-term average flows by month (Moore, R.D., Spittlehouse, D.L., Whitfield, P.H. and Stahl, K. 2010). In western North America, streamflow regimes can generally be characterised as rain-dominated, snow-dominated (nival), hybrid rain-snow regimes, and glacier-fed (Fleming et al. 2007).

Rain-dominated regimes in western North America have high flows during the autumn-winter wet season. They mainly occur in low-elevation catchments near the coast that receive the majority of their winter precipitation as rain, with high flows in autumn and winter and low flows during summer. Snow-dominated catchments typically lie at sufficiently high elevations or sufficiently removed from the moderating effect of the Pacific Ocean that air temperatures are low enough that most winter precipitation falls mainly as

snow. In these regimes, winters are dominated by low flows, and the bulk of annual streamflow occurs between April and June as a result of seasonal snow melt. Hybrid regimes commonly result in catchments in which lower elevations dominantly receive winter precipitation as rain, while higher elevations receive snow. Glacier-fed regimes are similar to nival regimes, except that high flows are sustained through July and August, and sometimes into September, by melting of glacier ice once the seasonal snowpack has melted.

The objective of this section is to characterize the streamflow regimes within the Basin, with particular attention to the influence of glacier cover.

5.3.2 Methods

Rather than using the raw mean monthly discharges or water yields, we computed Parde coefficients by normalizing each monthly streamflow by the long-term mean annual streamflow (Trubilowicz et al. 2013). We then followed the approach of Trubilowicz et al. (2013), who used a multivariate regression tree to classify streamflow regimes catchments throughout British Columbia.

Fitting a multivariate regression tree involves an iterative approach of cycling through a set of predictor variables. For each predictor variable, the algorithm finds a binary split that maximizes the difference among the objects with values above and below the threshold value. Following each split, the algorithm is applied to each group. The result is a tree diagram. Although the algorithm could be continued until each object (in this case, catchment) is in its own group, a cross-validation approach is used to determine an optimal stopping point so as to avoid over-fitting the model.

In this analysis, we used the *mvpart()* function in the R package mvpart. Predictor variables included the fractional coverage of the catchment by biogeoclimatic ecological classification (BEC) zone, fractional coverage by glaciers (based on the 1985 coverage), and median elevation of the catchment.

5.3.3 Results

As shown in Figure 5.4, the primary split in the classification tree is based on the presence of an alpine zone in the catchment, represented by the coverage of the IMA (Interior Mountain Alpine) BEC zone. Catchments on the left-hand major branch of the tree are those that have some coverage by alpine vegetation, whereas those on right-hand major branch lie entirely below regional treeline.

Catchments lacking an alpine zone have nival regimes, with the highest flows occurring in May. For these below-alpine catchments, the next splits are based on coverage dominated by the ESSF (Engelmann Spruce Subalpine Fir) BEC zone, which represents subalpine vegetation, and then by median catchment elevation. Catchments with > 63.7% ESSF coverage tend to have lower late-winter flows and higher flows in June

relative to those with less ESSF coverage. For the catchments with less than 63.7% ESSF, there is a subtle difference between catchments with median elevations above and below 1471 m, with higher catchments having a more even distribution of flow between May and June. Overall, for the below-alpine catchments, the main differences among regimes relate to catchment hypsometry, with higher catchments having lower late-winter flows and a snowmelt freshet that extends later into the summer.

For catchments with alpine coverage, the highest flows occur in June. There are three splits based on the fractional coverage by glaciers. As the fraction of glacier coverage increases, there is a tendency for late-winter flows to decrease and July flows to increase. Indeed, for catchments with greater than 2% glacier coverage, flows in June and July are roughly equal, and flows in August (and, to a lesser extent, September) are higher than for the other regimes.

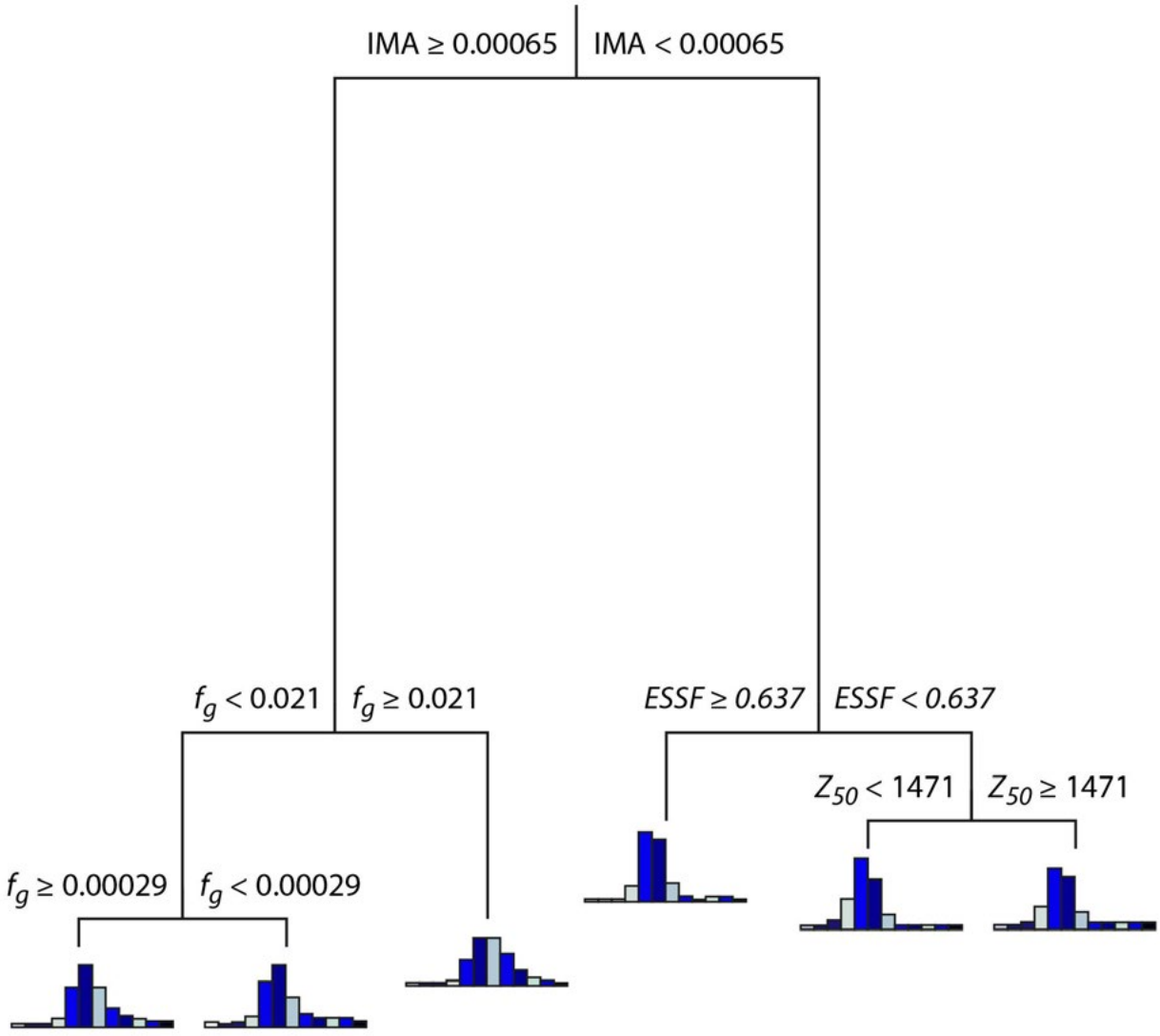

Figure 5.4 *Multivariate regression tree for classifying streamflow regimes in the Columbia River basin. The bars represent the mean monthly discharges, normalized by mean annual discharge, over a calendar year (Jan-Dec). IMA, ESSF and f_g indicate the fraction of the catchment covered by the Interior Mountain Alpine and Engelmann Spruce Subalpine Fir BEC zones and glaciers, respectively. Z_{50} is the median elevation.*

5.3.4 Discussion

The results indicate that the influence of glaciers on streamflow regime is detectable with as little as 2% glacier cover. Therefore, in the analyses to follow, 2% glacier cover will be used as a threshold to distinguish between catchments with and without significant glacier influences on streamflow.

5.4 Glacier influences on the variability of August streamflow

5.4.1 Introduction

Glaciers have a particularly important influence on August streamflow (Figure 5.4). Glacier-melt contributions not only maintain streamflow during the typically warm and dry weather in late summer, but also help maintain lower stream temperatures, which can be critical for cold- and cool-water fish species like bull trout (Moore 2006; Moore et al. 2013; Parkinson et al. 2016). The objective of this section is to document interannual variations and trends in August streamflow within the Basin, with a particular focus on the effects of glacier cover.

5.4.2 Methods

This analysis broadly followed the approach applied to all of BC by Stahl and Moore (2006). However, whereas Stahl and Moore (2006) standardized monthly streamflow data and predictor variables, we converted each monthly streamflow value from a mean discharge in $m^3 s^{-1}$ to a runoff depth in mm, and retained the predictor variables in their original units.

In addition to streamflow, the analysis involved time series of mean monthly air temperature and total monthly precipitation for each gauging station. These values were extracted from the ClimateWNA application for locations corresponding to the gauging station (Hamann et al. 2013). Because these values were used only as indices of the interannual variability of climatic conditions rather than as representative values for the catchment area, it was not necessary to correct for elevation differences. Glacier coverages for the years 1985, 2005 and 2013 were used to calculate fractional glacier coverage for each catchment, and its change through time.

A first analysis involved trend analysis of the August runoff time series by computing the Spearman correlation coefficient between August runoff and year. Regression analysis was then used to understand the drivers of interannual variability in August runoff (RO_{Aug}) (mm) by relating it to the following predictor variables: runoff in the preceding month (RO_{Jul}) (mm), mean August air temperature (T_{Aug}) (°C) and total

August precipitation (P_{Aug}) (mm). The inclusion of July runoff helps to account for effects of carry-over storage. Air temperature is an index of the magnitude of snow and ice melt as well as evapotranspiration from non-glacierized surfaces, and August precipitation represents the streamflow contribution from rainfall.

The regression model is:

[5.1] $$RO_{Aug}(t) = b_0 + b_1 \cdot RO_{Jul}(t) + b_3 \cdot P_{Aug}(t) + e(t)$$

where (b_i) are the estimated coefficients, (t) indicates year, and (e(t)) is the residual from the regression.

A further trend analysis was conducted on the residuals from the regression model. The logic underlying this analysis is that the three predictors account for external hydroclimatic influences and non-glacial storage influences, and that the residuals should contain information about any effects caused by internal changes in the catchment, particularly glacier retreat. Based on the degree-day melt model concept, we can express the sensitivity of glacier melt runoff to air temperature as follows:

[5.2] $$\frac{dM_{Aug}}{dT_{Aug}} = k_m \cdot n_d \cdot f_g$$

where (M_{Aug})is the glacier meltwater contribution to streamflow in August (mm), (k_m)is the degree-day factor (mm $\cdot^{o-1} \cdot d^{-1}$), and (n_d) is the number of days in August (31). By inspection, we can compute an apparent degree-day factor by combining Eqs. (5.1) and (5.2):

[5.3] $$k_m = \frac{b_2}{n_d \cdot f_g}$$

5.4.3 Results

5.4.3.1 Temporal variability of hydroclimatic variables

As seen in Figure 5.5 the variations in August air temperature and precipitation display a high amount of regional coherence, while July and August runoff are somewhat less consistent among stations. August precipitation displays a downward trend while August air temperature appears to have an upward trend between about 2005 to 2017.

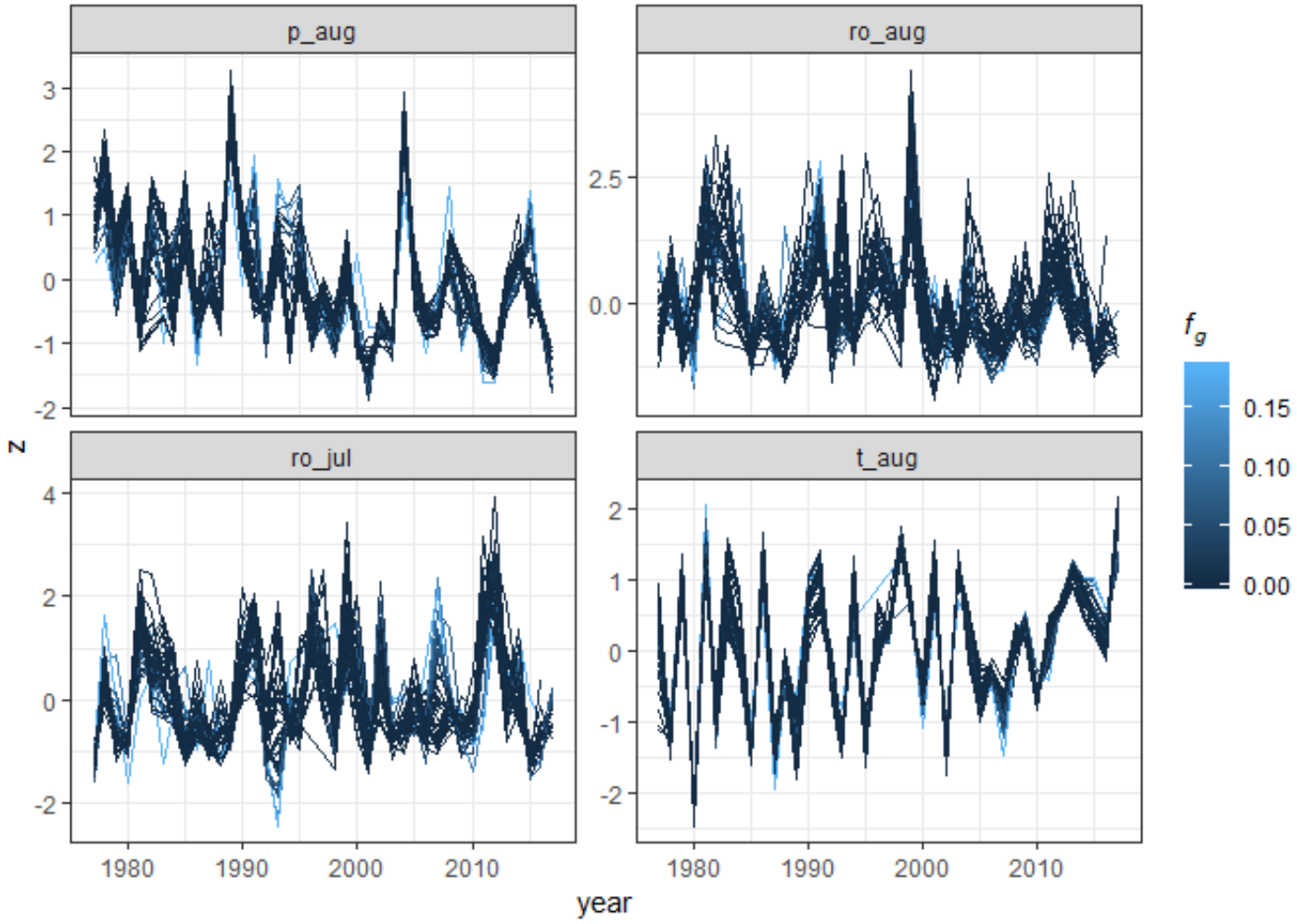

Figure 5.5 *Time series of August air temperature, August precipitation, and July and August runoff. Each trace represents a station. All data were standardized prior to plotting.*

5.4.3.2 Trend of August streamflow

Only two of the 25 catchments with less than 2% glacier cover had apparently significant trends. It should be noted that, when testing at (P)< 0.05, one would expect to find significance for 5% of the catchments, even if none had significant trends in reality. Considering the apparent decline in August precipitation and increase in August air temperature, one might expect to find declining trends in August streamflow. However, it appears that the substantial year-to-year variability in air temperature, precipitation and winter snow accumulation effectively obscures the expression of a negative trend in August water yield.

As seen in Figure 5.6, all of the catchments with more than 2% glacier cover had negative trends for August streamflow, although the trends were only statistically significant at (P)< 0.05 for three catchments (Table 1). Finding three significant trends out of nine catchments is substantially more than one would expect to find by chance if there were, in reality, no trend. For the six catchments for which the trends are not significant, it may be that the trend is obscured by the interannual variability in climatic conditions.

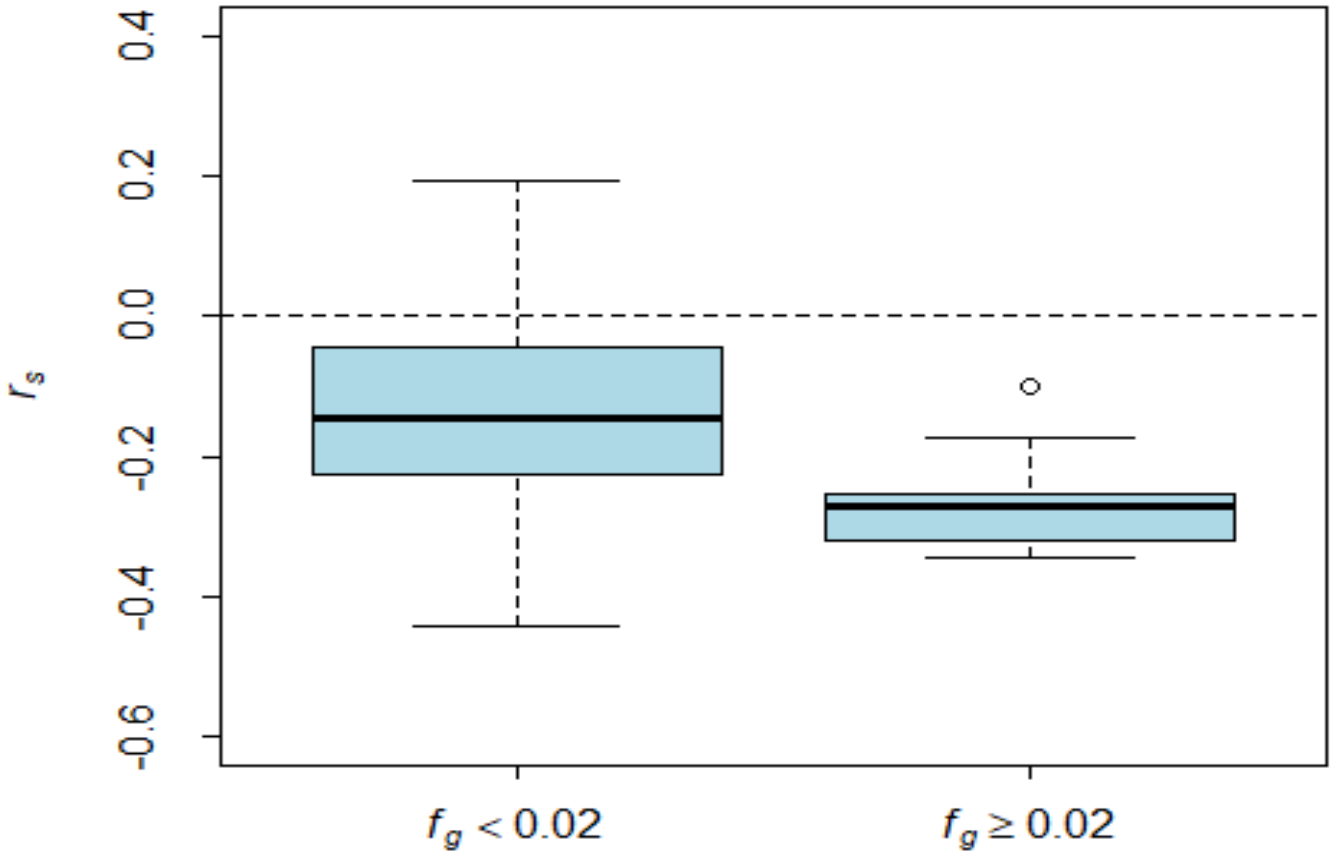

Figure 5.6 *Spearman's correlation coefficients (r_s) between August runoff and year binned according to fraction of glacier cover (f_g). Negative values indicate declining trends.*

Table 5.1 *Significance of trends in August runoff by glacier cover class, assessed using $p < 0.05$.*

	$f_g < 0.02$	$f_g \geq 0.02$
significant	2	3
not significant	24	6

5.4.3.3 Regression analysis

Figure 5.7 shows the relations between the fitted regression coefficients and glacier cover. Coefficient (b_1), which represents the effect of carry-over storage, is roughly 0.3, but declines for catchments with greater

glacier coverage. This result is consistent with our process understanding, in that high flows in July would be associated, in many years, with heavy snow accumulation and a late disappearance of snow. Persistence of snow on glaciers would reduce glacier melt runoff in August due to the higher albedo of snow relative to exposed glacier ice.

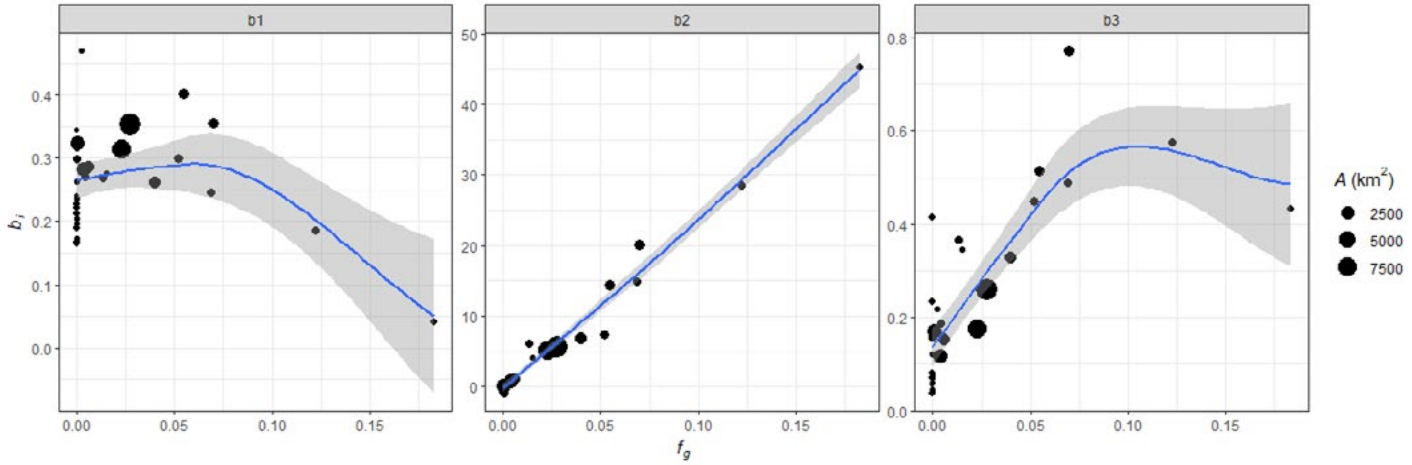

Figure 5.7 *Plot of fitted regression coefficients b_i against fractional glacier cover f_g. The trend lines are generated using the loess algorithm (span = 1, degree = 1). The grey bands represent 95% confidence limits on the trend lines.*

Coefficient (b_3), which reflects the effects of rainfall-runoff in August, tends to increase with glacier cover. This relation is consistent with the tendency for more heavily glacierized catchments to have higher elevations, and thus a greater orographic enhancement of precipitation. Coefficient (b_2) displays a linear relation with fractional glacier coverage. That is, the sensitivity of August water yield to August air temperature increases linearly with fractional glacier coverage, consistent with the conceptual model based on a degree-day melt model

(Eq. 2). The slope corresponds to a melt factor of km = 7.97 mm · day^{-1} · °C^{-1}. This value is somewhat higher than melt factors for ice derived for glaciers in western Canada by Shea et al. (2009), which averaged 4.6 mm · day^{-1} · °C^{-1}. However, the values derived by Shea et al. (2009) were for the entire ablation season, whereas the value of km derived here is based only on August.

5.4.3.4 Trend analysis of the residuals

As seen in Figure 5.8, all of the catchments with more than 2% glacier cover had negative trends for the residuals from the regression model, whereas catchments with less glacier cover exhibited both negative and positive trends. As seen in Table 5.2, none of the residual series had significant trends for catchments with less than 2% glacier cover. However, all but two of the eleven catchments with more than 2% glacier cover exhibited significant trends with time.

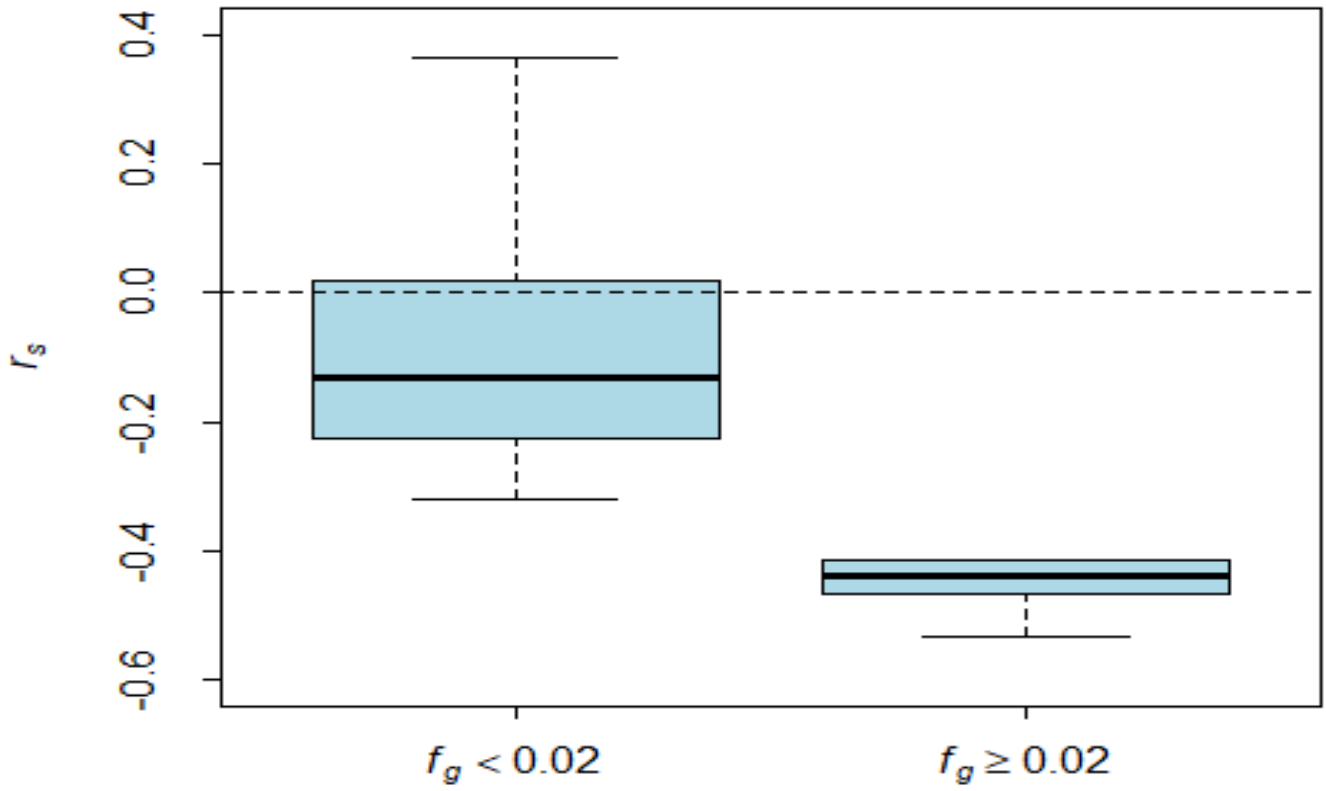

Figure 5.8 *Distributions of the Spearman correlation coefficient between the regression residuals and time as a function of glacier cover.*

Table 5.2 *Significance of trends in regression residuals by glacier cover class, assessed using $p < 0.05$.*

	$f_g < 0.02$	$f_g \geq 0.02$
significant	2	9
not significant	24	0

Through comparison of Figures 5.6 and 5.8, and the summaries in Tables 5.1 and 5.2, it is clear that the glacier-related negative trend is expressed more clearly after using the regression model to account for the effects of carry-over storage and climatic conditions in August.

5.5 Assessment of glacier wastage contributions to streamflow at Nordic and Zillmer glaciers

5.5.1 Introduction

The water balance of a catchment over a defined time interval can be expressed as

[5.4] $$Q - P - E - Q_{gw} - \Delta S_{ng} - \Delta S_g$$

where (Q) is streamflow, (P) is precipitation, (E) is evapotranspiration, (Q_{gw})is the water that leaves the catchment as groundwater, and (ΔS_{ng}) and (ΔS_g) are changes in non-glacial and glacial storage, respectively. All terms in Eq. (5.4) can be represented as an equivalent depth of water over the catchment (m). The change in glacial storage can be expressed as

[5.5] $$\Delta S_g = f_g \cdot b_n$$

where (f_g) is the fractional glacier coverage in the catchment and (b_n) is the specific glacier net balance (mm). Eqs. (5.4) and (5.5) can be combined to yield the following expression:

[5.6] $$Q = P - E - Q_{gw} - \Delta S_{ng} - f_g \cdot b_n$$

When the glacier net balance is negative, the last term in Eq. (5.6), ($- f_g \cdot b_n$), represents the wastage flux contribution to streamflow, denoted (Q_{wf}).

The objective of this section is to use the mass balance data collected at Nordic and Zillmer glaciers, along with the streamflow data measured downstream of the glaciers, to assess the contribution of the wastage flux to annual water yield for Nordic Creek and Canoe River.

5.5.2 Data sources

Mass balance data were collected at Nordic Glacier and Zillmer Glacier (the latter within the Canoe River catchment) using both geodetic and glaciologic methods (Pelto et al. 2019). See Chapter 4 for details. In this analysis, we use mass balances determined using the glaciological method.

Water Survey of Canada maintains stream gauges on Nordic Creek, just downstream of the glacier, and on Canoe River, which includes Zillmer glacier in its catchment (Table 5.3). Zillmer Glacier is just one of several glaciers that drain into Canoe River, so we assume here that its annual net balance is representative of all glaciers in the catchment.

Table 5.3 *Catchment characteristics for Canoe River and Nordic Creek*

Station no.	Station name	A (km^2)	f_g (1985)	f_g (2005)	f_g (2013)
08NC004	Canoe River below Kimmel Creek	305	0.189	0.177	0.17
08NB020	Nordic Creek at the outlet of Nordic Glacier	7.49	0.669	0.591	0.577

5.5.3 Results

As seen in Table 5.4, Nordic Creek has substantially greater water yield as a consequence of its higher median elevation. The wastage flux contribution to streamflow appeared to be more variable among years at Nordic Glacier, likely because a greater percentage of the gauged catchment area has glacier coverage (Table 5.3), allowing for greater glacier runoff contribution in years of large mass loss. The wastage flux contribution to Canoe River streamflow ranged from 8% to 13% of annual water yield and averaged 10.0%. The wastage flux contribution to Nordic Creek streamflow ranged from 9.0 to 19.3% of annual water yield and averaged 14.9%.

Table 5.4 *Glacier contributions to streamflow below Nordic and Zillmer glaciers. b_n is annual net balance, WY is annual water yield, and Q_{wf} is the glacier wastage flux contribution to annual water yield.*

Year	Glacier	b_n (m)	WY (m)	Q_{wf} (m)	Q_{wf} (%)
2015	Nordic	-1.310	3.925	0.756	19.3
2016	Nordic	-0.490	3.125	0.283	9.0
2017	Nordic	-0.900	2.852	0.519	18.2
2018	Nordic	-0.590	2.629	0.340	13.0
2015	Zillmer	-1.066	1.739	0.129	10.4
2016	Zillmer	-0.830	1.645	0.146	8.6
2017	Zillmer	-0.720	1.549	0.177	7.9
2018	Zillmer	-1.080	1.405	0.16	13.1

5.6 Representativeness of the five-year enhanced monitoring period

As seen in Figure 5.9, streamflow in catchments with greater than 2% glacier cover generally fell within the range of streamflow in the historic period from 1977 to 2014. However, there is a tendency toward higher flows in late winter and early spring in 2016. In 2015, 2016 and 2018, peak flow occurred earlier in the season compared to the historical period.

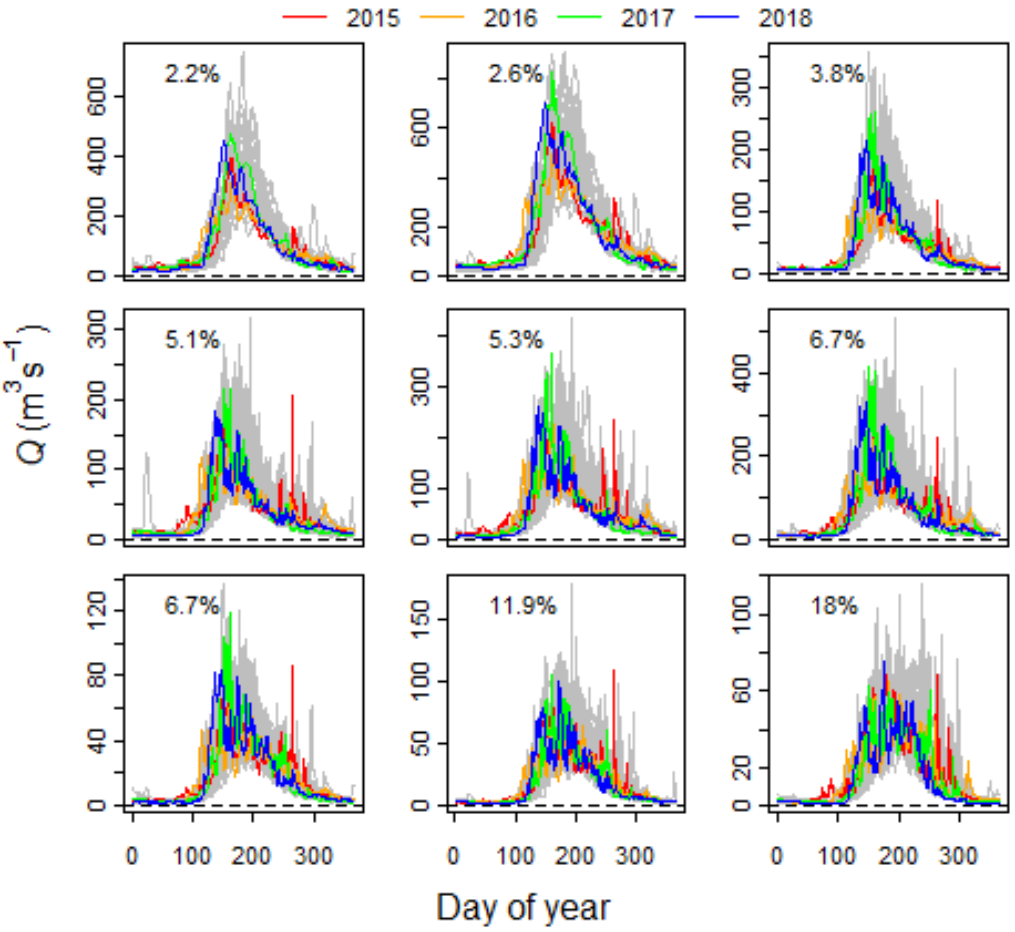

Figure 5.9 *Comparison of hydrographs of daily streamflow for catchments with more the 2% glacier cover (based on average of values for 1985 and 2005). Grey lines are for the 1977 to 2014 and the coloured lines are for the enhanced monitoring period: 2015 (red), 2016 (orange) and 2017 (green). Catchment glacier cover is shown in the left-hand corner of each panel.*

5.7 Summary of key results

Glaciers make important contributions to streamflow within the Columbia River Basin. For the more heavily glacierized catchments, such as Nordic Creek and Canoe River, the glacier wastage flux contributed on

the order of 12% of annual water yield, on average. However, this contribution varied from year to year, particularly for the high-elevation, highly glacierized Nordic Creek.

Glacier-melt contributions to August water yield are detectable even for catchments with as low as 2% glacier coverage. The magnitude of this contribution is linearly related to both August air temperature and the fractional glacier coverage within the catchment. The net effect of this contribution is to moderate inter-annual variability in August streamflow. For example, in a hot, dry August, when non-glacier-fed streams would experience extreme low flows, the increase in glacier-melt contributions would help maintain streamflow.

All catchments included in this analysis experienced retreat between 1985 and 2013, resulting in a decrease in glacier coverage ranging up to 2% of catchment area. All glacier-fed streams experienced negative trends in August streamflow, with three of the nine stations with more than 2% glacier cover exhibiting statistically significant trends. In contrast, catchments with less than 2% glacier cover exhibited no significant trends.

After statistically removing the effects of carry-over storage and August climatic conditions, August streamflow declined significantly in all nine catchments having at least 2% glacier cover. This finding indicates that the buffering effect of glacier melt -- that is, the ability of glaciers to maintain streamflow during warm, dry weather -- has declined in step with the decrease in glacier cover. It is anticipated that, as glaciers continue to retreat, the buffering effect of glaciers will also decline.

CHAPTER 6: SUMMARY OF FINDINGS AND IMPLICATIONS AND BIOGEOCHEMICAL AND ECOLOGICAL CONSEQUENCES OF GLACIER RECESSION

Authors: Janice Brahney, Ben Pelto and Brian Menounos

6.1 Introduction

Abundant snow and glacier melt from the Columbia Mountains provides the majority of the water resources to the Canadian Columbia Basin region as well as the downstream users. However, both snow and glacier melt contributions to streamflow in the Canadian Columbia basin are shifting as a result of anthropogenic climate change. Predicted changes include the loss of glaciers and their water tower effect as well as a loss of winter snow storage as greater proportions of winter precipitation fall as rain. This report as well as other studies have shown these predictions are underway and are expected to continue. These broad scale changes in regional hydrology are of widespread significance as these waters support several unique ecosystems including the world's only snowfed interior rainforest, fisheries, agriculture, and over 400 dams in the region that produce much of the energy needs for the Pacific Northwest. Importantly, the capacity for glacier melt to buffer drought years by supplying cold water in the later summer will diminish in the years to come. Beyond year to year variability, season shifts in the timing and volume of streamflow have ecosystem service implications (e.g. influence the Basin's capacity to store water) as well as ecological implications as the regions biota are largely adapted to pre-existing regimes. This chapter summarizes the findings of the network and discusses next steps and in broad terms the water quality and ecological consequences of cryosphere loss.

6.2 Summary of major findings from the five year study

Chapter two describes changes in temperature and precipitation over the last century at seven glacier locations. Data show regional consistency in trend direction but differ in absolute value as these glaciers are found at different latitudes and altitudes. Consistent increases in temperature and recent decreases in winter temperature indicate conditions are proceeding as predicted and further glacier retreat and reductions in the snow pack may be anticipated. Though clear changes in annual river discharge were not determined, these changes in precipitation and temperature suggest seasonal changes in flow timing that have been observed will continue. Specifically, a shift in the mass of water to earlier in the year resulting in lower late summer baseflows as glaciers retreat, snow melts earlier, and more winter precipitation

falls as rain and is immediately lost to runoff. However, extreme temperature and precipitation events have both occurred with more frequency in the latter half of the 20th century indicating that year to year generalizations on runoff will be difficult.

Chapter three reports on the methods of collecting snow depth and snow water equivalent data in British Columbia and throughout the Basin. At present, there are 245 snow monitoring stations throughout the Basin but significant gaps exist in the northern tip and southeastern part of the Basin. Data gaps also exist above 2200 m asl, which could be significant in that maximum snow depths were shown to occur above this threshold, ranging in elevation from 2250 to 2550. Fewer observations at mid elevations (around 1400 m) weaken the ability to study the effects of increasing snow lines with increased winter temperature and increased winter rain.

Chapter four reports on glaciological and geodetic data collected evaluating glacier mass change through the study period. In addition to the six glaciers that were evaluated using traditional mass balance methods (direct measurement on the glacier) an additional 74 glaciers were studied using LiDAR surveys. Both methods were comparable and indicated annual glacier mass loss of -0.76 ± 0.16 meter water equivalent (m w.e.) from 2015-2018. This offers promise for aerial surveying to capture greater glacier area, and thus better represent glacier change in the Basin, for similar cost. This is a four-fold increase relative to 2000-2009. Satellite imagery analysis indicates that Basin glaciers are shrinking at a rate of 0.47% per year, corresponding to a basin wide annual glacier mass loss of -0.36 ± 0.19 m.w.e or 11.34 gigatons of water from 2000 to 2018. This loss represents nearly one half of the total volume of Kinbasket Lake (24 km^3).

Chapter five characterizes the hydrology across the Basin with an emphasis on how glaciers influence surface runoff. Late summer streamflow in glacierized catchments is proportionally more influenced by glacier melt as snowmelt has already abated and precipitation this time of year tends to be low. The results indicate that the influence of glaciers on surface runoff is detectable at as little as 2% glacier cover. Catchments with glaciers above this threshold all show a decline in August streamflow over the period of instrumentation. The ability for glacial melt to buffer warm dry weather has thus declined in parallel. The two gauged basins with supersite glaciers, Canoe and Nordic, indicate that in catchments with significant glacier coverage, unsustainable mass loss, glacier wastage, comprises a significant portion of annual streamflow (10% in these cases). It follows that loss of glacier area and volume will significantly affect runoff in highly glacierized basins.

Our network provided a cursory assessment (Chapter 2) of meteorological forcing for glaciers and snowpack over the five year period of study. These differences may simply arise from the lack of available meteorological stations that are used in the Climate WNA downscaled (a semi-empirical downscaled climate

product). The Climate WNA cold season precipitation, for example, does not match the observed on-glacier or off-glacier snow data presented in chapters three and four. One avenue for improved insight into climate forcing includes high-resolution dynamical downscaling.

In turn, the off- and on-glacier LiDAR snow depth surveys are incongruous. This may not be surprising given the propensity for glaciers to exist at locations preferential to snow deposition and encourage further deposition themselves, yet these differences are entirely uncaptured by current snow forecasting and hydrologic models. Better understanding alpine snowpack is paramount to improving regional hydrological models.

6.3 Implications in terms of water availability

Year to year variations in the importance of runoff from snow and ice highly depends to a large degree on meteorological conditions, but long-term trends are set by the climate system. Though clear trends in annual streamflows were not detected in this study (Chapter 5), shifts in the timing of flows have been observed and declines in August flows in glacierized systems is apparent (Stahl and Moore 2006; Brahney et al. 2017a,b). Long term declines in regional April 1 snow water equivalent have also been observed (Jost and Weber 2012). Phase changes in precipitation (snow to rain) will affect seasonal water storage and may elevate forest fire risk. Aquatic systems remain vulnerable, especially those that lie in small, headwater basins where the fraction of flow from melting glaciers is highest. Though new lakes may form and existing lakes will expand, the degree of connectivity is expected to decline as glaciers fade. The significant runoff contribution found in the two gauged basins with supersite glaciers demonstrates that as these glaciers shrink, substantial reductions in late season runoff will occur in catchments with glacier cover greater than one or two percent.

6.4 Ecological and water quality implications

Demise of the cryosphere will have implications for both water quality and aquatic ecology. This provisioning of cold turbid water from glaciers creates habitat, keeps water temperatures within tolerance ranges for native fish, supplies nutrients, and shields aquatic organisms living in high elevations from harmful ultra-violet (UV) rays (Williamson et al. 2001; Fleming 2005; Hood and Berner 2009; Muhlfeld et al. 2011; Sommaruga 2015). As glaciers recede and fade, associated hydrologic changes will influence habitat ranges, species composition, biodiversity and ecosystem functioning through altered flow regimes, nutrient fluxes, water temperature, and light characteristics.

Because there are competing controls on the water quality and ecological attributes of alpine aquatic ecosystems, the specific future changes in ecosystem services in response to longer growing seasons and glacier retreat remain uncertain. Glacierized systems have been observed to both elevate fluxes of nutrients (Saros et al. 2010) and dilute nutrient concentrations during the melt season (Tockner et al. 2002; Hood and Berner 2009). Regardless of the direction and magnitude, changes in nutrient concentrations are anticipated which will have significant implications for species composition and trophic interactions across all aquatic habitats, particularly in mountain systems that are sensitive to small environmental changes (Moser et al. 2019).

Glacial melt influences water quality in receiving and downstream aquatic ecosystems through multiple mechanisms. Not only through shifts in nutrient fluxes as described above, but also through the release of organic and industrial pollutants that have accumulated in glaciers over time (Blais et al. 2001; Daly and Wania 2005; Geisz et al. 2008; Ferrario et al. 2017) . Elevated concentrations of heavy metals such as mercury, persistent organic pollutants (POP's) such as poly-chlorinated biphenyls PCB's as well as pesticides that have been banned for over half a century, such as dichlorodiphenyltrichloroethane (DDT), have been observed in glacial melt in western Canada. These contaminants have the capacity to enter the food chain and in some cases biomagnify (Morrissey et al. 2005).

Shifts in productivity and community composition in the near term may also vary from site to site. In general, the shift towards warmer temperatures in the long term is expected to increase primary production and biomass while near term community shifts are more complex. High suspended sediment loads combined with cold temperatures and a short growing season leads to a community of highly adapted specialized taxa with overall low taxonomic diversity. As the cryosphere fades, high UV:PAR ratios can initially lead to photoinhibition suppressing productivity adding additional constraints on taxonomic diversity (Sommaruga 2015). Over time, the encroachment of vegetation will increase fluxes of coloured dissolved organic matter that will suppress UV:PAR ratios reducing photoinhibition allowing for greater diversity in the pelagic regions. Further, as turbidity declines and light penetrates deeper into aquatic ecosystems new benthic habitats will open up. While specialized cold-adapted species will go extinct, warmer temperatures combined with a longer growing season will promote invasion from more temperate adapted species (Muhlfeld et al. 2011; Milner et al. 2017). Finally, phenological shifts in receiving ecosystems may have additional and hard to predict consequences. It is widely recognized that warming stream water temperatures, particularly in the late summer, will have negative consequences for native cold-water fish species (Fleming 2005). The direction response in the near or far term for any given system will likely vary with percent glacier cover, elevation, and whether systems are in an early or late phase response to glacier recession.

6.5 Directions for future work

This network successfully completed a major undertaking of glacier observations from glaciological and geodetic measurements. This dataset has great value for water resource management and improving models and projections of glacier response to ongoing climate change.

To maximize the value of this undertaking, it would be ideal to continue some of this monitoring since the value of monitoring changes in glaciers, snow and runoff directly scales to the duration of the monitoring itself. Our current understanding of alpine hydrology in the region is poor, due to limited observations and a lack of a historical baseline. The lag time in release of results generated by a university-led project due to publication constraints is not ideal, as this data would be more valuable were it released in near real-time. Ongoing work would best be coordinated by government agencies with clear mandates for long-term monitoring. We would strongly advocate for continued involvement with academic researchers and stakeholders in the Basin, however.

6.5.1 Continued snow research

Snow measurements are nearly nonexistent above tree line (>2,200 m asl) and sparse around 1400 m in the Basin. Significant spatial gaps in the network of snow observation also exist in the Basin's northernmost and southeastern regions. Additional measurements, either manual or automated, should be prioritized for these locations and elevations. Gradients of snow depth versus elevation for non-glacierized regions presented in this report demonstrate the potential for LiDAR to help fill the monitoring network gap; they also sample substantially more terrain than could be visited during a routine snow course survey. Uncertainty in snow depth derived from LiDAR measurements and the density used to convert snow depth to SWE, however require robust ground-truth validation. The quality and quantity of snow density measurements must improve, in part by using appropriate equipment to measure density. Snow depth measurements are also needed to further test in situ versus LiDAR snow depth.

6.5.2 Continued glacier research

Continuing in situ measurements and aerial surveying of glaciers provide one method to quantify the fraction of glacier wastage contributions to streamflow; these surveys also improve projections of glacier response to climate change. To complement estimates of current glacier runoff and improve projections of future glacier runoff, work is underway to further analyze our ice thickness data to provide an updated estimate of total ice volume in the Columbia River Basin.

A primary objective of this network was to estimate gradients of snow accumulation and glacier mass change (mass balance gradients). These gradients are critically needed to improve models that forecast

changes in streamflow in glaciated and alpine watersheds. While we produced mass balance gradients from in situ data, our geodetic mass balance data represent a glacier-average value of mass change. Efforts are underway to model ice dynamics of our study glaciers to estimate on-glacier balance gradients.

6.5.3 Continued streamflow research

Streamflow monitoring within the Basin has historically been geared towards providing relevant information for hydropower and flood control, and thus has been collected on major tributaries. Increasing the focus on smaller watersheds like the Canoe and Nordic is critical to quantify the relative contributions of snow melt and glacier wastage to streamflow, and thus forecast future changes to streamflow magnitude and timing.

REFERENCES

Arendt, A. A., K. A. Echelmeyer, W. D. Harrison, C. S. Lingle, and V. B. Valentine, 2002: Rapid wastage of Alaska glaciers and their contribution to rising sea level. *Science*, **297**, 382–386, https://doi.org/10.1126/science.1072497

Barnett, T. P., J. C. Adam, and D. P. Lettenmaier, 2005: Potential impacts of a warming climate on water availability in snow-dominated regions. *Nature*, **438**, 303–309, https://doi.org/10.1038/nature04141

Beedle, M. J., B. Menounos, and R. Wheate, 2014: An evaluation of mass-balance methods applied to Castle creek Glacier, British Columbia, Canada. *J. Glaciol.*, **60**, 262–276, https://doi.org/10.3189/2014JoG13J091

Belart, J. M. C., and Coauthors, 2017: Winter mass balance of Drangajökull ice cap (NW Iceland) derived from satellite sub-meter stereo images. *The Cryosphere*, **11**, 1501–1517, https://doi.org/10.5194/tc-11-1501-2017

Berthier, E., C. Vincent, E. Magnússon, and Á. Gunnlaugsson, 2014: Glacier topography and elevation changes derived from Pléiades sub-meter stereo images. *The Cryosphere*, **8**, 2275–2291, https://doi.org/10.5194/tc-8-2275-2014, 2014.

Bevington, A., H. Gleason, X. Giroux-Bougard, and J. T. de Jong, 2018: A Review of Free Optical Satellite Imagery for Watershed-Scale Landscape Analysis. *1*, **2**, https://doi.org/10.22230/jwsm.2018v2n2a18

Blais, J. M., D. W. Schindler, D. C. G. Muir, M. Sharp, D. Donald, M. Lafrenière, E. Braekevelt, and W. M. J. Strachan, 2001: Melting Glaciers: A Major Source of Persistent Organochlorines to Subalpine Bow Lake in Banff National Park, Canada. *AMBIO: A Journal of the Human Environment*, **30**, 410–415, https://doi.org/10.1579/0044-7447-30.7.410

Bolch, T., B. Menounos, and R. Wheate, 2010: Landsat-based inventory of glaciers in western Canada, 1985–2005. *Remote Sens. Environ.*, **114**, 127–137, https://doi.org/10.1016/j.rse.2009.08.015

Brahney, J., B. Menounos, X. Wei, and P. J. Curtis, 2017a: Determining annual cryosphere storage contributions to streamflow using historical hydrometric records. *Hydrol. Process.*, **31**, 1590–1601, https://doi.org/10.1002/hyp.11128

Brahney, J., F. Weber, V. Foord, J. Janmaat, and P. J. Curtis, 2017b: Evidence for a climate-driven hydrologic regime shift in the Canadian Columbia Basin. *Canadian Water Resources Journal / Revue canadienne des ressources hydriques*, **42**, 179–192, https://doi.org/10.1080/07011784.2016.1268933

Broxton, P. D., W. J. D. Leeuwen, and J. A. Biederman, 2019: Improving Snow Water Equivalent Maps With Machine Learning of Snow Survey and Lidar Measurements. *Water Resour. Res.*, **73**, 16, https://doi.org/10.1029/2018WR024146

Chilton, R. H., 1981: *A summary of climatic regimes of British Columbia*. Province of British Columbia, Ministry of Environment, Assessment and ...,.

Clarke, G. K. C., F. S. Anslow, A. H. Jarosch, V. Radić, B. Menounos, T. Bolch, and E. Berthier, 2013: Ice Volume and Subglacial Topography for Western Canadian Glaciers from Mass Balance Fields, Thinning Rates, and a Bed Stress Model. *J. Clim.*, **26**, 4282–4303, https://doi.org/10.1175/JCLI-D-12-00513.1

Clarke, G. K. C., A. H. Jarosch, F. S. Anslow, V. Radić, and B. Menounos, 2015: Projected deglaciation of western Canada in the twenty-first century. *Nat. Geosci.*, **8**, 372–377, https://doi.org/10.1038/ngeo2407

Cleveland, W. S., 1979: Robust Locally Weighted Regression and Smoothing Scatterplots. *J. Am. Stat. Assoc.*, **74**, 829–836, https://doi.org/10.1080/01621459.1979.10481038

Cogley, J. G., and Coauthors, 2011: Glossary of glacier mass balance and related terms, IHP-VII technical documents in hydrology No. 86, IACS Contribution No. 2. *International Hydrological Program, UNESCO, Paris*,.

Cohen, S. J., K. A. Miller, A. F. Hamlet, and W. Avis, 2000: Climate Change and Resource Management in the Columbia River Basin. *Water Int.*, **25**, 253–272, https://doi.org/10.1080/02508060008686827

Cook, B. I., R. Seager, and R. L. Miller, 2011: On the Causes and Dynamics of the Early Twentieth-Century North American Pluvial. *J. Clim.*, **24**, 5043–5060, https://doi.org/10.1175/2011JCLI4201.1

Crowley, T. J., 2000: Causes of climate change over the past 1000 years. *Science*, **289**, 270–277, https://doi.org/10.1126/science.289.5477.270

Cuffey, K. M., and W. S. B. Paterson, 2010: *The Physics of Glaciers*. Academic Press, 704 pp.

Dadic, R., R. Mott, M. Lehning, and P. Burlando, 2010: Wind influence on snow depth distribution and accumulation over glaciers. *J. Geophys. Res.*, **115**, 1064, https://doi.org/10.1029/2009JF001261

Daly, C., M. Halbleib, J. I. Smith, W. P. Gibson, M. K. Doggett, G. H. Taylor, J. Curtis, and P. P. Pasteris, 2008: Physiographically sensitive mapping of climatological temperature and precipitation across the conterminous United States. *Int. J. Climatol.*, **28**, 2031–2064, https://doi.org/10.1002/joc.1688

Daly, G. L., and F. Wania, 2005: Organic contaminants in mountains. *Environ. Sci. Technol.*, **39**, 385–398, https://doi.org/10.1021/es048859u

DeBeer, C. M., and M. J. Sharp, 2007: Recent changes in glacier area and volume within the southern Canadian Cordillera. *Ann. Glaciol.*, **46**, 215–221, https://doi.org/10.3189/172756407782871710

DeBeer, C. M., H. S. Wheater, S. K. Carey, and K. P. Chun, 2016: Recent climatic, cryospheric, and hydrological changes over the interior of western Canada: a review and synthesis. *Hydrol. Earth Syst. Sci.*, **20**, 1573, https://doi.org/10.5194/hess-20-1573-2016

Deemer, B. R., and Coauthors, 2016: Greenhouse Gas Emissions from Reservoir Water Surfaces: A New Global Synthesis. *Bioscience*, **66**, 949–964, https://doi.org/10.1093/biosci/biw117

Deems, J. S., T. H. Painter, and D. C. Finnegan, 2013: Lidar measurement of snow depth: a review. *J. Glaciol.*, **59**, 467–479, https://doi.org/10.3189/2013jog12j154

Demarchi, D. A., 2011: *An introduction to the ecoregions of British Columbia*. Third Edition. Ecosystem Information Section Ministry of Environment, 163 pp.

Elder, K., J. Dozier, and J. Michaelsen, 1991: Snow accumulation and distribution in an alpine watershed. *Water Resour. Res.*, **27**, 1541–1552, https://doi.org/ https://doi.org/10.1029/91WR00506.

Environment And Climate, 2018: National Water Data Archive: HYDAT. https://www.canada.ca/en/environment-climate-change/services/water-overview/quantity/monitoring/

Escher-Vetter, H., M. Kuhn, and M. Weber, 2009: Four decades of winter mass balance of Vernagtferner and Hintereisferner, Austria: methodology and results. *Ann. Glaciol.*, **50**, 87–95, https://doi.org/10.3189/172756409787769672

Farinotti, D., M. Huss, J. J. Fürst, J. Landmann, H. Machguth, F. Maussion, and A. Pandit, 2019: A consensus estimate for the ice thickness distribution of all glaciers on Earth. *Nat. Geosci.*, **12**, 168–173, https://doi.org/10.1038/s41561-019-0300-3

Fausto, R. S., and Coauthors, 2018: A Snow Density Dataset for Improving Surface Boundary Conditions in Greenland Ice Sheet Firn Modeling. https://doi.org/10.3389/feart.2018.00051

Ferrario, C., A. Finizio, and S. Villa, 2017: Legacy and emerging contaminants in meltwater of three Alpine glaciers. *Sci. Total Environ.*, **574**, 350–357, https://doi.org/10.1016/j.scitotenv.2016.09.067

Fleming, S. W., 2005: Comparative analysis of glacial and nival streamflow regimes with implications for lotic habitat quantity and fish species richness. *River Res. Appl.*, **21**, 363–379, https://doi.org/10.1002/rra.810

Fleming, S. W., 2008: Approximate record length constraints for experimental identification of dynamical fractals. *Ann. Phys.*, **17**, 955–969, https://doi.org/10.1002/andp.200810329

Fleming, S. W., 2019: *Where the River Flows: Scientific Reflections on Earth's Waterways*. Princeton University Press, 216 pp.

Fleming, S. W., and P. H. Whitfield, 2010: Spatiotemporal mapping of ENSO and PDO surface meteorological signals in British Columbia, Yukon, and southeast Alaska. *Atmosphere-Ocean*, **48**, 122–131, https://doi.org/10.3137/ao1107.2010

Fleming, S. W., and D. J. Sauchyn, 2013: Availability, volatility, stability, and teleconnectivity changes in prairie water supply from Canadian Rocky Mountain sources over the last millennium. *Water Resour. Res.*, **49**, 64–74, https://doi.org/10.1029/2012WR012831

Fleming, S. W., and H. E. Dahlke, 2014: Modulation of linear and nonlinear hydroclimatic dynamics by mountain glaciers in Canada and Norway: Results from information-theoretic polynomial selection. *Can. Water Resourc. J./Rev. Can. Ressour. Hydr.*, **39**, 324–341.

Fleming, S. W., and M. Barton, 2015: Climate Trends but Little Net Water Supply Shift in One of Canada's Most Water-Stressed Regions over the Last Century. *JAWRA Journal of the American Water Resources Association*, **51**, 833–841.

Fleming, S. W., P. H. Whitfield, R. D. Moore, and E. J. Quilty, 2007: Regime-dependent streamflow sensitivities to Pacific climate modes cross the Georgia--Puget transboundary ecoregion. *Hydrological Processes: An International Journal*, **21**, 3264–3287.

Francis, J. A., and S. J. Vavrus, 2012: Evidence linking Arctic amplification to extreme weather in mid-latitudes. *Geophys. Res. Lett.*, **39**, L06801, https://doi.org/10.1029/2012GL051000

Gardner, A. S., and Coauthors, 2013: A reconciled estimate of glacier contributions to sea level rise: 2003 to 2009. *Science*, **340**, 852–857, https://doi.org/10.1126/science.1234532

Geisz, H. N., R. M. Dickhut, M. A. Cochran, W. R. Fraser, and H. W. Ducklow, 2008: Melting glaciers: a probable source of DDT to the Antarctic marine ecosystem. *Environ. Sci. Technol.*, **42**, 3958–3962, https://doi.org/10.1021/es702919n

Glen, J. W., and J. G. Paren, 1975: The Electrical Properties of Snow and Ice. *J. Glaciol.*, **15**, 15–38, https://doi.org/10.3189/S0022143000034249

Gobena, A. K., F. A. Weber, and S. W. Fleming, 2013: The Role of Large-Scale Climate Modes in Regional Streamflow Variability and Implications for Water Supply Forecasting: A Case Study of the Canadian Columbia River Basin. *Atmosphere-Ocean*, **51**, 380–391, https://doi.org/10.1080/07055900.2012.759899

Government of Canada, 2019: National hydrometric network basin polygons. *Open Canada*,. https://open.canada.ca/data/en/dataset/0c121878-ac23-46f5-95df-eb9960753375 (Accessed January 14, 2019).

Grünewald, T., and Coauthors, 2013: Statistical modelling of the snow depth distribution in open alpine terrain. *Hydrol. Earth Syst. Sci.*, **17**, 3005–3021, https://doi.org/10.5194/hess-17-3005-2013

Grünewald, T., Y. Bühler, and M. Lehning, 2014: Elevation dependency of mountain snow depth. *The Cryosphere*, **8**, 2381–2394, https://doi.org/10.5194/tc-8-2381-2014

Hamann, A., T. Wang, D. L. Spittlehouse, and T. Q. Murdock, 2013: A Comprehensive, High-Resolution Database of Historical and Projected Climate Surfaces for Western North America. *Bull. Am. Meteorol. Soc.*, **94**, 1307–1309, https://doi.org/10.1175/BAMS-D-12-00145.1

Hamlet, A. F., and D. P. Lettenmaier, 1999: Columbia River streamflow forecasting based on ENSO and PDO climate signals. *of water resources planning and ...*, **125**, 333–341, https://doi.org/10.1061/(ASCE)0733-9496(1999)125:6(333)

Hamlet, A. F., P. W. Mote, M. P. Clark, and D. P. Lettenmaier, 2005: Effects of temperature and precipitation variability on snowpack trends in the Western United States*. *J. Clim.*, **18**, 4545–4561, https://doi.org/10.1175/JCLI3538.1

Hamlet, A. F., M. M. Elsner, G. S. Mauger, S.-Y. Lee, I. Tohver, and R. A. Norheim, 2013: An Overview of the Columbia Basin Climate Change Scenarios Project: Approach, Methods, and Summary of Key Results. *Atmosphere-Ocean*, **51**, 392–415, https://doi.org/10.1080/07055900.2013.819555

Helfricht, K., M. Kuhn, M. Keuschnig, and A. Heilig, 2014a: Lidar snow cover studies on glaciers in the Ötztal Alps (Austria): comparison with snow depths calculated from GPR measurements. *The Cryosphere*, **8**, 41–57, https://doi.org/10.5194/tc-8-41-2014

Helfricht, K., J. Schöber, K. Schneider, R. Sailer, and M. Kuhn, 2014b: Interannual persistence of the seasonal snow cover in a glacierized catchment. *J. Glaciol.*, **60**, 889–904, https://doi.org/10.3189/2014JoG13J197

Hirose, J. M. R., and S. J. Marshall, 2013: Glacier Meltwater Contributions and Glaciometeorological Regime of the Illecillewaet River Basin, British Columbia, Canada. *Atmosphere-Ocean*, **51**, 416–435, https://doi.org/10.1080/07055900.2013.791614

Hood, E., and L. Berner, 2009: Effects of changing glacial coverage on the physical and biogeochemical properties of coastal streams in southeastern Alaska. *J. Geophys. Res.*, **114**, 382, https://doi.org/10.1029/2009JG000971

Hsieh William W., Yuval null, Li Jingyang, Shabbar Amir, and Smith Stephanie, 2003: Seasonal Prediction with Error Estimation of Columbia River Streamflow in British Columbia. *Journal of Water Resources Planning and Management*, **129**, 146–149, https://doi.org/10.1061/(ASCE)0733-9496(2003)129:2(146)

Huss, M., 2013: Density assumptions for converting geodetic glacier volume change to mass change. *The Cryosphere*, **7**, 877–887, https://doi.org/10.5194/tc-7-877-2013

Huss, M., and D. Farinotti, 2012: Distributed ice thickness and volume of all glaciers around the globe. *J. Geophys. Res.*, **117**, https://doi.org/10.1029/2012JF002523

Huss, M., and R. Hock, 2015: A new model for global glacier change and sea-level rise. *Front Earth Sci. Chin.*, **3**, 54, https://doi.org/10.3389/feart.2015.00054

Huybers, P., and W. Curry, 2006: Links between annual, Milankovitch and continuum temperature variability. *Nature*, **441**, 329–332, https://doi.org/10.1038/nature04745

Jacoby, G. C., Jr, 1976: Long-term surface-water supply and streamflow trends in the Upper Colorado River basin based on tree-ring analyses. *Natl. Sci. Found. Lake Powell Res. Proj. Bull*, **18**, 1–70.

Joerg, P. C., F. Morsdorf, and M. Zemp, 2012: Uncertainty assessment of multi-temporal airborne laser scanning data: A case study on an Alpine glacier. *Remote Sens. Environ.*, **127**, 118–129, https://doi.org/10.1016/j.rse.2012.08.012

Jost, G., and F. Weber, 2012: Potential impacts of climate change on BC Hydro's water resources. *BC Hydro*, 1–28.

Jost, G., R. D. Moore, B. Menounos, and R. Wheate, 2012: Quantifying the contribution of glacier runoff to streamflow in the upper Columbia River Basin, Canada. *Hydrol. Earth Syst. Sci.*, **16**, 849–860, https://doi.org/10.5194/hess-16-849-2012

Kääb, A., 2005: *Remote sensing of mountain glaciers and permafrost creep*. Geographisches Institut der Universität Zürich, 264 pp.

Klug, C., and Coauthors, 2018: Geodetic reanalysis of annual glaciological mass balances (2001–2011) of Hintereisferner, Austria. *The Cryosphere*, **12**, 833–849, https://doi.org/10.5194/tc-12-833-2018

Kovacs, A., A. J. Gow, and R. M. Morey, 1995: The in-situ dielectric constant of polar firn revisited. *Cold Reg. Sci. Technol.*, **23**, 245–256, https://doi.org/10.1016/0165-232X(94)00016-Q

Luckman, B. H., 2000: The Little Ice Age in the Canadian Rockies. *Geomorphology* , **32**, 357–384, https://doi.org/10.1016/S0169-555X(99)00104-X

Machguth, H., O. Eisen, F. Paul, and M. Hoelzle, 2006: Strong spatial variability of snow accumulation observed with helicopter-borne GPR on two adjacent Alpine glaciers. *Geophys. Res. Lett.*, **33**, 317, https://doi.org/10.1029/2006GL026576

Mantua, N. J., S. R. Hare, Y. Zhang, J. M. Wallace, and R. C. Francis, 1997: A Pacific Interdecadal Climate Oscillation with Impacts on Salmon Production*. *Bull. Am. Meteorol. Soc.*, **78**, 1069–1080, https://doi.org/2.0.CO;2">10.1175/1520-0477(1997)078<1069:APICOW>2.0.CO;2

Marshall, S. J., 2014: Meltwater run-off from Haig Glacier, Canadian Rocky Mountains, 2002-2013. *Hydrol. Earth Syst. Sci.*, **18**, 5181, https://doi.org/10.5194/hess-18-5181-2014

Marti, R., S. Gascoin, E. Berthier, M. de Pinel, T. Houet, and D. Laffly, 2016: Mapping snow depth in open alpine terrain from stereo satellite imagery. *The Cryosphere*, **10**, 1361–1380, https://doi.org/10.5194/tc-10-1361-2016

McGrath, D., L. Sass, S. O'Neel, A. Arendt, G. Wolken, A. Gusmeroli, C. Kienholz, and C. McNeil, 2015: End-of-winter snow depth variability on glaciers in Alaska. *J. Geophys. Res. Earth Surf.*, **120**, 1530–1550, https://doi.org/10.1002/2015JF003539

McGrath, D., L. Sass, S. O'Neel, C. McNeil, S. G. Candela, E. H. Baker, and H.-P. Marshall, 2018: Interannual snow accumulation variability on glaciers derived from repeat, spatially extensive ground-penetrating radar surveys. *The Cryosphere*, **12**, 3617–3633, https://doi.org/10.5194/tc-12-3617-2018

Menounos, B., and Coauthors, 2019: Heterogeneous Changes in Western North American Glaciers Linked to Decadal Variability in Zonal Wind Strength. *Geophys. Res. Lett.*, **46**, 200–209, https://doi.org/10.1029/2018GL080942

Milner, A. M., and Coauthors, 2017: Glacier shrinkage driving global changes in downstream systems. *Proc. Natl. Acad. Sci. U. S. A.*, **114**, 9770–9778, https://doi.org/10.1073/pnas.1619807114

Mingo, L., and G. E. Flowers, 2010: Instruments and Methods An integrated lightweight ice-penetrating radar system. *J. Glaciol.*, **56**, 709–714, https://doi.org/10.3189/002214310793146179

Moholdt, G., C. Nuth, J. O. Hagen, and J. Kohler, 2010: Recent elevation changes of Svalbard glaciers derived from ICESat laser altimetry. *Remote Sens. Environ.*, **114**, 2756–2767, https://doi.org/10.1016/j.rse.2010.06.008

Moore, R. D., S. W. Fleming, B. Menounos, R. Wheate, A. Fountain, K. Stahl, K. Holm, and M. Jakob, 2009: Glacier change in western North America: influences on hydrology, geomorphic hazards and water quality. *Hydrol. Process.*, **23**, 42–61, https://doi.org/10.1002/hyp.7162

Moore, R. D., M. Nelitz, and E. Parkinson, 2013: Empirical modelling of maximum weekly average stream temperature in British Columbia, Canada, to support assessment of fish habitat suitability. *Canadian Water Resources Journal / Revue canadienne des ressources hydriques*, **38**, 135–147, https://doi.org/10.1080/07011784.2013.794992

Moore, R. D. (dan), 2006: Stream Temperature Patterns in British Columbia, Canada, Based on Routine Spot Measurements. *Canadian Water Resources Journal / Revue canadienne des ressources hydriques*, **31**, 41–56, https://doi.org/10.4296/cwrj3101041

Moore, R.D., Spittlehouse, D.L., Whitfield, P.H. and Stahl, K., 2010: Regional Hydrology. *Compendium of Forest Hydrology and Geomorphology in British Columbia. 280 Land Management Handbook 66*, R. G. Pike, T. E. Redding, R. D. Moore, R. D. Winkler, & K. D. Bladon, Ed., Kamloops: B.C. Ministry of Forest and Range, Forest Science Program, Victoria, B.C. and FORREX Forum for Research and Extension in Natural Resources, 85–110.

Morrissey, C. A., L. I. Bendell-Young, and J. E. Elliott, 2005: Identifying Sources and Biomagnification of Persistent Organic Contaminants in Biota from Mountain Streams of Southwestern British Columbia, Canada. *Environmental Science & Technology*, **39**, 8090–8098, https://doi.org/10.1021/es050431n

Moser, K. A., and Coauthors, 2019: Mountain lakes: Eyes on global environmental change. *Global and Planetary Change*, **178**, 77–95, https://doi.org/10.1016/j.gloplacha.2019.04.001

Muhlfeld, C. C., J. J. Giersch, F. R. Hauer, G. T. Pederson, G. Luikart, D. P. Peterson, C. C. Downs, and D. B. Fagre, 2011: Climate change links fate of glaciers and an endemic alpine invertebrate. *Clim. Change*, **106**, 337–345, https://doi.org/10.1007/s10584-011-0057-1

Najafi, M. R., F. Zwiers, and N. Gillett, 2017: Attribution of the Observed Spring Snowpack Decline in British Columbia to Anthropogenic Climate Change. *J. Clim.*, **30**, 4113–4130, https://doi.org/10.1175/JCLI-D-16-0189.1

Nolan, M., C. Larsen, and M. Sturm, 2015: Mapping snow depth from manned aircraft on landscape scales at centimeter resolution using structure-from-motion photogrammetry. *The Cryosphere*, **9**, 1445–1463, https://doi.org/10.5194/tc-9-1445-2015

Nolin, A. W., J. Phillippe, A. Jefferson, and S. L. Lewis, 2010: Present-day and future contributions of glacier runoff to summertime flows in a Pacific Northwest watershed: Implications for water resources. *Water Resour. Res.*, **46**, 303, https://doi.org/10.1029/2009WR008968

Nuth, C., and A. Kääb, 2011: Co-registration and bias corrections of satellite elevation data sets for quantifying glacier thickness change. *The Cryosphere*, **5**, 271–290, https://doi.org/10.5194/tc-5-271-2011

Oerlemans, J., and Coauthors, 1998: Modelling the response of glaciers to climate warming. *Clim. Dyn.*, **14**, 267–274, https://doi.org/10.1007/s003820050222

Osborn, T. J., and K. R. Briffa, 2006: The spatial extent of 20th-century warmth in the context of the past 1200 years. *Science*, **311**, 841–844, https://doi.org/10.1126/science.1120514

Parkinson, E. A., E. V. Lea, M. A. Nelitz, J. M. Knudson, and R. D. Moore, 2016: Identifying Temperature Thresholds Associated with Fish Community Changes in British Columbia, Canada, to Support Identification of Temperature Sensitive Streams: STREAM TEMPERATURE AND FISH COMMUNITIES. *River Res. Appl.*, **32**, 330–347, https://doi.org/10.1002/rra.2867

Paul, F., A. Kääb, M. Maisch, T. Kellenberger, and W. Haeberli, 2004: Rapid disintegration of Alpine glaciers observed with satellite data. *Geophys. Res. Lett.*, **31**, https://doi.org/10.1029/2004GL020816

Pelto, B. M., B. Menounos, and S. J. Marshall, 2019: Multi-year evaluation of airborne geodetic surveys to estimate seasonal mass balance, Columbia and Rocky Mountains, Canada. *The Cryosphere*, **13**, 1709–1727, https://doi.org/10.5194/tc-13-1709-2019

Pelto, M. S., 2006: The current disequilibrium of North Cascade glaciers. *Hydrol. Process.*, **20**, 769–779, https://doi.org/10.1002/hyp.6132

Pelto, M. S., 2018: How unusual was 2015 in the 1984--2015 period of the North Cascade glacier annual mass balance? Water, 10, 543. *Water*, **10**, 543, https://doi.org/10.3390/w10050543

Ragettli, S., W. W. Immerzeel, and F. Pellicciotti, 2016: Contrasting climate change impact on river flows from high-altitude catchments in the Himalayan and Andes Mountains. *Proc. Natl. Acad. Sci. U. S. A.*, **113**, 9222–9227, https://doi.org/10.1073/pnas.1606526113

R Development Core Team, 2013: *R: A language and environment for statistical computing*. R Foundation for Statistical Computing,.

Samimi, S., and S. J. Marshall, 2017: Diurnal Cycles of Meltwater Percolation, Refreezing, and Drainage in the Supraglacial Snowpack of Haig Glacier, Canadian Rocky Mountains. *Front. Earth Sci.*, **5**, 93, https://doi.org/10.3389/feart.2017.00006

Saros, J. E., and Coauthors, 2010: Melting Alpine Glaciers Enrich High-Elevation Lakes with Reactive Nitrogen. *Environmental Science & Technology*, **44**, 4891–4896, https://doi.org/10.1021/es100147j

Schiefer, E., B. Menounos, and R. Wheate, 2007: Recent volume loss of British Columbian glaciers, Canada. *Geophys. Res. Lett.*, **34**, L16503, https://doi.org/10.1029/2007GL030780

Schiefer, E., B. Menounos, and R. Wheate, 2008: An inventory and morphometric analysis of British Columbia glaciers, Canada. *J. Glaciol.*, **54**, 551–560.

Schnorbus, M., A. Werner, and K. Bennett, 2014a: Impacts of climate change in three hydrologic regimes in British Columbia, Canada. *Hydrol. Process.*, **28**, 1170–1189, https://doi.org/10.1002/hyp.9661

Schnorbus, M., A. Werner, and K. Bennett, 2014b: Impacts of climate change in three hydrologic regimes in British Columbia, Canada. *Hydrol. Process.*, **28**, 1170–1189.

Sevruk, B., 2004: Niederschlag als Wasserkreislaufelement. *Theorie und Praxis der Niederschlagsmessung. Zurich-Nitra: Eigenverlag ETH Zurich*,.

Shea, J. M., R. Dan Moore, and K. Stahl, 2009: Derivation of melt factors from glacier mass-balance records in western Canada. *J. Glaciol.*, **55**, 123–130, https://doi.org/10.3189/002214309788608886

Sold, L., M. Huss, M. Hoelzle, H. Andereggen, P. C. Joerg, and M. Zemp, 2013: Methodological approaches to infer end-of-winter snow distribution on alpine glaciers. *J. Glaciol.*, **59**, 1047–1059, https://doi.org/10.3189/2013JoG13J015

Sold, L., M. Huss, A. Eichler, M. Schwikowski, and M. Hoelzle, 2014: Recent accumulation rates of an alpine glacier derived from firn cores and repeated helicopter-borne GPR. *The Cryosphere Discuss.*, **8**, 4431–4462, https://doi.org/10.5194/tcd-8-4431-2014

Sold, L., and Coauthors, 2016: Mass balance re-analysis of Findelengletscher, Switzerland; benefits of extensive snow accumulation measurements. *Front Earth Sci. Chin.*, **4**, 18.

Solomon, S., G.-K. Plattner, R. Knutti, and P. Friedlingstein, 2009: Irreversible climate change due to carbon dioxide emissions. *Proc. Natl. Acad. Sci. U. S. A.*, **106**, 1704–1709, https://doi.org/10.1073/pnas.0812721106

Sommaruga, R., 2015: When glaciers and ice sheets melt: consequences for planktonic organisms. *J. Plankton Res.*, **37**, 509–518, https://doi.org/10.1093/plankt/fbv027

Stahl, K., and R. D. Moore, 2006: Influence of watershed glacier coverage on summer streamflow in British Columbia, Canada. *Water Resour. Res.*, **42**, W06201, https://doi.org/10.1029/2006WR005022

Stahl, K., R. D. Moore, and I. G. McKendry, 2006: The role of synoptic-scale circulation in the linkage between large-scale ocean-atmosphere indices and winter surface climate in British Columbia, Canada (vol 26, pg 541, 2006). *Int. J. Climatol.*, **26**, 561–561, https://doi.org/10.1002/joc.1268

Sturm, M., M. A. Goldstein, and C. Parr, 2017: Water and life from snow: A trillion dollar science question. *Water Resour. Res.*, **53**, 3534–3544, https://doi.org/10.1002/2017WR020840

Tennant, C., and B. Menounos, 2013: Glacier change of the Columbia Icefield, Canadian Rocky Mountains, 1919–2009. *J. Glaciol.*, **59**, 671–686, https://doi.org/10.3189/2013JoG12J135

Teucher, A., Hazlitt, S., & Albers, S., 2018: *Bcmaps: Map layers and spatial utilities for british columbia*.

Tockner, K., F. Malard, U. Uehlinger, and J. V. Ward, 2002: Nutrients and organic matter in a glacial river—floodplain system (Val Roseg, Switzerland). *Limnol. Oceanogr.*, **47**, 266–277.

Trubilowicz, J., R. D. Moore, and F. Anslow, 2010: *Glacier Inventory of the Canadian Columbia River Basin and Recommendations for Monitoring*. University of British Columbia, 26 pp.

Trubilowicz, J. W., R. D. Moore, and J. M. Buttle, 2013: Prediction of stream-flow regime using ecological classification zones. *Hydrol. Process.*, **27**, 1935–1944, https://doi.org/10.1002/hyp.9874

Vincent, L. A., X. Zhang, R. D. Brown, Y. Feng, E. Mekis, E. J. Milewska, H. Wan, and X. L. Wang, 2015: Observed trends in Canada's climate and influence of low-frequency variability modes. *J. Clim.*, **28**, 4545–4560.

Viviroli, D., H. H. Dürr, B. Messerli, M. Meybeck, and R. Weingartner, 2007: Mountains of the world, water towers for humanity: Typology, mapping, and global significance. *Water Resour. Res.*, **43**, 14,827, https://doi.org/10.1029/2006WR005653

Wang, T., A. Hamann, D. Spittlehouse, and C. Carroll, 2016: Locally Downscaled and Spatially Customizable Climate Data for Historical and Future Periods for North America. *PLoS One*, **11**, e0156720, https://doi.org/10.1371/journal.pone.0156720

Wan, H., X. Zhang, and F. Zwiers, 2019: Human influence on Canadian temperatures. *Clim. Dyn.*, **52**, 479–494, https://doi.org/10.1007/s00382-018-4145-z

Whitfield, P. H., R. D. (dan) Moore, S. W. Fleming, and A. Zawadzki, 2010: Pacific Decadal Oscillation and the Hydroclimatology of Western Canada—Review and Prospects. *Canadian Water Resources Journal / Revue canadienne des ressources hydriques*, **35**, 1–28, https://doi.org/10.4296/cwrj3501001

Williamson, C. E., P. J. Neale, G. Grad, H. J. De Lange, and B. R. Hargreaves, 2001: Beneficial and Detrimental Effects of UV on Aquatic Organisms: Implications of Spectral Variation. *Ecological Applications*, **11**, 1843, https://doi.org/10.2307/3061100

Wilson, N. J., G. E. Flowers, and L. Mingo, 2013: Comparison of thermal structure and evolution between neighboring subarctic glaciers. *J. Geophys. Res. Earth Surf.*, **118**, 1443–1459, https://doi.org/10.1002/jgrf.20096

Woodhouse, C. A., and S. T. Gray, 2006: Updated streamflow reconstructions for the Upper Colorado River basin. *Water Resour.*, **42**, https://doi.org/10.1029/2005WR004455

World Glacier Monitoring Service (WGMS), 2018: Fluctuations of Glaciers Database. https://doi.org/10.5904/WGMS-FOG-2018-11

Wu, A., W. W. Hsieh, and A. Shabbar, 2005: The Nonlinear Patterns of North American Winter Temperature and Precipitation Associated with ENSO. *Journal of Climate*, **18**, 1736–1752, https://doi.org/10.1175/jcli3372.1

Zemp, M., M. Hoelzle, and W. Haeberli, 2009: Six decades of glacier mass-balance observations: a review of the worldwide monitoring network. *Ann. Glaciol.*, **50**, 101–111, https://doi.org/10.3189/172756409787769591

Zemp, M., and Coauthors, 2019: Global glacier mass changes and their contributions to sea-level rise from 1961 to 2016. *Nature*, **568**, 382–386, https://doi.org/10.1038/s41586-019-1071-0

Published by the Canadian Columbia Basin Glacier and Snow Research Network with support from Columbia Basin Trust.

February 2020